Departamento de Biología Celular, Biología Funcional y Antropología Física

Instituto de Biotecnología y Biomedicina (BIOTECMED). Universitat de València

DOCTORADO EN BIOMEDICINA Y BIOTECNOLOGÍA

IMMUNE SURVEILLANCE OF NEURAL STEM CELLS

Pablo Martí Rodrigo

VNIVERSITAT DE VALÈNCIA

Directores de la tesis doctoral:

Isabel Fariñas Gómez y Alberto Yáñez Boyer

VALENCIA, AGOSTO DE 2022

Dña. Isabel Fariñas Gómez, catedrática del Departamento de biología celular, biología funcional y antropología física de la Universitat de València, y de la ERI BIOTECMED, como directora.

D. Alberto Yáñez Boyer, Investigador Ramón y Cajal del Departamento de microbiología y ecología de la Universitat de València, y de la ERI BIOTECMED, como director.

D. Daniel Gozalbo Flor, catedrático del Departamento microbiología y ecología de la Universitat de València, como tutor.

INFORMAN QUE:

D. Pablo Martí Rodrigo ha realizado bajo la dirección de Isabel Fariñas Gómez y Alberto Yáñez Boyer la tesis doctoral titulada “Immune surveillance of neural stem cells”, y que hallándose concluida, autorizan su presentación a fin de que pueda ser juzgada por el tribunal correspondiente para la obtención del grado de Doctor por la Universitat de València.

Valencia, agosto de 2022.



Isabel Fariñas Gómez Alberto Yáñez Boyer Daniel Gozalbo Flor

Esta investigación ha sido financiada por los siguientes proyectos a cargo de Isabel Fariñas:

- 2021-2024. Regulación molecular de la heterogeneidad celular en los nichos neurogénicos adultos. MICINN (PID2020- 117937GB-I00).
- 2021-2025. Una aproximación multidisciplinar al estudio de la respuesta al daño genómico en células madre neurales: de levadura a mamíferos y vuelta. Consellería de Educación de la Generalitat Valenciana. Programa Prometeo de Proyectos de Excelencia (PROMETEO/2021/028).
- 2018-2020. Regulación del comportamiento de las células madre neurales por el medio sistémico: el nicho extendido. MINECO (SAF2017-86690-R).
- 2017-2021. Efectos directos y remotos de la respuesta inflamatoria sobre las células madre neurales. Generalitat Valenciana. Programa Prometeo de Proyectos de Excelencia (PROMETEO/2017/030).
- 2017-2020. RETIC de Terapia Celular. ISCIII (RD16/0011/0017).
- 2006-vigente. CIBER de Enfermedades Neurodegenerativas (CIBERNED). ISCIII (CB06/05/0086).

Pablo Martí recibió una beca predoctoral de la fundación “la Caixa” (ID 100010434) cuyo código identificativo es LCF/BQ/DE18/11670015. / *The project that gave rise to these results received the support of a fellowship from ”la Caixa” Foundation (ID 100010434). The fellowship code is LCF/BQ/DE18/11670015.*

TABLE OF CONTENTS

ABSTRACT

Antigen presentation through major histocompatibility complexes and the subsequent immune surveillance by cytotoxic T lymphocytes is considered a preventive mechanism against damaged or infected cells. At the same time, the central nervous system has long been considered an isolated territory where immune responses could not be fully developed. However, in the light of recent findings, these assumptions need to be revisited. On one hand, it has been demonstrated that quiescent adult stem cells down-regulate antigen exposure and evade immune surveillance in the hair follicle and the muscle. On the other hand, the identification of lymphatic routes for the drainage of brain-derived antigens have challenged the concept of brain immune privilege, and it is now assumed that the formation of neoantigens in neural cells is constantly monitored by the immune system. Specifically, the subependymal zone is the largest neurogenic niche in the adult mammalian brain and contains neural stem cells that can either be in a quiescence or in an activated state. The latter proliferate to give rise to the neurogenic lineage that generates mainly neurons for the olfactory bulb or small numbers of glial cells for the corpus callosum or the striatum. In addition, subependymal neural stem cells have been identified as the cells-of-origin of primary glioblastoma, the most aggressive form of brain tumor. However, whether adult neural stem cells undergo immune surveillance had not been studied before and we decided to explore it by using the adoptive transfer of T lymphocytes engineered to kill cells that express the green fluorescent protein in transgenic mice, in which this reporter protein is specifically expressed in the subependymal neurogenic lineage. Our results indicate that activated neural stem cells can be eliminated by T lymphocytes, while the quiescent ones evade immune surveillance. The analysis of antigen presentation and other mediators of cellular immunity reveals that the susceptibility of neural stem cells to T lymphocyte-mediated killing is determined by a finely tuned balance between activation signals, essentially major histocompatibility complexes exposure, and inhibitory mechanisms that include immune checkpoints and protective mechanisms. Also, we demonstrate that antigen presentation is subjected to post-translational regulation and depends on CD99 expression in some neural stem cells.

LIST OF ABBREVIATIONS

aNSC	Activated NSC
APC	Antigen-presenting cell
BBB	Blood-brain barrier
bFGF	Basic fibroblast growth factor
BSA	Bovine serum albumin
cDNA	Complementary DNA
CK	Cytokine
CNS	Central nervous system
CP	Choroid plexus
CSF	Cerebrospinal fluid
CTL	Cytotoxic T cell
CTLA-4	Cytotoxic T-lymphocyte antigen 4
DAMP	Damage-associated molecular pattern
DAPI	4’,6-diamidino-2-phenylindole
DC	Dendritic cell
DNA	Deoxyribonucleic acid
E	Embryonic day
EDTA	Ethylenediaminetetraacetic acid
EGF	Ependymal growth factor
EGFR	EGF receptor
ENB	Early neuroblast
ER	Endoplasmic reticulum
FACS	Fluorescence-activated cell sorting
FBS/FCS	Fetal calf/bovine serum
FcR	Antibody constant region receptor
FMO	Fluorescence minus one control
FSC	Forward scatter
GAS	γ-activated sequences
GBM	Glioblastoma
gDNA	Genomic DNA
GFAP	Glial fibrillary acidic protein
GFP/EGFP	(Enhanced) green fluorescent protein
GLAST	Glutamate aspartate transporter

GSC	Glioma/glioblastoma stem cell
HBSS	Hank's Balanced Salt Solution
HC	Heavy chain of the MHCI complex
HS	Horse serum
i.p.	Intraperitoneal
i.v.	Intravenous
IFN	Interferon
IL	Interleukin
ISF	Interstitial fluid
ISRE	IFN-stimulated regulatory elements
JAK	Janus kinase
JEDI	Just Egfp Inducing Death
LIN-	Lineage-negative (negative for TER119, O4, CD45 and CD31)
LNB	Late neuroblast
LPS	Lipopolysaccharide
LV.EGFP	Lentivirus encoding EGFP
MFI	Median fluorescence intensity
MHC	Major histocompatibility complex
MHCI	MHC class I
MHCII	MHC class II
mRNA	Messenger RNA
NB	Neuroblast
NLRC5	NOD-, LRR- and CARD-containing 5
NPC	Neural progenitor cell
NSC	Neural stem cell
OB	Olfactory bulb
PAMP	Pathogen-associated molecular pattern
PB	Phosphate buffer
PBS	Phosphate-buffered saline
PCR	Polymerase Chain Reaction
PD-1	Programmed Cell Death Protein 1
PD-L1/2	Programmed Cell Death Ligand 1 or 2
PEI	Polyethylenimine
PES	Polyethersulfone
PFA	Paraformaldehyde

pNSC	Primed NSC
PRR	Pattern recognition receptor
qNSC	Quiescent NSC
RBC	Red blood cell
RFP	Red fluorescent protein
RMS	Rostral migratory stream
RNA	Ribonucleic acid
RT	Room temperature
RT-qPCR	Reverse transcription quantitative PCR
SAS	Subarachnoid space
SC	Stem cell
SD	Standard deviation
SEZ	Subependymal zone
SGZ	Subgranular zone
shRNA	short hairpin RNA
SLO	Secondary lymphoid organ
SSC	Side scatter
STAT	Signal transducer and activator of transcription
TAP	Transporter associated with antigen processing
TCR	T cell receptor
TGN	Trans-Golgi network
TNF	Tumor necrosis factor
Treg	Regulatory T cell
TU	Transduction units
V-SVZ	Ventricular-subventricular zone
β2M	β2-microglobulin

INTRODUCTION

The present work lies at the interface of two different disciplines: neurobiology and immunology. On one hand, the project focuses on the neural stem cells (NSCs) of the adult subependymal zone (SEZ), which, when mutated, can be the cells-of-origin of primary glioblastoma (GBM). On the other hand, it addresses how these cells interact with the adaptive immune system, specifically with $CD8^+$ T lymphocytes. Therefore, to provide the necessary knowledge to understand the goals and results of this work, I will give a basic overview of the central aspects related to T cell-mediated immunity, NSC biology and tumor initiation.

1. The adaptive immune response: T cell generation and biology

1.1. T lymphocytes are part of a complex system

The molecules, cells and tissues that protect us from infections constitute the immune system. However, they do not only react against external pathogens, but can elicit responses against damaged and mutated cells (Abbas et al., 2016). The vast majority of immune cells in adult mammals are generated from hematopoietic stem cells (SCs) in the bone marrow, which give rise to myeloid or lymphoid lineage-committed progenitors of all blood circulating cells. A wide array of cell types are generated from these progenitors, and they constitute both the innate and the adaptive immune systems (Abbas et al., 2016; Savino et al., 2005).

Innate immunity is the first line of defense against any invader or unusual antigen. It is comprised by physical and chemical barriers (epithelia, antimicrobial substances, etc.), phagocytic cells (mainly neutrophils, monocytes, macrophages and dendritic cells (DCs)) and many other cell types, as well as blood proteins such as the complement system and other mediators of inflammation (Abbas et al., 2016). Innate immune cells detect pathogen-associated molecular patterns (PAMPs) frequently found in pathogens, or damage-associated molecular patterns (DAMPs) which become available upon tissue injury. These elements are recognized through pattern recognition receptors (PRRs) to initiate microbicidal and pro-inflammatory responses required to eliminate infectious agents or deal with tissue damage (Iwasaki and Medzhitov, 2015). Moreover, innate immune cells trigger adaptive immune responses by presenting abnormal “non-self” antigens to T lymphocytes. The adaptive immune system elicits specific responses that are

orchestrated by B and T lymphocytes (Boehm and Swann, 2014). There are two broad classes of adaptive immune responses: antibody responses in which B cells are activated to produce antibodies to label and block dangerous molecules or antigens, and T-cell mediated responses, in which T lymphocytes directly recognize foreign or abnormal antigens that are bound to MHC molecules on the surface of cells through their T cell receptor (TCR) (Abbas et al., 2016; Bonilla and Oettgen, 2010). It takes days to weeks to mount a full adaptive immune response that will ultimately generate a variety of defensive molecules that neutralize the extracellular antigens, mark them for easier phagocytosis or eliminate infected cells in a very specific manner. Depending on the nature of the antigen, different types of lymphocytes will be more important in the response. The two major T cell subsets, $CD4^+$ or helper T lymphocytes and $CD8^+$ or cytotoxic T cells (CTLs), function as the main mediators of cellular adaptive immunity. $CD4^+$ T cells secrete cytokines (CKs) that modulate T and B lymphocytes, as well as macrophages and other cells of the innate immune system. On the other hand, $CD8^+$ T cells recognize and kill cancer cells as well as cells infected with intracellular pathogens such as viruses (Abbas et al., 2016).

1.2. Antigen presentation

For lymphocytes to be able to recognize foreign antigens through specific TCRs, antigen-presenting cells (APCs) must expose them at their surface bound to MHC (HLA in humans) class II (MHCII) or class I (MHCI) molecules. MHCII expression is restricted to professional APCs, mainly DCs, macrophages and B lymphocytes (Neefjes et al., 2011). Conversely, MHCI molecules are expressed by nearly every nucleated mammalian cell to expose a sample of their intracellular peptides at the cell surface, which enables the immune system to recognize presented self- and foreign-derived antigens (Chemali et al., 2011; Neefjes et al., 2011). MHC genes are generally divided into three categories: class I, II (which are related to MHCI and MHCII respectively) or III. Genes encoding for MHCI and MHCII molecules are polygenic (there are multiple genes) and the most polymorphic known (there are multiple variants of them) (Elmer and McAllister, 2012), leading to a great diversity of sets of MHC molecules. MHC class III genes code for other immune system proteins, including components of the complement system and proinflammatory CKs, as well as proteins not involved in immune function (Janeway et al., 2001).

The main professional APCs are DCs, which are constantly sampling the extracellular milieu and phagocytizing damaged or defective cells. Phagocytic vesicles, which might contain abnormal molecules, are targeted to the lysosomal pathway. There, protein degradation results in peptides of 10 to 30 residues that bind to MHCII molecules at the endoplasmic reticulum (ER) before they traffic to the cell surface (Neefjes et al., 2011). Antigens presented by MHCII can only be recognized by $CD4^+$ T cells as the co-receptor CD4 specifically binds MHCII molecules. In addition, MHC class I (MHCI) molecules expose fragments of 8 to 11 amino acids of virtually all intracellular proteins on the surface of, theoretically, all nucleated cells in the organism (Neefjes et al., 2011; Peaper and Cresswell, 2008). This also includes professional DCs and other professional APCs, which present peptides derived from the lysosomal pathway through MHCI in a process termed cross-presentation. We are interested in the study of NSCs, which are not professional APCs and thus not expected to express MHCII. Therefore, we will focus on MHCI.

For the generation of protein fragments that are loaded into MHCI complexes **(Figure 1)**, the nuclear and cytoplasmic proteasomes are constantly degrading intracellular proteins into peptides. While most cytoplasmic and nuclear peptides diffusing into the cytosol are degraded by aminopeptidases, some of them escape degradation and can be translocated as antigenic peptides from the cytosol into the ER by ABC transporters of the transporter associated with antigen processing (TAP) family, TAP1 and TAP2, and then loaded into MHCI complexes (Neefjes et al., 2011). These complexes are formed by two non-covalently linked polypeptide chains: a light and constant subunit called β2-microglobulin (β2M) and a variable heavy chain (HC) or alpha (α) subunit. HCs are transmembrane immunoglobulin-like subunits encoded by several polymorphic genes (in mice, H2-K, -D, -L, and 2-I-A and I-E allomorphs) (Cresswell et al., 2005). As the repertoire of peptides to present is virtually infinite, the existence of many HCs increases the probability of one being able to load a given antigen fragment (Chapman and Williams, 2010). The specific MHC genes and variants that an individual expresses comprise its MHC haplotype (Elmer and McAllister, 2012). MHCI assembly in the ER involves binding to a multicomponent complex, containing the TAP and the ER-resident chaperons, calnexin, calreticulin, tapasin, and Erp57 that assist the correct folding of MHCs until a peptide fragment with affinity for the peptide-binding groove displaces them (Chapman and Williams, 2010). Once this happens, antigen-MHCI complexes reach

the cell surface via the Trans-Golgi Network (TGN) in vesicles that fuse to the plasma membrane to present the peptide fragment extracellularly (Neefjes et al., 2011; Peaper and Cresswell, 2008).

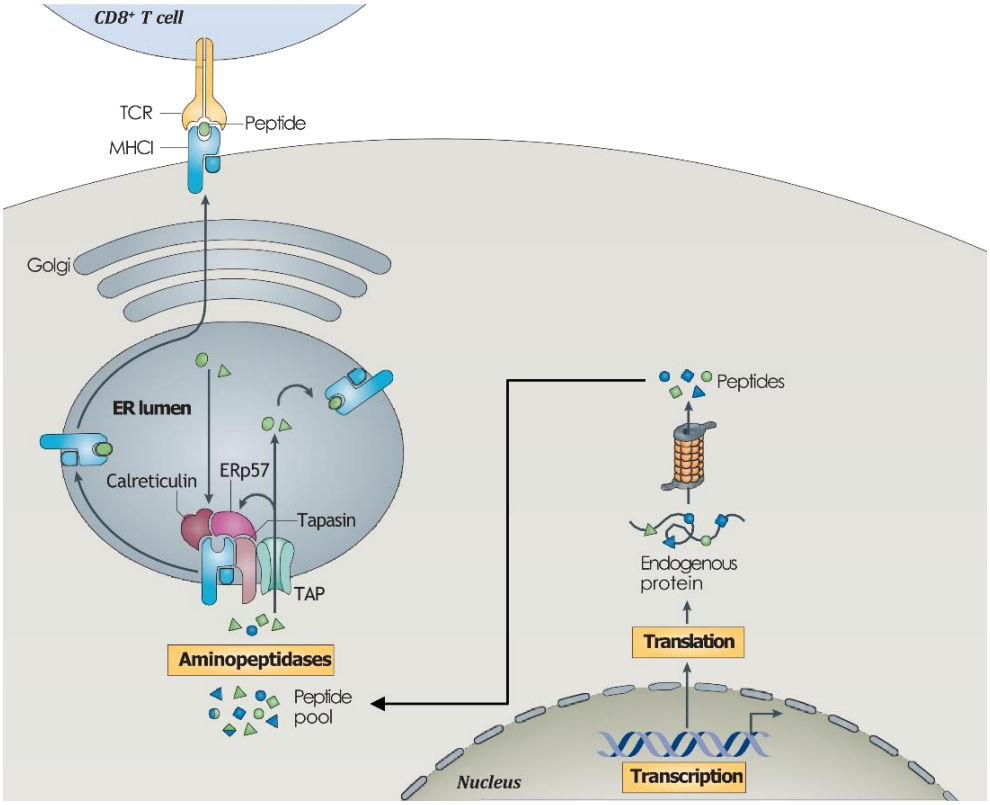

Figure 1. The basic MHCI antigen presentation pathway. Intracellular proteins are degraded by the proteasome into peptides. Peptides that are not degraded by cytoplasmic aminopeptidases are transported to the ER by TAP transporters. Once there, they displace the chaperones stabilizing pre-MHCI complexes (calreticulin, tapasin and ERp57) and get associated with the light chain β2M and a MHCI α subunit. When antigen-MHCI complexes are assembled, they reach the cell surface via the TGN. $CD8^+$ T cells contact antigen-loaded MHCI complexes and, if they detect abnormal or foreign proteins, they might perform effector functions (adapted from Neefjes et al., 2011).

Once assembled and loaded, MHCI complexes have been generally considered to rapidly egress from the ER upon dissociation from TAPs and to arrive at the cell surface through the secretory pathway by bulk flow, without requirements for

specific signals. However, some evidence indicates that positive sorting can take place, suggesting that MHCI ER-to-Golgi transport may depend on previously unrecognized export sequences or may involve association of MHCI molecules with cargo transport receptors (Pereira and DaSilva, 2016; Sohn et al., 2001). Interestingly, the cytosolic tail of the HC does not contain any described ER-Golgi trafficking peptide signal (Dancourt and Barlowe, 2010), which suggests that MHCI may bind to cargo receptors, the identity of which remains elusive. One such cargo has been proposed to be BAP31, a transmembrane protein that cycles between the ER and the Golgi, and interacts with both human and murine MHCI (Ladasky et al., 2006). However, knockdown of Bap31 does not lead to a decrease in MHCI levels at the cell surface, suggesting that additional and redundant mechanisms facilitate MHCI exit from the ER (Donaldson and Williams, 2009). Once MHCI complexes reach the plasma membrane, their loaded peptides can be identified by T lymphocytes as “self” or “non-self” antigens, leading to different responses (Neefjes et al., 2011; Peaper and Cresswell, 2008). The presence of “non-self” peptides, for instance belonging to proteins of infecting viruses or mutated genes, might trigger a specific attack by CTLs that recognize the neoantigen through their antigen-specific TCR.

The transcription of MHCI genes is controlled by several cis-acting regulatory elements at their proximal promoters. Specifically, a region termed enhancer A, which contains NF-kB-binding sites, an interferon (IFN)-stimulated response element (ISRE) and an SXY module are important for their constitutive expression and induction. By binding to these sites, NF-kB and IRF transcription factors can induce MHCI expression. At the same time, NOD-, LRR- and CARD-containing 5 (NLRC5) is a specific transactivator of MHCI genes required for their constitutive expression, and it is considered to be their master regulator. Moreover, NLRC5 can also be induced by IFN gamma (IFNγ), and its expression correlates with the capacity to induce MHCI in response to the proper stimuli, which basically means, again, IFNγ (Kobayashi and Van Den Elsen, 2012; Ludigs et al., 2015). Levels of MHCI are also determined by general processes affecting protein degradation. On one hand, proteasomes are key to generate the peptides that are loaded into MHCI complexes, and many reports show that the inhibition or disruption of their activity can down-regulate the MHCI-mediated presentation of most peptides (Benham et al., 1998; Fehling et al., 1994; Finn et al., 2010; Rock et al., 1994; Schwarz et al., 2000). On the other hand, autophagy is the process that enables cells to digest their

cytoplasmic contents in lysosomes. It is different from other cytoplasmic digestive processes, including proteasomal degradation, as it can eliminate large targets such as toxic protein aggregates, defunct or disused organelles and invading microorganisms. Autophagy has functions in immunity that include the direct elimination of microorganisms, the control of inflammation, the secretion of immune mediators and the control of adaptive immunity through the regulation of antigen presentation (Deretic et al., 2013). It affects MHCI by competing with the proteasome for the degradation of newly synthesized cytoplasmic proteins (Wenger et al., 2012). More interestingly, enhanced autophagy or lysosome function in cancer cells can promote immune evasion by degrading MHCI molecules (Yamamoto et al., 2020).

1.3. Generation and selection of T cells

Common lymphoid progenitors in the bone marrow are responsible for B and T lymphopoiesis. The fate of these precursors depends on the cell surface receptors that get activated by extracellular signals, as these activate different transcription factors and chromatin rearrangements. Common lymphoid progenitors give rise to both B-cell and T-cell lineages, but the development of B cells and T cells occurs separately, with B cells developing in the bone marrow and T cells in the thymus (Nemazee, 2006). Accordingly, in the case of T cells, lymphocyte progenitors, which are called thymocytes, will circulate to the thymus to complete their maturation (Abbas et al., 2016; Tanigaki and Honjo, 2007). At this step, Notch receptors will be activated by extracellular ligands (Radtke et al., 2004). Together with GATA3 (Hozumi et al., 2008), NOTCH1 activation will trigger epigenetic rearrangements and thus enable the expression of genes involved in T cell development. Among these, the ones encoding the proteins Rag1 and Rag2, as well as components of the pre-T cell receptor (Abbas et al., 2016; Tanigaki and Honjo, 2007).

The adaptive immune system can recognize almost any pathogen or foreign protein that the host can encounter throughout life. Therefore, B and T Lymphocytes together can respond to an astounding number of foreign antigens. However, as every T cell responds only to the MHC-bound antigens that match the structure of its specific TCR, which is unique in every clone of lymphocytes, an astonishing number of T cell clones must be generated (Abbas et al., 2016; Buchholz et al.,

2016). Additionally, these T cells must be selected so that they do not react against "self" antigens that are normally present in the host. This is exactly what the process of T cell development has evolved to achieve. As we focus on adaptive immunity, we will only refer to αβ T cells (T cells or T lymphocytes from now on). However, there is another, yet numerically smaller, subset of T lymphocytes called γδ T cells. These cells express TCRs with limited diversity, are functionally related to the innate immune system and will not be discussed in this thesis (Abbas et al., 2016).

Every clone of T cells expresses a different TCR, made up of different β and α polypeptide chains. T cell receptor *loci Tcrb* and *Tcra* undergo V(D)J recombination events **(Figure 2)** to generate billions of different β and α chains that together form TCRs. For V(D)J recombination to occur, the presence of the lymphoid-specific recombination proteins Rag1 and Rag2 and the ubiquitously expressed DNA repair factors of the non-homologous end joining pathway are required (Sleckman, 2005). In a nutshell, each germline TCR *locus* is arranged with a 5' cluster of many different V gene segments, then D segments (only in the β *loci*), and then a cluster of J segments all separated by non-coding sequences. V(D)J recombination is the process by which these TCR *loci* are intragenically rearranged so they can generate novel β and α chains. To do so, one V gene segment, one D segment (only in the β chain), and one J segment are randomly selected and brought next to each other (Bonilla and Oettgen, 2010; Sleckman, 2005). The process is mediated by Rag proteins that generate double-strand breaks for the different segments to be joined together (Arya and Bassing, 2017; Sleckman, 2005). After cleaving the DNA sequence, broken ends are repaired by the non-homologous end joining machinery that introduces additional diversity at the junctions. As a result, unique TCR sequences are created in every developing T cell clone (Abbas et al., 2016; Nemazee, 2006).

The most immature thymocytes, known as pro-T cells, start recombining their β chain *loci* as it has been explained. Only around one third of gene rearrangements produce in-frame products and can therefore express functional proteins. When a functional β chain starts to be expressed, it assembles in the cell surface together with other proteins called pre-Tα, CD3 and ζ, to form the pre-TCR complex, and cells start to be called pre-T cells (Nemazee, 2006). This pre-TCR complex inhibits the β chain recombination in the other inherited *locus*, so only one β chain is generated,

and that triggers the recombination of the α chain *loci*. Successful pre-TCR complexes provide pro-survival signals that keep thymocytes alive, possibly in a ligand-independent manner. Thus, when no functional β chains are produced, the absence of these signals makes thymocytes die by apoptosis (Abbas et al., 2016; Nemazee, 2006). In contrast to the β chain, there is no allelic exclusion in the α chain *locus*, and productive rearrangements can occur in both chromosomes. If this happens, and it does in around 30% of cases, the T cell clone will express two different α chains, and therefore two different TCRs. When the recombination of the α chain *loci* is finished and α chains are expressed, they assemble with β chains, CD3 and ζ to constitute the mature αβ TCR (or TCR). Because many of these TCRs will recognize MHCs bound to self-antigens, and many others will not be able to bind MHC complexes at all, the next steps in the process of T cell maturation will focus on eliminating the useless and the self-reactive ones (Abbas et al., 2016).

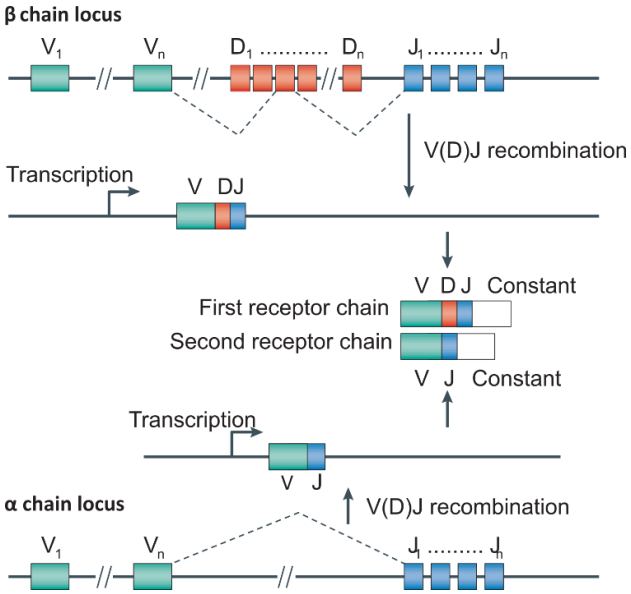

Figure 2. General scheme of V(D)J recombination for the assembly of TCR genes. Antigen receptors consist of two protein chains that are encoded by independent *loci*. One *locus* (*Tcrb*) is generated by the assembly of individual germline variable (V), diversity (D) and joining (J) minigene elements from among multiple minigene elements. The other *locus* (*Tcra*) lacks D elements and is assembled by direct V-to-J joining. V, D and J elements are recombined through the activity of recombination-activating gene 1 (RAG1)–RAG2 protein complexes and the non-homologous end-joining machinery to generate VDJ or VJ joins (adapted from Nemazee, 2006).

In order to select the proper clones of developing T cells, the thymus is packed with APCs that express both MHCI and MHCII complexes loaded with an organism-wide representative sample of peptides (Abbas et al., 2016). These APCs include DCs, macrophages and thymic epithelial cells. Medullary thymic epithelial cells express a very wide repertoire of proteins that are otherwise specific to other tissues thanks to the unconventional transcription factor called AIRE that forces their expression. Besides, recirculating DCs bring antigens collected from many different tissues to the thymus (Takaba and Takayanagi, 2017; Wang et al., 2020). Thus, thymocytes will interact within the thymus with APCs expressing MHCI and MHCII. In principle, at this stage, they will mostly encounter MHCs loaded with self-peptides, and a strong activation of the TCR, which means that they are recognizing these peptides that need to be tolerated, will lead to the death of the lymphocyte. This will contribute to central tolerance (Stritesky et al., 2012; Takaba and Takayanagi, 2017). On the other hand, useful TCRs have to be able to recognize MHCs, as foreign antigens will always be presented to them through MHCI or MHCII. Therefore, TCRs that do not recognize MHC complexes at all will not produce pro-survival signals and thymocytes will undergo apoptosis. In the end, only thymocytes that are able to bind MHCs in the thymus, but that do it rather weakly as they recognize MHC molecules but not the antigens that they are presenting at this point, survive (Carpenter and Bosselut, 2010; Kurd and Robey, 2016; Takaba and Takayanagi, 2017). In addition, when the TCR starts to be expressed in the cell surface, thymocytes express both CD4 and CD8 co-receptors, and are called double-positive thymocytes. CD4 and CD8 recognize MHCII and MHCI, respectively, and allow the TCR to bind antigen-MHC complexes (Abbas et al., 2016). The recognition of MHCI will lead to the suppression of CD4, and binding to MHCII will stop CD8 expression, finally committing double-positive thymocytes into $CD8^+$ or $CD4^+$ T cells **(Figure 3)**. Mature naïve T cells will now exit the thymus and start trafficking through secondary lymphoid organs (SLOs) looking for APCs presenting their specific antigens (Abbas et al., 2016; Carpenter and Bosselut, 2010).

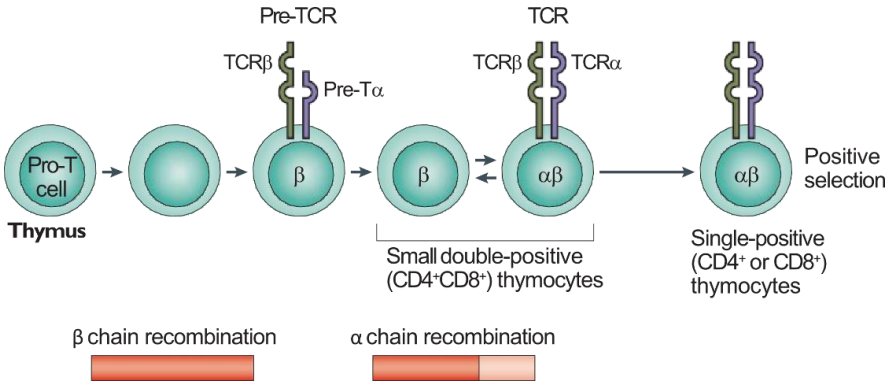

Figure 3. T cell developmental pathway. The development of T cells occurs in the thymus. In progenitor (pro)-T cells, the first antigen-receptor chain *locus* undergoes V(D)J recombination, generating the TCR β chain. This β chain then associates with the surrogate α chain precursor (Pre-Tα), yielding a pre-TCR complex. Next, lymphocytes stop dividing and recombine the genes that encode the α receptor chain, generating the TCR. Continued rearrangement at the *Tcra locus* often occurs because of autoreactivity or lack of positive selection, creating either a non-functional rearrangement (denoted by the reverse arrow) or an edited receptor with a new TCR. Positive selection ultimately stops gene rearrangements and promotes the loss of either CD4 or CD8 (adapted from Nemazee, 2006).

1.4. Recirculation of T cells and antigen recognition

T cells have the ability to recognize a virtually infinite repertoire of foreign antigens. However, there are hundreds of millions of different specificities of T cells, and therefore very few naïve T cells of each one (Abbas et al., 2016). In addition, a pathogen or a defective cell can appear anywhere in the body and in tiny quantities. Thus, the chance of them being recognized by a specific T cell must be maximized, and this is where SLOs are key.

Naïve T cells are T cells that have never encountered their specific antigens. They are in a quiescent state and are constantly recirculating from the blood to SLOs, which basically are lymph nodes, the spleen and mucosal lymphoid tissues. T cells usually go through several lymph nodes, get back to the blood via lymphatic vessels and access lymph nodes again through their high endothelial venules. This process is guided by the expression of integrins and chemokine receptors, among others,

and naïve T cells spend most of their time in SLOs (Abbas et al., 2016; Bonilla and Oettgen, 2010). At the same time, DCs, which are present in peripheral tissues, are constantly sampling and phagocytizing material from all over the body and traveling to SLOs through lymphatic vessels. There, they present what they have collected via both MHCI (cross-presentation) and MHCII. Therefore, both T cells and antigens from all tissues, presented by DCs, are concentrated in SLOs (Eisenbarth, 2019; Guermonprez et al., 2002). The mere recognition of their specific antigen-MHC complex is not enough to activate a naïve T cell. Subsequent signals, mainly the binding of CD28 on the T cell to CD80 or CD86 on the APC (or signal 2) as well as the proper CKs (signal 3) are needed (Chen and Flies, 2013; Curtsinger and Mescher, 2010; Guerder and Flavell, 1995). CD80 and CD86 are called costimulatory molecules and are highly expressed in DCs. These professional APCs also induce the expression of signal 3 (and enhance signal 2) upon the binding of PAMPs and DAMPs to their PRRs. These are some of the reasons why DCs are the APCs that most efficiently activate naïve T cells, although other APCs can also induce the expression of costimulatory ligands and CKs in response to inflammation (Abbas et al., 2016). Additionally, DCs have higher pH and lower protease content within endosomes compared to other APCs, which favors epitope conservation and antigen presentation (Delamarre et al., 2005). In some cases, mainly when intense inflammation is produced or when the DCs express the antigen themselves, DCs alone can activate naïve $CD8^+$ T cells. However, in most other cases such as the recognition of tumor cells that usually trigger weak immune responses, $CD4^+$ T cells are also needed. In this case, the activation of $CD4^+$ T cells by DCs will make them produce CKs, such as IFNγ, that stimulate $CD8^+$ T cell differentiation and effector function (Abbas et al., 2016; Kaech et al., 2002). In addition, activated $CD4^+$ T cells express CD40 ligand (CD40L). By binding to CD40 on the surface of DCs, $CD4^+$ T cells increase the expression of costimulatory molecules in DCs making them more efficient at activating $CD8^+$ T cells (Schoenberger et al., 1998).

When naïve T cells are activated in SLOs, they start secreting CKs and expressing new CK receptors, proliferating and differentiating into effector or memory cells. Some of these CKs, mainly interleukin (IL) 2 (IL-2), act as a paracrine and autocrine growth factor for the T cells when binding its receptor CD25 (Buchholz et al., 2016; Zhang and Bevan, 2011). Proliferation of the recently activated T cells is necessary to amplify the T cell clone so that enough cells with the proper specificity differentiate into effector cells (Buchholz et al., 2016). Only when proliferation and

differentiation are completed, $CD8^+$ T cells leave the lymphoid organs, enter the blood flow and migrate to peripheral tissues where an immune response is needed **(Figure 4)**. To do so, activated T cells down-regulate adhesion molecules that retain them in SLOs such as CD62L and CCR7, and up-regulate others that favor their migration to peripheral sites of tissue injury and inflammation. These are, among others, LFA-1, VLA-4, E- and P-selectins, and CD44. Upon inflammation in a given tissue, the endothelium adapts and changes its expression of adhesion molecules, guiding T cells to the sites where they might be needed (Abbas et al., 2016; Ley et al., 2007).

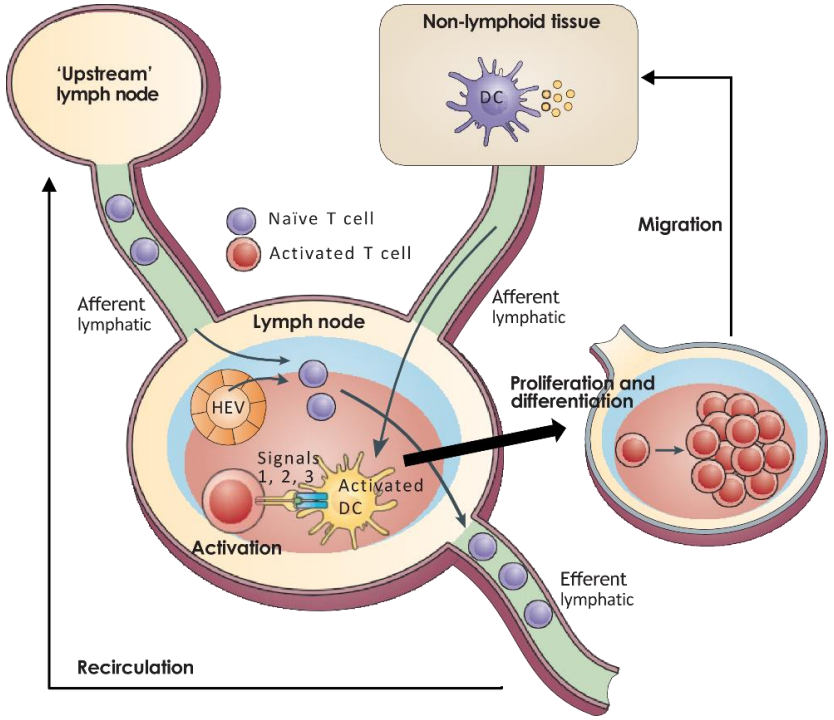

Figure 4. T cell recirculation through lymph nodes, activation by DCs and migration to sites of infection or tissue injury. T cells enter lymph nodes from blood through high endothelial venules (HEVs), from upstream lymph nodes or from non-lymphoid tissues via afferent lymphatics. DCs also get to lymph nodes through the lymphatic system and present antigens to T cells there. If naïve T cells do not get activated, they exit lymph nodes via efferent lymphatics, eventually return to the blood via lymph drainage in the thoracic duct and, at some point, start trafficking through lymph nodes again. If they become activated by DCs, T lymphocytes proliferate and differentiate before leaving the lymph nodes and then travel to peripheral tissues where their effector functions might be required (adapted from Masopust and Schenkel, 2013).

1.5. Memory and effector function of CD8$^+$ T cells

Differentiation of naïve CD8$^+$ T cells generates effector T cells, which might fight infections or destroy tumor cells. Besides, naïve T cells also differentiate into memory cells (Kaech et al., 2002; Sallusto et al., 2004; Tscharke et al., 2015). These might stay in SLOs and provide an expanded pool of cells to start future immune responses, in case the same antigen is encountered again. In that case, they are called central memory T cells, express CCR7 and L-selectin, and are retained in the lymph nodes. Conversely, memory cells might not express CCR7 or L-selectin and home to peripheral sites, mainly mucosal tissues. These are called effector memory T cells and provide an immediate, yet limited, source of effector T cells to face future contacts with the same antigen. Interestingly, memory and effector T cells do not need costimulation to get activated (Abbas et al., 2016; Mahnke et al., 2013; Mueller et al., 2013). Therefore, any MHCI-expressing cell, not necessarily professional APCs, can activate effector and memory CD8$^+$ T cells in peripheral tissues.

Once effector CTLs recognize cells exposing their target antigen-MHCI complexes in peripheral sites, they start secreting IFNγ (Kaech et al., 2002), which promotes antigen presentation in the neighboring cells by up-regulating the expression of MHC-related genes, and potentiates their own killing capacity (Abbas et al., 2016; Zhang and Bevan, 2011). CTLs bind target cells and form a close region of contact known as immune synapse (Bustos-Morán et al., 2016). Once conjugated to the target cell, the CTLs cytotoxic secretory granules containing deadly proteins like perforin and granzymes are released at the immunological synapse (Martínez-Lostao et al., 2015; Trapani and Smyth, 2002; Voskoboinik et al., 2006, 2015). As these proteins do not generally diffuse outside the synapse, this process of killing is highly cell-specific (Abbas et al., 2016). Granzymes, which are serine proteases, might have extracellular functions that can occur in the absence of perforin, but their capacity to induce target-cell death by cleaving intracellular substrates is entirely dependent on perforin. Indeed, perforin monomers assemble in pre-pore formations and insert in the membrane of the target cell. This allows granzymes to diffuse into the target cell, digest intracellular proteins and induce cell death. Granzyme B induces caspase-dependent apoptosis and is the most powerful pro-apoptotic granzyme, while granzyme A does not require caspases to induce target-cell death. It remains unclear whether other granzymes have cytotoxic activity

(Voskoboinik et al., 2006, 2015). CTLs also use a granule-independent mechanism of killing that is mediated by interactions of membrane molecules on the CTLs and their target cells: on activation, CTLs express a membrane protein called Fas ligand (FasL) that binds to the death receptor Fas, which is expressed on many cell types. This interaction also results in activation of caspases and apoptosis of Fas-expressing targets (Abbas et al., 2016).

1.6. Inhibition of CTLs by immune checkpoints

Activation of a naïve $CD8^+$ T cell requires the engagement of its TCR (signal 1), costimulation (signal 2) and the proper CKs (signal 3), and it is usually carried out by professional APCs. Conversely, once previously activated, a T lymphocyte can attack a cell by only recognizing its specific antigen (signal 1 alone) (Abbas et al., 2016). However, other signals can modulate the outcome of this APC-T cell interaction. Specifically, the balance between stimulatory signals (MHCs and costimulators) and immune checkpoints or co-inhibitory receptors, can be determinant in avoiding CTL-mediated killing. Many immune checkpoints have been described, including the immunoreceptors Programmed Cell Death Protein 1 (PD-1), Cytotoxic T-lymphocyte antigen 4 (CTLA-4), LAG3, TIM3, TIGIT and BTLA in T cells, and their corresponding ligands in APCs (Chen and Flies, 2013) **(Table 1)**. The activation of these receptors can lead to cell cycle arrest, inhibition of effector functions and apoptosis of the lymphocytes. The most studied immune checkpoints are CTLA-4 and PD-1. CTLA-4 is a member of the CD28 family and acts as a competitive inhibitor of CD28. As explained before, the activation of CD28 is key for naïve T cell activation in SLOs (Abbas et al., 2016). CD28 and CTLA-4 are both expressed by T cells and bind the same ligands on the APC, which are the costimulatory proteins CD80 and CD86. Upon engagement of these ligands, CD28 promotes T cell activation, while CTLA-4 does not. Therefore, the role of CTLA-4 is to compete with CD28 for its ligands, reduce its signaling, and thus inhibit T cell activation. This mechanism is very important in SLOs (Van Coillie et al., 2020; Greenwald et al., 2005). PD-1 is another inhibitory receptor of the CD28 family. It is mainly expressed in activated T cells, and APCs can express its ligands Programmed Cell Death Ligand 1 (PD-L1) or 2 (PD-L2). Activated PD-1 stops TCR and CD28 signaling, and therefore inhibits activated T cells that might be in peripheral tissues already (Sun et al., 2018). These mechanisms evolved as additional elements

ensuring immune tolerance to self-antigens. However, cancer cells, and possibly other cell types, can adopt them to evade $CD8^+$ T cell-mediated killing. This is the reason why antibodies targeting PD-1, PD-L1 or CTLA-4 have revolutionized the treatment of different types of tumors (Bagchi et al., 2021). Other immune checkpoints and their ligands are shown in Table 1 (Chen and Flies, 2013; He and Xu, 2020).

LIGANDS IN APCs		**RECEPTORS IN T CELLS**
GENE	PROTEIN	
Cd86	CD86	CTLA-4
Cd80	CD80	
Pdcd1lg2	PD-L2	PD-1
Cd274	PD-L1	
Tnfrsf14	HVEM	BTLA
Vsir	VISTA	Unknown
Havcr1	TIM1	
Timd4	TIM4	
Cd48	CD48	2B4
Pvr	CD155	TIGIT
Nectin2	CD112	
Nectin3	CD113	
Ceacam1	CEACAM1	TIM3
Hmgb1	HMGB1	
Lgals9	GALECTIN 9	
Ps	PS	
Clec4g	LSECtin	LAG3
Lgals3	GALECTIN 3	
Fgl1	FGL1	

Table 1. Immune checkpoints: ligands that can be expressed in APCs and their receptors (proteins) on the surface of T cells (adapted from Chen and Flies, 2013).

1.7. Additional mechanisms modulating CTL-mediated killing

Apart from the TCR and immune checkpoints, T cell responses can be modulated at other levels by APCs: by determining CTL location with chemokines; by expressing serine protease inhibitors (serpins) that can inactivate granzymes; or by affecting the release of CKs or the response to them. In this framework, a great variety of chemokines are known to fine tune T cell trafficking and effector functions. Chemokines are chemotactic CKs that control the traffic and position of immune cells and have key roles controlling all aspects of immunity (Abbas et al., 2016; Viola et al., 2006). Most chemokines have four characteristic cysteines, and depending on the motif displayed by the first two of them, they have been classified into CXC or alpha, CC or beta, C or gamma, and CX3C or delta chemokine classes. Chemokine receptors are G-protein coupled seven-domain transmembrane receptors. Based on the chemokine class that they bind, these receptors have been named CXCR1, 2, 3, 4, and 5 (bind CXC chemokines); CCR1 through CCR9 (bind CC chemokines); XCR1 (binds the C chemokine); and CX3CR1 (binds the CX3C chemokine) (Rossi and Zlotnik, 2000). The focus of this project is on the interaction between $CD8^+$ T cells and NSCs in the SEZ. Therefore, we will focus on the main chemokines regulating CTL effector functions when T lymphocytes are already at peripheral sites. In this context, the key chemokine receptor in $CD8^+$ T cells is CXCR3, which determines the location of these cells (Griffith et al., 2014). CXCR3 is activated by CXCL9 and CXCL10 and promotes T cell recruitment within the tissue and granzyme B expression, among others. In fact, CXCL10 is considered a critical factor regulating CTL effector function, and it has been shown to be presented on the cell surface of some APCs and promote antigen-independent T cell recruitment (Griffith et al., 2014). Another CXC chemokine, CXCL11, can also bind to CXCR3, but with opposite effects (Karin, 2018).

In addition, APCs can develop mechanisms to avoid killing by CTLs, even if they are recognized and attacked. Specifically, the expression of SERPINB9, and the consequent increased resistance to CTLs, have been described in cancer cells (Jiang et al., 2018). The serpin superfamily is a group of structurally related proteins that function as intracellular or extracellular protease inhibitors and control a wide range of physiological processes such as complement activation, blood coagulation and apoptosis. Many different serpins have been found in humans, where three of them have been reported as granzyme inhibitors so far (SERPINA1, SERPINB9 and

SERPINC1). Additional granzyme inhibitors have been identified in mice (Serpinb9, Serpinb9b and Serpina3n) and other species. The best-studied example of a granzyme-regulating serpin is SERPINB9 (or PI-9), which is a potent inhibitor of granzyme B. SERPINB9 has a broad tissue distribution, being present at high and relatively stable levels in CTLs to protect them from granzyme leaking from granules, as well as in professional APCs, many endothelial and mesothelial cells and at sites of immune privilege such as testis and placenta (Kaiserman and Bird, 2010).

Immune responses are also orchestrated by a plethora of different CKs, which are relatively small proteins that usually mediate communication between immune cells. When it comes to adaptive immune responses against virus or mutated cells, IFNγ is the key CK (Abbas et al., 2016). Originally named for their ability to interfere with viral replication, IFNs form a diverse family of CKs. Each class of IFN (type I, II and III) signals through a distinct heterodimeric receptor and regulates gene expression through the Janus kinase (JAK)-signal transducer and activator of transcription (STAT) signaling pathway. The type II IFN class has only one member, IFNγ, which is crucial for immunity against intracellular pathogens and for tumor control. IFNγ is a homodimer formed by the non-covalent association of two 17 kDa polypeptide subunits. During synthesis, after multiple N-glycosylations, both subunits bind in an antiparallel manner, constituting a mature 50 kDa molecule. Its expression is induced by mitogens and CKs, such as IL-12, IL-15, IL-18, and type I IFN. The pleiotropic functions of this CK are mediated by cell-specific expression of hundreds of IFNγ-regulated genes that include inflammatory signaling molecules, apoptosis and cell cycle regulators, as well as transcriptional activators (Castro et al., 2018). This CK is mainly produced by natural killer and natural killer T cells as part of the innate immune response, and by Th1 $CD4^+$ and $CD8^+$ effector T cells in antigen-specific immunity (Castro et al., 2018; Schoenborn and Wilson, 2007). IFNγ receptors are transmembrane heterodimers of IFNGR1 and IFNGR2. While IFNGR1 is constitutively expressed in most cell types, the levels of IFNGR2 are finely tuned and determine the sensitivity to IFNγ. Once activated, this receptor promotes the activation of JAK1 and JAK2 proteins, which in turn phosphorylate STAT transcription factors, mainly STAT1. Phosphorylated STAT proteins form dimers and translocate to the nucleus, where they modulate the expression of IFN-stimulated genes. STAT1 homodimers act on γ-activated sequences to induce the expression of target genes such as *Irf1*, that will regulate the expression of additional genes,

including those encoding MHC proteins, by acting on ISREs **(Figure 5)** (Castro et al., 2018; Negishi et al., 2018; Schoggins, 2019). Although IFNγ is essential for the activation, differentiation and effector functions of $CD8^+$ T cells, it also up-regulates the antigen presentation machinery in APCs and promotes the recruitment of T cells by inducing CXCL9 and CXCL10 expression. However, IFNγ can also perform immunosuppressive functions, for example limiting tissue damage in chronic inflammatory conditions. For instance, IFNγ can stimulate the function of regulatory T cells (Tregs), which are immunosuppressive $CD4^+$ T cells, and up-regulate the expression of immune checkpoint ligands such as PD-L1. Therefore, IFNγ can stimulate or inhibit CTL-mediated responses depending on the microenvironmental context and the magnitude of its signal (Castro et al., 2018).

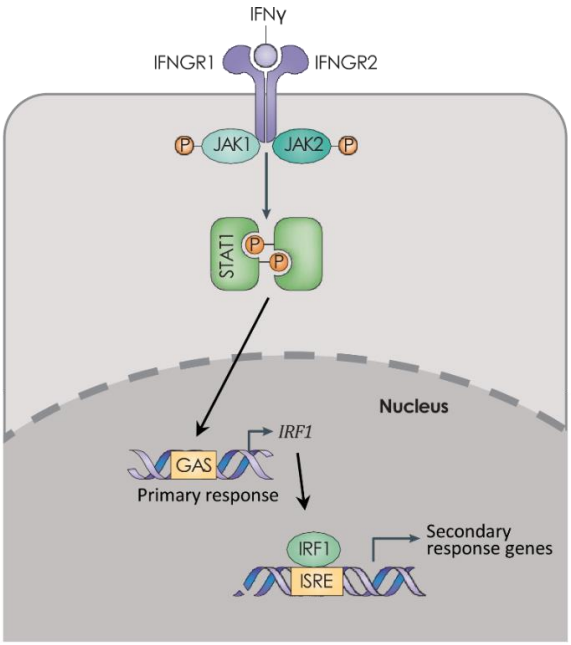

Figure 5. Basic overview of the IFNγ pathway. IFNγ signals through a heterodimeric transmembrane receptor at the cell surface. Upon binding of its ligand, IFNGR activates JAK kinases, which phosphorylate STAT1 transcription factors that in turn form homodimers. These move to the nucleus where they act on γ-activated sequences (GAS) to induce the expression of target genes such as IRF1. Some of these, in turn, promote the expression of secondary response genes (adapted from Kobayashi and Van Den Elsen, 2012).

2. T-cell mediated immunity in the CNS: a changing field

2.1. The immune uniqueness of the CNS

The central nervous system (CNS) is made up of thousands of millions of neurons accompanied by an even larger number of assisting glial cells. Neurons are intricately interconnected postmitotic cells and the vast majority of them are generated during fetal development and never replaced. Protection of these perennial neurons and circuits against pathogens and physical trauma essentially requires the activity of the immune system. Surprisingly, it was assumed for a long time that the CNS was not under the surveillance of adaptive immunity. On the contrary, the brain and spinal cord were thought to be immunoprivileged structures where immune cells that battle infections were kept outside by the blood-brain barrier (BBB). However, experimental evidence gathered in the last decade has indicated that the brain and the immune system are more intertwined than previously thought (Kwon, 2022).

For protection, the CNS is covered by a rigid bone layer. Thus, inflammatory reactions can be fatal since they would lead to overpressure, cell death and disruption of the brain milieu (Ransohoff and Engelhardt, 2012). However, both the immune system and the CNS are together in charge of detecting and responding to stress, function in a continuous crosstalk, and regulate each other through many different mechanisms (Steinman, 2004). An illustrative example of the evolutionary significance of this close relationship can be seen upon infection: generally, an infected host will adopt an antisocial behavior aimed to limit the spreading of the pathogen (Kipnis, 2016). In spite of the essential relationship between immunity and the CNS, whether the latter is immune-privileged or not has been a matter of debate for a long time. The reason is that tissue grafts, bacterial or viral antigens introduced for the first time into the brain parenchyma did not seem to be rejected as it happens in the periphery (Engelhardt et al., 2017). This immune uniqueness was attributed to the lack of immune cells with the exception of microglia, the apparent absence of lymphatic drainage, and the low expression of MHC molecules (Engelhardt et al., 2017; Louveau et al., 2015b, 2015a). Indeed, the transfer of cells and molecules into the adult CNS parenchyma is strictly regulated by the BBB and the blood-cerebrospinal fluid (CSF) barrier. Populations of circulating adaptive and innate immune cells, including monocytes, T and B lymphocytes, and neutrophils,

were thought to only enter the CNS in a consistent manner upon disruption of the barriers as it happens during trauma or disease, for example in multiple sclerosis, cerebral ischemia, or neurodegeneration (Prinz and Priller, 2014; Salter and Stevens, 2017). Immune protection of the CNS under homeostatic conditions has, therefore, long been considered to be restricted to microglia, the innate immune cells of the CNS parenchyma.

2.2. Microglia: the parenchymal immune cells

Microglia, the long-lived resident macrophages of the brain and spinal cord parenchyma, colonize the CNS very early in development and never exit it. Although they permanently monitor and regulate the neural parenchyma (Ransohoff and Cardona, 2010; Shemer et al., 2015), they are not capable of migrating to the vascular system to act as APCs, activate naïve lymphocytes and initiate adaptive immune responses. Therefore, their role in the induction of an adaptive immune response would be constrained to local reactivation of infiltrating lymphocytes rather than initial antigen processing (Papadopoulos et al., 2020). Microglial cells represent around 5-10% of all brain cells and are ubiquitously distributed throughout the CNS (Lawson et al., 1990; Pelvig et al., 2008). They are endowed with highly ramified motile processes which constantly survey their surroundings (Nimmerjahn et al., 2005) and are key players in defense processes and responses to brain damage. Fate mapping studies have revealed that their embryonic origin differs from that of other myeloid cells. They derive from uncommitted c-Kit^{+} SCs of the yolk sac, which is the first site of hematopoiesis in the embryo. These primitive SCs develop into CSF1R^{+} c-Kit^{+} CD45^{low} CX3CR1^{+} erythro-myeloid progenitor cells at embryonic day (E) 8.5 and start colonizing the CNS at E9.5 (Ginhoux et al., 2010; Gomez Perdiguero et al., 2013; Kierdorf et al., 2013; Schulz et al., 2012). Since microglial cells become separated from circulation very early in fetal life they develop isolated from the hematopoietic system. Differentiation of microglia is dependent on macrophage and B cell-specific transcription factor PU.1 and on the IRF8 transcription factor of the IFN regulatory factor family (Kierdorf et al., 2013). It requires signaling through the receptor for colony-stimulating factor 1 (CSF1) and IL-34, CSF1R, which also regulates proliferation, differentiation, and survival of osteoclasts and monocytes/macrophages (Li et al., 2006; Patel and Player, 2009). Immediately after birth, microglial cells extensively proliferate and

expand their numbers to reach a maximum at two weeks of age that becomes reduced by the sixth week of life and is maintained throughout life (Shigemoto-Mogami et al., 2014). In the adult CNS, infiltration of circulating myeloid cells is highly restricted under physiological conditions and, therefore, the microglial population is maintained by self-renewal of resident cells with no contribution from peripheral bone marrow-derived cells (Ginhoux et al., 2010; Mildner et al., 2007). However, under inflammatory conditions, monocytes can transiently enter the brain and differentiate into macrophages with a phenotype that is very close to microglia (Ajami et al., 2007, 2011; Bennett et al., 2018; Hashimoto et al., 2013). Although as a part of the innate immune system they affect and are affected by adaptive immunity, the focus here will be on the latter.

2.3. A unique anatomical setting

The steady state CNS parenchyma is virtually devoid of immune cells apart from microglia, and does not harbor DCs, which partly accounts for its immune uniqueness (Galea et al., 2007). However, different evidence supports an active immune surveillance within the CNS. For instance, if external tissue is grafted in the brain parenchyma after being placed at a peripheral site, it provokes a normal immune response. Also, several opportunistic pathogens infecting the CNS, such as *Cryptococcus*, *Toxoplasma gondii*, cytomegalovirus, herpes simplex virus, John Cunningham virus, or West Nile and measles virus are reactivated when the adaptive immune system is compromised, for example in patients with human immunodeficiency virus infections (Louveau et al., 2015b; Papadopoulos et al., 2020). Additionally, meningeal lymphatics have a central role in the immune response triggered by GBM formation (Hu et al., 2020; Song et al., 2020b).

The brain is separated from the periphery by a specialized system of barriers that determines its unique interactions with the immune system **(Figure 6)**. Starting from the cranium, three meningeal layers surround the brain: the dura mater, the arachnoid mater and the pia mater (Engelhardt et al., 2017). The dura mater is a thick fibrous structure with an inner and outer layer, which contain large venous sinuses between them. Its outer layer is attached to the skull, and extends vascular connections into the bone. Blood vessels within the dura are fenestrated and do not have tight junctions. The other two layers constitute the leptomeninges. The

arachnoid mater is an avascular membrane contiguous to the dura mater and is composed of two layers of squamous epithelial cells with long cytoplasmic processes and connected by tight junctions. Beneath the arachnoid mater there is a CSF-filled space called subarachnoid space (SAS). There, fibroblast-like cells and collagenous trabeculae connect the inner arachnoid membrane to the pia mater, which is the third meningeal layer. The pia mater is composed of epithelial cells producing a basement membrane and fibroblast-like cells, but does not have tight junctions. Underneath the pia mater, the surface of the CNS parenchyma consists of a basement membrane and astrocytic endfeet that form the glia limitans. Arterial blood enters the cranial cavity through the internal carotid arteries and the vertebral arteries. Second-order branches traverse the SAS and give rise to smaller arterioles that enter the brain parenchyma. The glia limitans and the pia mater follow penetrating arteries until points of branching as well as postcapillary venules and veins that exit the parenchyma. In these cases, the basal membrane of the endothelium and the basal membrane of the pia are not in direct contact, and penetrating (and exiting) vessels are surrounded by perivascular spaces, filled with CSF and brain interstitial fluid (ISF). Perivascular spaces vary in size and are much bigger in postcapillary venules than in arterioles. The pia mater separates the SAS from the perivascular spaces and the brain parenchyma. This meningeal layer contains fenestrations that allow the free movement of CSF/ISF between perivascular spaces and the SAS (Mastorakos and McGavern, 2019) and, therefore, it does not constitute an absolute barrier separating the CSF and the parenchyma (Papadopoulos et al., 2020).

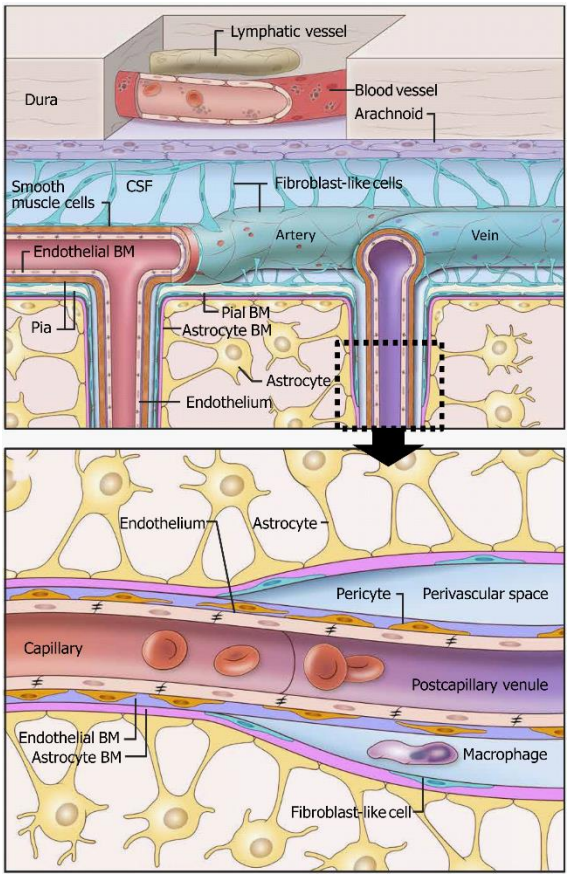

Figure 6. Anatomy of the meninges and perivascular spaces. The dura mater contains lymphatics and fenestrated blood vessels without tight junctions. The arachnoid mater is an epithelial barrier between the peripheral vasculature of the dura mater and the CSF that harbors tight junctions and efflux pumps. Leptomeningeal blood vessels lack astrocytic ensheathment, but their endothelial cells are connected by tight junctions. However, small stomata in the connective tissue (fibroblastic reticular cells) covering pial vessels allow the exchange of fluid between the CSF and perivascular spaces. Pial arteries penetrate the brain and are covered by a dense perivascular layer of astrocytic foot processes; astrocytic, pial, and endothelial basement membranes (BMs); and smooth muscle cells. Veins exiting the parenchyma have a perivascular space flanked by astrocytic foot processes as well as endothelial BMs (adapted from Mastorakos and McGavern, 2019).

Additionally, the BBB is a summation of mechanisms that control the exchange of solutes and cells between circulation (blood) and the CNS. It is composed of endothelial cells, basement membrane, pericytes, glia limitans (astrocytic endfeet) and microglia, which collectively restrict the movement of most substances into the CNS, but can also selectively transport small and large molecules through passive diffusion, facilitated diffusion and active transport (Mastorakos and McGavern, 2019). The glia limitans and basement membranes are the rate-limiting barrier between the CSF and the ISF, through which molecule exchange mainly depends on size, lipophilicity, concentration gradients and astrocytic transport mechanisms. Also, they create a barrier between circulating immune cells, which access the CSF, and the CNS parenchyma. Besides, blood-CSF barriers are present in the choroid plexus (CP). The CP is a vascularized structure that produces CSF by filtering blood and is attached to the walls of the ventricles. The ventricles are CSF-filled cavities that are interconnected between them and with the SAS (Engelhardt et al., 2017; Mastorakos and McGavern, 2019; Papadopoulos et al., 2020). In the CP, a blood-CSF barrier determines the CSF initial composition of solutes and immune cells. Its endothelium lacks tight junctions and is open to peripheral circulation. However, choroidal capillaries are covered by an epithelial layer of ependymal cells with tight junctions that restrict the exchange between fenestrated blood vessels and the CSF. In any case, tracers that do not enter the brain parenchyma can be found in the leptomeninges, CP and perivascular spaces when are administered intravascularly. Also, the brain border regions (ventricles, CP and meninges) are populated by a plethora of immune cells, including DCs, macrophages and T cells, and show an immune reactivity that is similar to other organs (Mundt et al., 2019b, 2019a).

2.4. Antigen drainage and T cell trafficking

Apart from the CSF, which fills the CNS interfaces, the brain parenchyma is filled with ISF. The formation of brain ISF is carried out through CSF influx, vascular extravasation or metabolism, and is balanced by fluid efflux that occurs through multiple routes, including return to the CSF directly (Papadopoulos et al., 2020) or through perivascular spaces of capillaries and arteries, which are connected with the CSF (Iliff et al., 2012; Mastorakos and McGavern, 2019). This system of convective fluid fluxes with rapid interchange of CSF and ISF is sometimes termed glymphatic system based on its similarity to the lymphatic system in the peripheral

tissue (Jessen et al., 2015). The glia limitans - pia mater is the largest interface between ISF and CSF and is not an absolute barrier. On one hand, its permeability to macromolecules is dependent on concentration gradient, size, and solubility in the CSF. On the other hand, parenchymal solutes also move as a consequence of bulk flow, carried by the movement of the surrounding fluid, and become available in the CSF (Engelhardt et al., 2017; Papadopoulos et al., 2020). Different studies suggest an extensive exchange of CSF and ISF solutes, including metabolites and antigens. The CSF drains into venous blood or lymphatic vessels, despite the CNS parenchyma lacking a conventional drainage system, as an extensive network of lymphatic vessels in the dura mater permits CSF drainage to lymph nodes **(Figure 7)** (Alves De Lima et al., 2020; Louveau et al., 2018; Papadopoulos et al., 2020). There, specific T cell-mediated immune responses can be initiated (Louveau et al., 2015b; Mundt et al., 2019b, 2019a). In the healthy CNS, as well as in other tissues, a substantial fraction of antigens drains in the fluid itself rather than carried by APCs (Papadopoulos et al., 2020). The arachnoid mater is the boundary between CSF-filled spaces and the dura mater, where lymphatic vessels drain ISF and CSF-derived solutes. It has tight junctions that limit the exchange of substances (Papadopoulos et al., 2020). However, different experiments reveal areas of increased uptake capacity along meningeal lymphatic vessels that serve as entry points for solutes and immune cells from the SAS and CSF (Louveau et al., 2018; Da Mesquita et al., 2018). Antigens have been suggested to move from the CSF to CNS-draining lymph nodes through perineural routes as well, although these do not seem to be essential for immune surveillance (Papadopoulos et al., 2020). In addition, it was recently discovered that CNS-derived antigens in the CSF accumulate around the dural venous sinuses. Unlike the brain parenchyma, the dural meninges display homeostatic infiltration by circulating leukocytes, enabling efficient immune surveillance of this tissue. Thus, antigens are captured by local APCs and are presented to circulating T cells to promote effector functions and tissue retention. Instead of being evenly distributed along the dura mater, immune cells (both APCs and T cells) accumulate in immune hubs that are important for CNS immune surveillance (Rustenhoven et al., 2021).

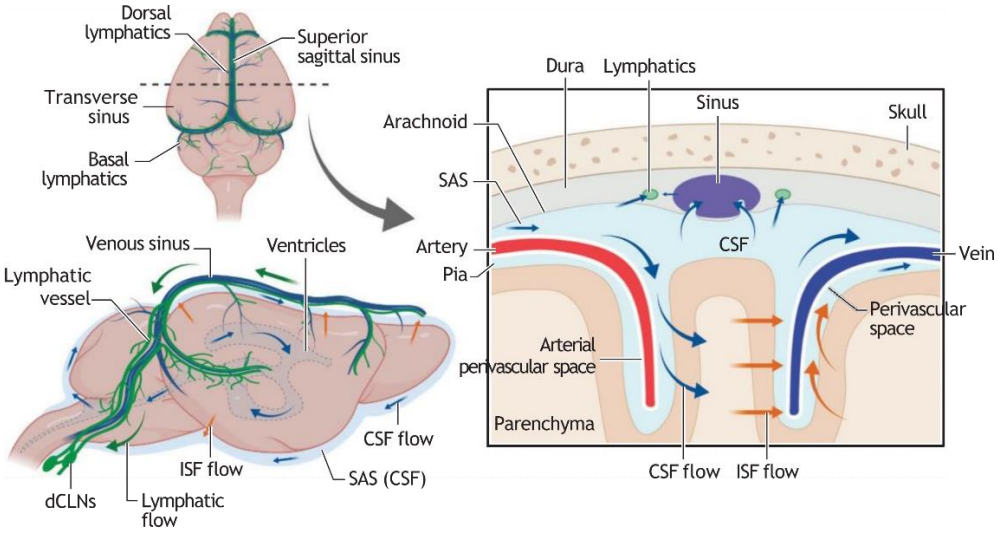

Figure 7. Meningeal lymphatic vasculature and pathways of CSF drainage. Dorsal meningeal lymphatics are situated within the dura mater, closely surrounding the dural sinus, and additional basal lymphatics are located at the base of the skull and the cerebellar ring. CSF is produced by the CPs within the ventricles and circulates toward the cisterna magna, where it fills the SAS. Here, the CSF can be drained via meningeal lymphatic vessels toward the deep cervical lymph nodes (dCLNs), or it may enter the dural sinuses (adapted from Alves De Lima et al., 2020).

Immune surveillance and the initiation of CNS immune responses also depends on APCs residing within the CNS barriers: in perivascular spaces, leptomeningeal vessels, CPs and the SAS (Engelhardt et al., 2017; Mastorakos and McGavern, 2019). These spaces contain DCs, which are the most efficient APCs also in the CNS (Mundt et al., 2019b) and macrophages. Similar to microglia, most macrophages that reside in the leptomeninges and perivascular spaces are derived from yolk sac-derived erythromyeloid progenitors and have minimal turnover in steady state. This is not the case for macrophages in the CP and dura mater, as these organs contain fenestrated blood vessels, are open to peripheral circulation and permit high amounts of immune cell traffic. Whereas diffusion of solutes from the CSF parenchyma is regulated mostly in capillaries, the extravasation of immune cells often occurs at the level of postcapillary venules (Engelhardt and Ransohoff, 2012; Mastorakos and McGavern, 2019). To access the brain parenchyma, immune cells need to migrate across barriers in a two-step process. First, they have to cross

endothelial cells and the inner basement membrane to access perivascular spaces. Second, they need to go through the glia limitans and the outer basement membrane to access the parenchyma. In homeostatic conditions, the brain endothelium does not allow myeloid cell adhesion due to a lack of P-selectin expression at the cell surface, and only a few $CD8^+$ and $CD4^+$ T cell can move through the BBB (Engelhardt and Ransohoff, 2012; Mastorakos and McGavern, 2019). α4-integrins mediate the capture of T cells on the BBB endothelium by binding to vascular cell adhesion molecule 1 (VCAM1) (Mastorakos and McGavern, 2019). In contrast to the general idea of immune cell restriction by brain interfaces, the endothelial cells of blood vessels within the CNS do not limit the extravasation of activated T cells independently of their antigen specificity, which can accumulate in the meningeal and perivascular areas, separated from the parenchyma only by the glia limitans (Mundt et al., 2019a). Nevertheless, only after T cells recognize their cognate antigen again, presented by border-associated APCs (a process termed antigen reconfirmation), mainly perivascular DCs, they can cross the glia limitans and access the parenchyma to exert effector functions **(Figure 8)** (Mastorakos and McGavern, 2019; Mundt et al., 2019b, 2019a). Many questions regarding antigen drainage from the brain parenchyma and CNS immune surveillance remain to be answered. However, It is already assumed that, even with its peculiarities, the CNS is under close immune surveillance for aberrant cells and pathogens (Engelhardt et al., 2017; Mastorakos and McGavern, 2019; Papadopoulos et al., 2020; Ransohoff and Engelhardt, 2012).

2.5. Antigen presentation in the CNS

MHCI expression is widely detected in the mouse developing brain. It is at its highest during early postnatal development, but the levels gradually decrease as mice reach adulthood (Liu et al., 2013). MHCI in the adult rodent CNS was for many years thought to be restricted to glial and endothelial cells (Wong et al., 1984). Indeed, it has generally been presumed that MHCI is hardly expressed by cells of the adult CNS parenchyma, including neurons, astrocytes and oligodendrocytes under homeostatic conditions (Cebrián et al., 2014a; Lampson, 1995; Wong et al., 1984). When present, MHCI molecules in neurons are predominantly known not for their involvement in immunity, but for their roles in developmental neural refinement and adult synaptic plasticity (Cebrián et al., 2014a). Proper

development of the CNS requires the establishment of appropriate connections between neurons, and this process is controlled by a balance between synaptogenic molecules and proteins that negatively regulate synapse formation and plasticity. Over the past decades, it has become clear that MHCI molecules play a significant non-immune role in the development and plasticity of the CNS, acting as synapse-limiting molecules and inhibiting neural development (Elmer and McAllister, 2012; Shatz, 2009). Increasing evidence has demonstrated that MHCI can be expressed by some neuronal populations in response to immune signals that may be produced under pathological conditions. Neurons have been shown to exhibit MHCI *in vitro* after their exposure to IFNγ and *in vivo* in response to brain injury or neurodegeneration (Cebrián et al., 2014b, 2014a; Neumann et al., 1995; Salvioni et al., 2019; Zalocusky et al., 2021). In line with this, IFNγ can also up-regulate antigen presentation in astrocytes, oligodendrocytes and microglia, as well as in endothelial and ependymal cells (Sethna and Lampson, 1991; Wong et al., 1984).

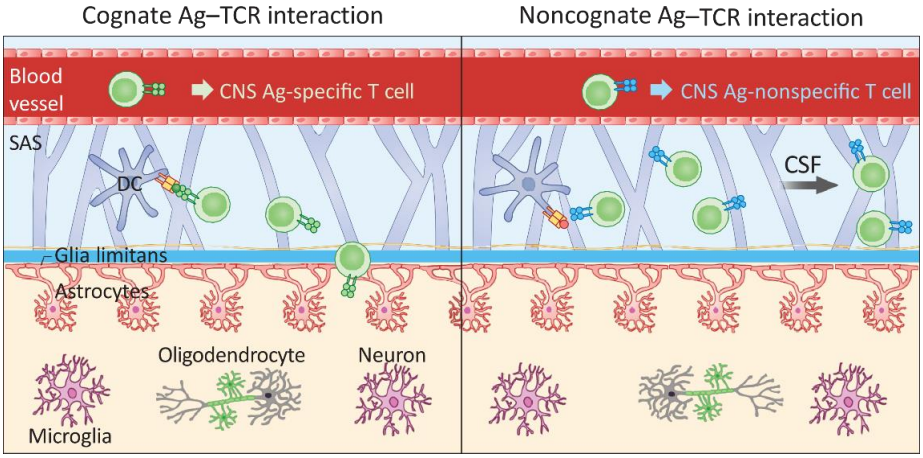

Figure 8. Antigen-specific T cell trafficking within the healthy brain. Activated T cells can leave the leptomeningeal blood vessels to screen the SAS for their cognate antigen (Ag). CNS Ag-ignorant T cells remain in this location, where they might either undergo cell death or be released again to the periphery via the CSF flow. In the case of confirmatory cognate Ag presentation by CNS-associated APCs (especially DCs) CNS-specific T cells become reactivated and are able to breach the glia limitans of the BBB and infiltrate the CNS parenchyma (adapted from Mundt et al., 2019a).

3. Adult stem cells, immunity, and the case of NSCs

3.1. Adult stem cells as units of regeneration and their interaction with T cells

Most tissues in adult mammals contain SCs, which are essential for their homeostasis and regeneration. SCs are rare cells with the potential to generate differentiated cell types and, therefore, their life-long maintenance is essential to sustain tissue renewal and repair. Both SCs and the immune system evolved to prevent, mitigate and resolve tissue injury and it is not surprising that they are in continuous crosstalk and can modulate each other. In fact, immune cells are essential to create the proper microenvironment in SC niches so SCs can develop and function, and can promote SC activation in the right circumstances (Aurora and Olson, 2014). Conversely, SCs sense, communicate with and recruit immune cells to maintain tissue homeostasis or deal with stress (Naik et al., 2018). In contrast, their malignant transformation might turn them into cancer-initiating cells. Therefore, somatic SCs need to be monitored by the immune system while avoiding uncontrolled killing. Cells can become tumorigenic as they accumulate somatic mutations due to environmental factors or DNA replication errors (Blokzijl et al., 2016; Tomasetti et al., 2017). These random genetic alterations can promote tumor development when they favor sustained proliferation, evasion from tumor suppressors, resistance to cell death, replicative immortality, angiogenesis and/or invasive capacity, as well as resistance to immune destruction, among others (Hanahan, 2022). As SCs have self-renewal capacity, they are the longest living proliferative cells in multicellular organisms and therefore have increased risk of accumulating mutations and becoming tumorigenic (Ermolaeva et al., 2018; Tomasetti et al., 2017; Zindl and Chaplin, 2010). Besides, most SCs are largely quiescent. While this non-proliferative state might help them preserve their genomic integrity, DNA damage checkpoints and several DNA repair pathways depend on the cell cycle. Moreover, upon SC activation and entrance to the G1 phase of the cell cycle, DNA damage is primarily repaired by error-prone non-homologous end joining, which favors the accumulation of mutations (Mandal et al., 2011), especially since SCs are resistant to DNA damage-induced apoptosis or senescence (Barazzuol et al., 2017; Insinga et al., 2013). Interestingly, the repeated activation of quiescent SCs has been shown to explain, at least in part, their accumulation of DNA damage during aging (Walter et al., 2015).

When it comes to immune surveillance, all nucleated cells in the body were thought to express MHCI and expose antigens to $CD8^+$ T cells (Abbas et al., 2016). However, recent evidence shows that this is not the case for quiescent SCs in some peripheral tissues. Specifically, Agudo et al made use of the *Just Egfp Inducing Death* (JEDI) mouse model, in which $CD8^+$ T cells recognize (enhanced) green fluorescent protein (EGFP/GFP) as their cognate antigen, to explore whether adult tissue SCs are subjected to immune surveillance. CTLs from JEDI mice were transferred into Lgr5-GFP reporter mice, where epithelial SCs of the intestine, ovary, mammary gland and hair follicle express GFP. Interestingly, they found that quiescent SCs in the hair follicle and the muscle are resistant to CTL-mediated killing, while fast cycling epithelial SCs in the gut and ovary were subjected to immune detection and clearance. This shows that immune privilege is not a general property of adult SCs, but might be a unique characteristic of slowly-cycling SCs. Additionally, they showed that quiescent SCs down-regulate the antigen presentation machinery by suppressing NLRC5 expression. When they enter the cell cycle, NLRC5 and antigen presentation are induced and cells become susceptible to antigen-specific $CD8^+$ T cells (Agudo et al., 2018; Boyd and Rodrigues, 2018). The immune protection of quiescent SCs preserves the capacity to restore a damaged tissue after an inflammatory response associated with autoimmune attack or when SCs harbor immunogenic mutations. However, it also renders SCs more susceptible to neoplastic transformation, as the formation of neoantigens cannot be checked by the immune system (Agudo et al., 2018).

3.2. Stem cells of the brain and olfactory neurogenesis

In the adult mammalian brain NSCs generate new astrocytes, oligodendrocytes and neurons throughout life. They are located in two main neurogenic niches, which are the subgranular zone (SGZ) in the hippocampus, and the subependymal zone (SEZ, also known as ventricular-subventricular zone or V-SVZ), which is the biggest one. Located along the walls of the lateral ventricles, the SEZ of a young adult mouse contains up to 15,000 NSCs (Mirzadeh et al., 2008), which are estimated to sustain the production of approximately 10 million neurons throughout the mouse lifespan (Obernier and Alvarez-Buylla, 2019). Subependymal NSCs are specialized astrocytes with a radial morphology that resembles embryonic radial glia, from which they are originated during mid-embryonic development (Chaker et al., 2016; Doetsch, 2003;

Doetsch et al., 1999a; Fuentealba et al., 2015; Furutachi et al., 2015; Kriegstein and Alvarez-Buylla, 2009). Adult NSCs are embedded in a structured niche that contributes to maintaining their epithelial apico-basal polarity. NSCs extend a small apical process with a primary cilium that contacts the ventricular CSF at the center of multicilliated ependymal cell rosettes (pinwheels). On the basal end, they contact the vascular plexus through long cytoplasmic processes (Chaker et al., 2016; Fuentealba et al., 2012; Mirzadeh et al., 2008; Tavazoie et al., 2008). This radial morphology enables their access to secreted factors in the CSF and in blood vessels that contribute to the fine tuning of NSCs biology and of the neurogenic output. NSCs are also exposed to factors from neighboring cells, including other NSCs, their immediate progeny, ependymal cells, parenchymal astrocytes, microglia and neurons **(Figure 9)** (Morante-Redolat and Porlan, 2019; Obernier and Alvarez-Buylla, 2019; Porlan et al., 2013; Silva-Vargas et al., 2016; Sirerol-Piquer et al., 2019).

NSCs in different states of activation coexist in the SEZ. Most of them are in quiescence, which is an actively maintained and reversible state characterized by cell cycle arrest, low metabolic activity, as well as reduced RNA and protein synthesis (Urbán et al., 2019). Once activated, NSCs produce young migrating neurons (neuroblasts or NBs) through the generation of rapidly dividing transit-amplifying progenitors (neural progenitor cells or NPCs) (Doetsch et al., 1997, 1999a). NPCs divide symmetrically 3 or 4 times before they convert into NBs. NBs can then cycle once or twice to amplify the NB pool (Calzolari et al., 2015; Ponti et al., 2013). We term the proliferating subpopulation of NBs as early NBs (ENBs) and the migrating pool as late NBs (LNBs). Newly-born NBs along the SEZ migrate tangentially in chains towards the olfactory bulb (OB) creating the rostral migratory stream (RMS) (Doetsch and Alvarez-Buylla, 1996; Lois et al., 1996). Within the OB, NBs differentiate into interneurons that integrate into the pre-existing neural circuits and participate in fine odor discrimination and odor-reward association (Lledo and Saghatelyan, 2005; Obernier and Alvarez-Buylla, 2019). NSCs generate different subtypes of interneurons depending on their location within the SEZ. This regional specification among the anterior-posterior and the dorsal-ventral axes is intrinsic (Merkle et al., 2007, 2014) and early set during mid-embryonic development (Fuentealba et al., 2015). Therefore, the SEZ constitutes a cellular mosaic with some regional differences that produce lineage-restricted progeny. Whereas neurons are the most abundant progeny, NSCs also generate

oligodendrocytes for the corpus callosum and striatal astrocytes (Menn et al., 2006; Sohn et al., 2015).

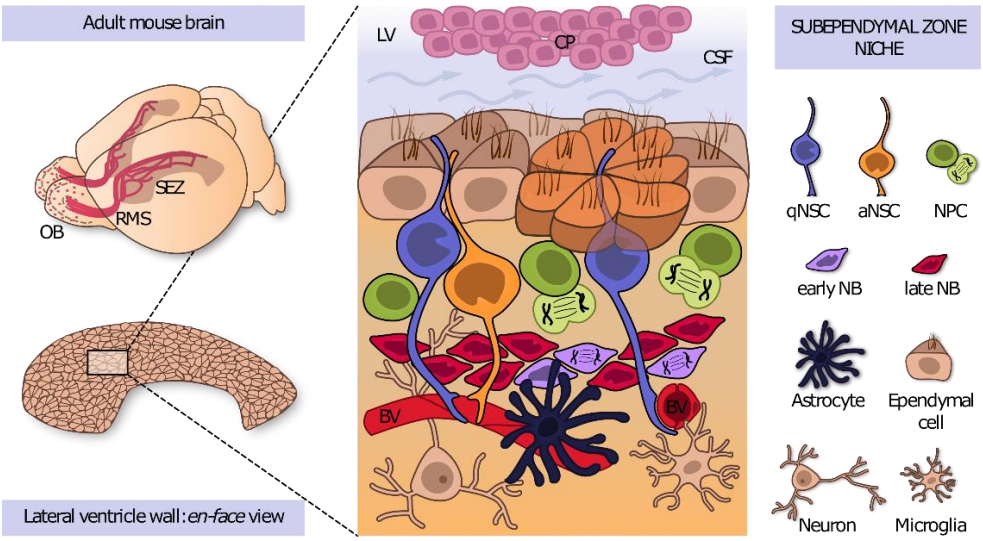

Figure 9. The adult SEZ niche. The SEZ is located along the walls of the lateral ventricles (LV), where newly-born neurons migrate through the RMS towards the OB. The SEZ niche has a special architecture with ependymal cells acting as rosette-like organized cobblestones (pinwheels) paving the wall. Underneath, quiescent (qNSCs) and activated NSCs (aNSCs) extend an apical process to contact the CSF through ependymal pinwheels and a basal process to contact blood vessels (BV). aNSCs generate rapidly-dividing NPCs, which in turn give rise to new young neurons (NBs). Extrinsic signals from niche elements, such as the CP, microglia, neurons, blood vessels and their own progeny regulate their physiology (Illustration by Ana Domingo).

Based on their astrocytic nature, NSCs have traditionally been identified histologically by pan-astrocytic markers, such as glial fibrillary acidic protein (GFAP), glutamate aspartate transporter (GLAST) and brain lipid-binding protein (BLBP) (Doetsch, 2003; Doetsch et al., 1999a). However, it was not possible for a long time to use a single marker to specifically discriminate bona fide NSCs from niche astrocytes, or NSCs with different proliferation dynamics. The recent implementation of fluorescence activated cell sorting (FACS, flow cytometry) strategies to identify and isolate the different populations of the neurogenic lineage

allowed more detailed studies of the molecular identity of NSCs and their different states of activation. In fact, the detection of surface markers such as GLAST, Prominin-1/CD133, or Plexin B2 and/or the usage of GFAP::GFP reporter mice together with fluorescent epidermal growth factor (EGF) that binds the activation-associated EGF receptor (EGFR) has revealed that NSCs co-exist in two main proliferative states, activated (aNSCs) and quiescent (qNSCs) NSCs that differ transcriptionally and phenotypically (Basak et al., 2018; Belenguer et al., 2020; Codega et al., 2014; Daynac et al., 2013; Dulken et al., 2017; Llorens-Bobadilla et al., 2015; Mich et al., 2014; Pastrana et al., 2009). aNSCs are characterized by the expression of genes related to cell cycle and DNA repair, their metabolism depends on oxidative phosphorylation and have increased protein synthesis and proteasome activity. In contrast, the transcriptome of qNSCs is highly enriched in genes involved in cell adhesion and communication, extracellular matrix and inflammation, as well as in transmembrane transporters and ion channels. Besides, qNSCs depend on glycolysis, fatty acid metabolism and lysosomal function and have increased expression of signaling receptors (mainly G protein-coupled receptors), which supports the idea that quiescence is an actively regulated state (Belenguer et al., 2020; Chaker et al., 2016; Codega et al., 2014; Leeman et al., 2018; Llorens-Bobadilla et al., 2015). In addition, recent single cell RNA-seq data revealed that qNSCs and aNSCs populations are heterogeneous, and contain cells with different molecular profiles (Basak et al., 2018; Dulken et al., 2017; Llorens-Bobadilla et al., 2015; Mizrak et al., 2019). It is relevant the identification of primed NSCs (pNSCs) (Belenguer et al., 2020; Llorens-Bobadilla et al., 2015) as a subpopulation of NSCs in a state of shallow quiescence similar to the G_{Alert} state described for SCs in the skeletal muscle niches (Rodgers et al., 2014) or that of the short-term hematopoietic SCs in the bone marrow (Laurenti et al., 2015). pNSCs are quiescent and show a singular gene expression profile, but they are more prone to activation than qNSCs and seem to stand in the transition between quiescent and active NSCs. In line with activation, they display higher ribosomal activity and lower glial marker expression than qNSCs (Belenguer et al., 2020; Llorens-Bobadilla et al., 2015). At the opposite end of the quiescent state, genetic and label retention studies have revealed the existence of deeply quiescent or 'dormant' NSCs, a subset of NSCs that are originated and specified during mid-embryonic development and remain largely quiescent until their activation in adult life (Fuentealba et al., 2015; Furutachi et al., 2015). The existence of several levels of quiescence calls into question the use of traditional nucleoside retaining methods during adulthood as

ways to unequivocally label quiescent cells, since many of them may never become activated and thus might not be detected. Therefore, current and future studies on NSC behavior will necessarily rely on more informative methods such as flow cytometry for the study of NSCs in different activation states.

3.3. Adult neurogenesis and immunity

The SEZ is at the interface between the brain parenchyma and the lateral ventricle, and therefore constitutes a brain-CSF interface with special characteristics. This barrier between the SEZ and the lateral ventricle is formed by ependymal cells with intercalated NSCs (Lim and Alvarez-Buylla, 2016). Mature ependymal cells are polygonal cells which display polarized structure and function. At the basal side, they present basal lamina, whereas apically their luminal pole is in contact with the ventricular CSF and displays motile cilia, which participate in the movement of CSF. Multiciliated ependymal cells are joined with adherens junctions involving cadherins, which are important for the integrity of the monolayer (Morante-Redolat and Porlan, 2019). In steady state conditions, the absence of tight junctions in the ependymal barrier and the proximity (and contact) of NSCs to the CSF suggest that the SEZ might have easy drainage of antigens to the CSF, and increased leukocyte infiltration. Indeed, leukocytes can potentially enter the brain parenchyma from the CSF crossing the ependymal cell layer that delineate the ventricles (Bechmann et al., 2007; Engelhardt and Ransohoff, 2012; Wilson et al., 2010). Furthermore, multiciliated ependyma has been shown to produce effector molecules that support leukocyte transmigration in infectious and inflammatory conditions (Jiménez et al., 2014). Thus, the SEZ might present an immune reactivity more similar to brain interfaces than other parts of the parenchyma.

Different studies found that mouse models of severe combined immunodeficiency, which lack B and T cells, or nude mice, which only lack T cells, have reduced neurogenesis and NSC/NPC proliferation in both the SGZ and the SEZ (Ziv et al., 2006). Also, neurogenesis is reduced in the SGZ of MHCI or MHCII-deficient mice (Huang et al., 2010) or when $CD4^+$ T cells, but not B or $CD8^+$ T cells, are impaired or depleted. Repopulation of immunodeficient mice with $CD4^+$ T cells rescues neurogenesis (Huang et al., 2010; Wolf et al., 2009a; Ziv et al., 2006), whereas $CD8^+$ T cells are necessary for enhancing it through physical activity or environmental

enrichment (Zarif et al., 2018). It seems that only activated and especially CNS-reactive T cells support neurogenesis (Derecki et al., 2010; Rolls et al., 2008; Song et al., 2020a; Wolf et al., 2009b; Xu et al., 2017; Ziv et al., 2006), and several mechanisms have been proposed to explain that, including the regulation of microglia (Qi et al., 2016; Ziv et al., 2006) and astrocytes (Zarif et al., 2018) as well as the production of neurotrophins (i.e. BDNF) (Derecki et al., 2010; Kipnis et al., 2012; Ziv et al., 2006). Summarizing, it seems that T cells might have functions unrelated to immune responses against CNS-derived antigens that support neurogenesis from outside the brain parenchyma. Conversely, the infiltration of $CD8^+$ T cells has been reported in the SEZ of old mice, where they decrease cell proliferation (Dulken et al., 2019). In any case, antigen-specific interactions or cell-cell contacts between NSCs and T cells in the healthy and young SEZ have not been identified.

On the other hand, inflammatory conditions in the CNS can have devastating consequences, and $CD8^+$ T cells have been linked to the pathogenesis of Alzheimers' disease (Gate et al., 2020), Parkinson's disease (Dhanwani et al., 2022; Krot and Rolls, 2021; Sulzer et al., 2017; Tan et al., 2020), autoimmune encephalomyelitis and multiple sclerosis (Kaskow and Baecher-Allan, 2018; Sospedra and Martin, 2005; Wagner et al., 2020), and ischemia (Zhang et al., 2021). After brain injury, even in non-neurogenic sites, NSCs/NPCs from neurogenic niches can proliferate and migrate to the affected site, attempting, with very limited success in mammals, to limit the damage and partly restore the tissue (Arvidsson et al., 2015; Covacu et al., 2014; Faiz et al., 2015; Otsuki and Brand, 2020). Tissue damage is normally associated with inflammation, and immune responses can be associated with collateral tissue damage and autoimmunity (Abbas et al., 2016). Adult tissue SCs are precious players in tissue homeostasis and regeneration, and therefore need to be kept safe in these circumstances (Blanpain and Fuchs, 2014). It has been shown that NSCs actively preserve their stemness during inflammation (Belenguer et al., 2020), which indicates that additional mechanisms might be in place to protect them from the immune system, as it happens in other adult SC niches in the periphery (Agudo et al., 2018).

Although the immune surveillance of NSCs has not been studied, compelling evidence indicates that SEZ NSCs are, in both rodents and humans, the cells-of-origin of GBM (Alcantara Llaguno and Parada, 2021; Alcantara Llaguno et al., 2009,

2019; Lee et al., 2018; Matarredona and Pastor, 2019). GBM is the most frequent type of CNS cancer in adults, with a peak incidence in the seventh decade of life, and an annual incidence of around 1 case per 30,000 individuals. It is the most aggressive variant of diffuse gliomas, generally resistant to all current standard-of-care therapeutic interventions (surgery, radiotherapy, and systemic chemotherapy), and invariably lethal (Lim et al., 2018). These tumors have been proposed to contain small populations of cancer cells with stem-like properties, that some authors call glioma SCs (GSCs), that retain most of the NSC properties and plastic behavior. Single cell RNA-seq analysis have shown striking similarities between GSCs and radial glial cells (Bhaduri et al., 2020) and unbiased clonal evolution analysis of barcoded GBM cells during serial transplantation has indicated that heterogeneity in clonal expansion does not derive from genetic diversity. This suggests that GBM initiation may be associated with the aberrant activation of normal developmental programs (Lan et al., 2017). Mutations leading to dysregulation of receptor tyrosine kinases, phosphatidylinositol 3-kinases, RAS pathways, p53 and retinoblastoma signaling, and well as reactivation of telomerase, are central in GBM initiation (Brennan et al., 2013; McLendon et al., 2008). In line with this, alterations in *TP53*, *EGFR*, *PTEN*, *NF1, RB1* and *TERT* have been found to drive NSCs malignant transformation influencing their physiology and, eventually, enabling them to migrate, invade neural tissue and form a brain tumor (Alcantara Llaguno et al., 2009, 2019; Lee et al., 2018). Accordingly, engineered mouse models of brain cancer have been developed by targeting all these pathways at many different levels in NSCs and NPCs (Alcantara Llaguno et al., 2009, 2019, 2015; Galvao et al., 2014; Holland et al., 2000; Huse and Holland, 2009; Noorani, 2019; Simeonova and Huillard, 2014; Zhu et al., 2005).

AIMS

1. To determine whether the SEZ is subjected to immune surveillance and/or allows more infiltration of $CD8^+$ T cells than other parts of the brain.

2. To determine if the different neurogenic populations in the SEZ have distinct susceptibilities to $CD8^+$ T cells.

3. To determine which mechanisms underlie differential susceptibilities of the different neurogenic populations in the SEZ to $CD8^+$ T cells.

METHODOLOGY

1. Animal models

1.1. Mouse handling

Mice were bred and housed at the animal housing facility of the *Universitat de València* (Servei Central de Suport a la Investigació Experimental, Burjassot) according to the European Union 2010/63/UE and Spanish RD-53/2013 guidelines under official veterinary supervision. Housing established 12 h periods of light/darkness, room temperature of 20-22 °C and free availability of food (pellets) and water. Litters were weaned 21 days after birth. All experimental procedures were approved by the Ethics Committee of *Universitat de València*.

1.2. Mouse strains

Experiments were carried out using 2 to 4-months-old mice unless stated otherwise. The strains that were used are the following:

- C57BL/6J: These mice were obtained from The Jackson Laboratory (strain 000664) and used as *wild-type* mice for different *in vivo* and *in vitro* experiments.
- Rag1: *B6.129S7-Rag1tm1Mom/J*, which lack B and T lymphocytes, strain 002216 at The Jackson Laboratory (Mombaerts et al., 1992) were kindly shared by Dr. Rosa Noguera from *Universitat de València*. They were used to assess neurogenesis in the absence of lymphocytes.
- JEDI: *Ptprca TcrbLn1Bdb TcraLn1Bdb H2d/J* mice were also obtained from The Jackson Laboratory (strain 028062) and were the source of JEDI T cells (Agudo et al., 2015).
- mTmG: *Gt(ROSA)26Sortm4(ACTB-tdTomato,-EGFP)Luo/J* mice (strain 007576 at The Jackson Laboratory) (Muzumdar et al., 2007) were kindly shared by the group of Dr. Eva González at CNIO in Madrid. Upon receipt, they were housed and bred in the animal facility of the *Universitat de València*.
- hGfapCre: *B6.Cg-Tg(Gfap-cre)73.12Mvs/J* mice were obtained from The Jackson Laboratory (strain 012886) (Zhuo et al., 2001) and were used for crossing with the mTmG strain to obtain R26mTmG;hGfap-Cre mice.

- CX3CR1-EGFP: *B6.129P2(Cg)-Cx3cr1tm1Litt/J knock-in* mice were also obtained from The Jackson Laboratory (strain 005582) (Jung et al., 2000) and were used as a model of $EGFP^+$ microglia.
- B10D2: *B10.D2-Hc0 H2d H2-T18c/oSn* were obtained from The Jackson Laboratory (strain 000461). They carry the allele H2Kd and were used for crossing with other strains such as C57BL/6J, CX3CR1-EGFP or R26mTmG;hGfap-Cre so their F1 progeny was histocompatible with the JEDI T cells.

1.3. Genotyping

Only when strains were not maintained in homozygosis, genetic modifications were genotyped by end-point Polymerase Chain Reaction (PCR) of genomic DNA (gDNA) extracted from an ear punch using the Phire Animal Tissue Direct PCR kit (Thermo Fisher, F140WH). 20 to 50 ng of gDNA were used for amplification with specific primers and the Phire II polymerase provided in the gDNA extraction kit. PCR products were resolved by electrophoresis in a 2-3% agarose gel in TAE buffer (40 mM Tris-HCl pH 7.6, 20 mM glacial acetic acid, 1 mM ethylenediaminetetraacetic acid (EDTA)). Touchdown PCR programs were used, starting with annealing temperatures of 65 °C and progressively decreasing until 55 °C. The primers we used are indicated in the following table:

Rag1	
Common	CAT TCC ATC GCA AGA CTC CT
WT	TCT GGA CTT GCC TCC TCT GT
Mutated	CCT CGT TCC ACT CTA CTG TC
mTmG	
Common	CTT CCC TCG TGA TCT GCA AC
WT	CAG GAC AAC GCC CAC ACA
Mutated	GTT ATG TAA CGC GGA ACT CCA
hGfapCre	
Mutated	GCG GTC TGG CAG TAA AAA CTA TC
Mutated	GTG AAC AGC ATT GCT GTC ACT T
Control	CTA GGC CAC AGA ATT GAA AGA TCT
Control	GTA GGT GGA AAT TCT AGC ATC ATC C

1.4. *In utero* electroporation

Embryonic age was determined based on the day when the vaginal plug was observed (E0.5). E15.5 pregnant mice were placed in an induction chamber with 2.5% (v/v) isoflurane at 0.8 l/min until they were completely anaesthetized (determined by low respiratory rate and absence of pedal reflex). Then, they were transferred to a heating pad and continuous delivery of isoflurane (Karizoo) was secured through a nose mask. 0.1 mg/kg of buprenorphine (Rb Pharmaceuticals) was subcutaneously injected for analgesia and lubricant was applied to prevent eyes from drying. The mouse abdomen was shaved with an electric razor and washed with 70% (v/v) ethanol and iodine wipes. A 30 mm long incision through the abdominal skin was performed, and skin was carefully separated from the muscle with a blunt spatula. A second incision in the abdominal wall allowed us to access the abdominal cavity and pull the uterus, which was maintained with warm saline solution, out of the abdominal cavity with ring forceps.

Plasmid DNA (1-2 µg/µl) with 1/20 volume of 1% Fast Green (Sigma-Aldrich, F7252) in TE buffer was injected into the lateral ventricles of the embryos. That was done through a mouth-controlled aspirator tube until the fast green dye could be noticed inside the ventricle. Then, forceps-type platinum electrodes were laterally placed around the head of the injected embryo and oriented with the positive electrode contacting the ventrolateral region of the injected hemisphere. Finally, five pulses of 50 V and 80 ms, with 950 ms intervals, were applied with a square wave electroporator (BTX, ECM830). The uterus was placed back into the abdominal cavity. The abdominal wall, and then the skin, were closed with absorbable sutures and animals were maintained on the heating pad until recovery. Polymyxin B, Bacitracin and Neomycin were topically applied to prevent infection and additional analgesia was applied at this point and the next day (Mateos-White et al., 2020).

1.5. Lipopolysaccharide injection

Lipopolysaccharide (LPS) (Sigma, L263) was reconstituted at 1 mg/ml in saline solution and intraperitoneally (i.p.) injected at a single dose of 5 mg/kg.

2. Isolation and adoptive transfer of JEDI T cells

Naïve JEDI T cells were isolated by magnetic sorting from the spleens of 2 to 4-months-old JEDI mice. The EasySep Mouse Naïve $CD8^+$ T Cell Isolation Kit (Stemcell, 19858) was used following the manufacturer's instructions. However, we used the antibody cocktail and the magnetic particles at half the concentration recommended in the datasheet, as we obtained cell extracts with similar purity **(Figure 1)**. This kit allows the negative selection of mouse naïve $CD8^+$ T cells by removing cells that express CD4, CD11b, CD11c, CD19, CD44, CD45R/B220, CD49b, TCRγ/δ and TER119. Briefly, splenocytes were extracted by perfusing spleens with blocking buffer, consisting in 2% fetal calf serum (FCS or FBS) and 2 mM EDTA in 0.1 M Phosphate-buffered saline, pH 7.4, with 0.09% NaCl (PBS) with a 25 G needle. They were then cut in 4 to 6 pieces and disaggregated with the piston of a 1 ml syringe. Cell suspensions were filtered through a 0.45 µm polyethersulfone (PES) filter. The cell suspension was centrifuged (500x*g*, 5 min) and resuspended in blocking buffer (1 ml/spleen). Rat serum was added, and then a cocktail of biotinylated antibodies for negative selection. Following a 10 min incubation, streptavidin-coated magnetic particles were added and, after incubation, labeled cells were removed with an EasySep Magnet (Stemcell, 18000). In order to concentrate the isolated cells, the suspension obtained after magnetic sorting was centrifuged again (500x*g*, 5 min) and resuspended in the proper volume of PBS.

Unless stated otherwise, the number of naïve JEDI T cells injected to each receptor mouse was equivalent to the JEDIs extracted from 1-1.5 JEDI mice, which is around 5 million. JEDI T cells were resuspended in sterile PBS. Then, for *in vivo* experiments, lentiviral particles encoding EGFP (LV.EGFP) (see below) were added to the mixture. JEDI T cells and LV.EGFP were injected together into mice previously anaesthetized with isoflurane (4% for induction) in a final volume of 100 µl/mouse by retro-orbital intravenous (i.v.) injection.

For co-culturing with NSCs, total $CD8^+$ T cells (not only naïve) were isolated from spleens. This time we used the EasySep Mouse $CD8^+$ T Cell Isolation Kit (Stemcell, 19853) following the manufacturer's instructions (1x reagents).

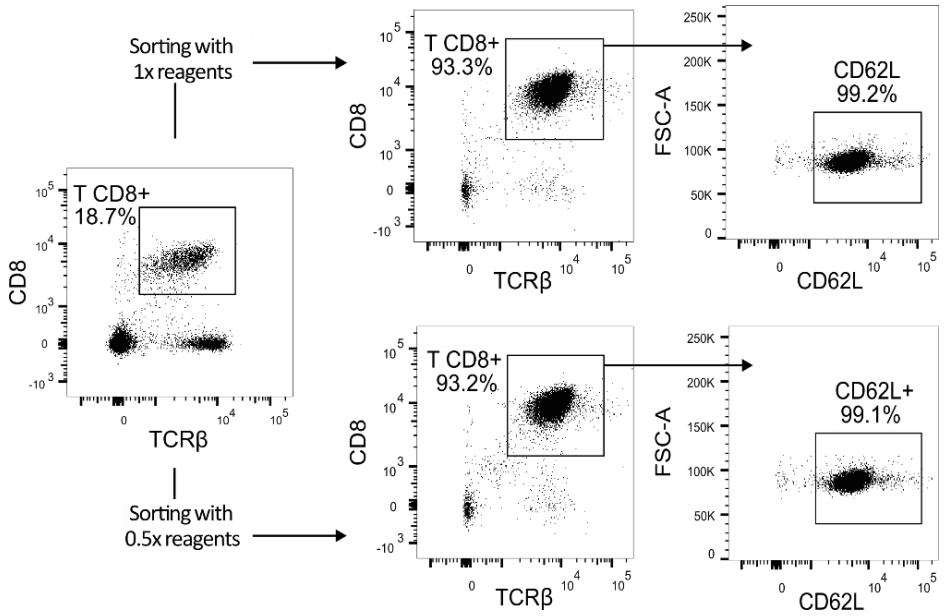

Figure 1. Naïve CD8⁺ T cell isolation. Comparison of the purity obtained by using the EasySep Mouse Naïve CD8⁺ T Cell Isolation Kit (Stemcell, 19858) with 1x or 0.5x the recommended concentration in the datasheet of biotinylated antibodies cocktail and streptavidin-coated magnetic particles. CD8⁺ JEDI T cells were defined as TCRβ⁺ CD8⁺, and the naïve state identified as CD62L⁺. The dot plot at the left of the figure shows the percentage of CD8⁺ T cells in a representative spleen extract, with no cell sorting.

3. Lentivirus production and titration

LV.EGFP are third generation lentiviral particles and were generated in HEK293T cells. To do that, 15 cm dishes were seeded with 14 million HEK293T cells in DMEM-F12 (Gibco, 13210-074) supplemented with 10% FBS (Biowest, S181B) and penicillin/streptomycin (Sigma, P4333). The following day, cell culture media was changed and antibiotics removed. Then, cells were transfected using linear polyethylenimine (PEI) (Polysciences, 23966) 1 mg/ml (1 µl of PEI solution/µg of total plasmid DNA) and the following amounts of plasmid for each 15 cm dish:

- 9.4 µg of envelope plasmid CMV-VSVG-PolyA
- 13.4 µg of packaging plasmid CMV-GAG-POL-RRE
- 6.7 µg of packaging plasmid CMV-REV

- 26.8 µg of transfer plasmid with the gene of interest: 5'LTR-CMV-EGFP-LTR for the *in vivo* activation of JEDI T cells.

After 16 to 18 h, cell culture media was changed and antibiotics added again. 24 h later, cell culture medium was changed, and conditioned media was collected. This was centrifuged (300x*g*, 5 min) and the supernatant filtered through a 0.45 µm PES filter. Then, lentiviral particles were concentrated by ultracentrifugation (90,000x*g*, 90 min at 10 °C), resuspended in PBS containing 1% bovine serum albumin (BSA), and kept in the fridge until the next day. After another period of 24h, cell culture media was collected again and the process repeated. Finally, viral suspensions from both days were pooled and ultracentrifuged again (90,000x*g*, 90 min at 10 °C). Pellets were thoroughly resuspended in PBS with 1% BSA in a volume around 500 times lower than the amount of cell culture media initially collected (approximately 80 µl for each 15 cm dish). Lentiviral particles were divided in aliquots of 40 µl and kept at -80 °C until they were used.

For titration, 50,000 HEK293T cells were seeded per well in 6-well plates. After 24 h, their media was removed and 1 ml of fresh media containing 16 µg/ml of polybrene (Sigma, TR-1003-G) added to each well. An aliquot of lentiviral particles was thawed, and serial dilutions, from $1/10^3$ to $1/10^8$ were prepared with cell culture media. 1 ml of each dilution was added to each well, and 72 h later, cells were harvested and resuspended in PBS containing 2% FCS and 2 mM EDTA. The percentage of $EGFP^+$ cells was assessed by flow cytometry, and transduction units (TU)/ml were calculated as follows:

TU/ml = cells in each well the day of infection (around 100,000) * (1/virus dilution) * (%$EGFP^+$/100).

High viral concentrations increase the probability of several viral particles infecting the same cell. However, this equation assumes that each $EGFP^+$ cell was infected with only one viral particle. Therefore, we only considered the viral dilutions that provided a percentage of $EGFP^+$ cells between 0.05 and 20, and averaged the results obtained with all of them. Viral titers in the final suspensions were usually around $5 \cdot 10^9$ TU/ml.

4. Immunofluorescence of the SEZ

4.1. SEZ dissection and whole-mounts

Mice were sacrificed by cervical dislocation. Skin was removed and the brain extracted and placed on a silicone pad with sterile ice-cold PBS. The OBs and the cerebellum were discarded and both hemispheres were then separated along the brain midline. The lateral ventricle was accessed by separating the hippocampus, septum and diencephalon from the cortex underneath the corpus callosum line. The SEZ was isolated after removing the surrounding tissue, and white matter tracts (corpus callosum and capsule/stria terminalis) were used as reference lines. The SEZ was finally separated from the striatum and extracted as a thin slice of tissue. Images of the process and a more detailed explanation can be found in Belenguer et al., 2016, 2021 (Belenguer et al., 2016, 2021).

When we needed these SEZs for other experiments requiring live cells (for example flow cytometry), perfusion was not an option. Instead, SEZ dissection was performed in freshly isolated brains and whole-mounts were fixed by immersion in 4% paraformaldehyde (PFA) with 0.5% Triton-X-100 for 1 h at room temperature (RT). Next, they were thoroughly washed with PBS and kept at 4 °C in PBS with 0.05% azide until they were further processed. Prior to staining, whole-mounts were incubated for 1 h at RT in blocking solution (PBS with 10% horse serum (HS) and 0.2% Triton X-100). Then, overnight incubations with the following primary antibodies were performed: for JEDI T cell staining, mouse anti-mouse CD45.1 conjugated to BV650 (BD, 563754) at 4 µg/ml (1:50); to mark proliferating cells, rabbit anti-mouse Ki67 (Abcam, ab15580) at 3 µg/ml (1:300); and to enhance the detection of EGFP, goat anti-EGFP/GFP (1:1000). After washing primary antibodies with PBS, secondary antibodies were incubated at 1:800 dilution at RT for 1 h in the dark: Alexa Fluor 647 donkey anti-rabbit (Molecular probes, A31573) and Alexa Fluor 488 donkey anti-goat (Jackson, AB2340428). Finally, nuclei were counterstained with DRAQ5 (Thermo, 62251) and samples were mounted using Fourmount-GT medium (Electron Microscopy Sciences, 17984). Images were acquired using an Olympus FV10i confocal microscope (with 405, 458, 488 and 633 nm lasers).

4.2. Perfusion and tissue sections

In other cases, SEZs were not needed for additional techniques. This was the case, for example, of SERPINB9 staining. This time, animals were deeply anaesthetized and transcardially perfused with approximately 28 ml of saline buffer (0.9% NaCl) and 83 ml of 4% PFA in 0.1 M phosphate buffer pH 7.4 (PB) at a flow rate of 5.5 ml/min. Fixed brains were carefully and then post-fixed for 1 h by immersion in 4% PFA. After abundantly washing off the fixative with PBS, brains were embedded in 4% agar and vibratome-sectioned at 30-40 µm (Leica VT1000). Sagittal sections were collected and preserved at 4 °C in 0.05% sodium azide in PBS until use.

Prior to specific antigen detection with primary antibodies, potential non-specific or reactive sites were blocked by incubating the tissue slices in blocking buffer (10% HS and 0.2% Triton X-100 in 0.1 M PBS for 1 h at RT). Next, samples were incubated with primary antibodies (anti-SERPINB9, Santa cruz, sc-390406 conjugated to AF647) diluted in blocking solution overnight at 4°C. After washing thoroughly with 0.1 M PBS, nuclei were counterstained with 4',6-diamidino-2-phenylindole (DAPI) (1 µg/ml in distilled water) for 5 min and sections were mounted with FlourSave Reagent (Calbiochem, 345789). TdTomato and EGFP detection did not require antibody staining. Images were acquired using an Olympus FV10i confocal microscope.

5. Cell phenotyping by flow cytometry

5.1. Characterization of SEZ neurogenic cells

First of all, SEZs were dissected as explained before for immunofluorescence in whole-mounts (section 4.1). Then, they were minced and enzymatically digested using the Neural Tissue Dissociation kit (T) (Miltenyi, 130-093-231) following the manufacturer's instructions in a gentleMACS Octo Dissociator (Miltenyi). Trypsin was stopped with 3 ml of 100 µg/ml trypsin inhibitor (Sigma, T6522) diluted in blocking buffer, consisting of Hanks' Balanced Salt solution (HBSS) 1x, HEPES 1 mM, EDTA 20 mM and BSA 0.5% in distilled water. The remaining tissue was mechanically dissociated by pipetting up and down with a plastic Pasteur pipette. Then, the cell suspensions were filtered through a 40 µm nylon filter and cells were pelleted (300x*g*, 10 min). Cells were washed with blocking buffer and spun down

again. Then, they were resuspended in 100 µl of blocking buffer containing fluorescently-labeled primary antibodies and incubated in the dark, on ice, for 30 min. After washing with blocking buffer, labeled samples were centrifuged and resuspended in blocking buffer, and finally analyzed. If using a biotinylated anti-GLAST antibody, this was added to the mixture with the rest of primary antibodies. Then, after washing, fluorescent streptavidin (BD, 612775, conjugated to BUV737) was incubated alone for 20 min on ice before the final washing steps and resuspension. Samples were analyzed with a LSR-Fortessa cytometer (Becton Dickinson) with 350, 405, 488, 561 and 640 nm lasers whose configuration will be detailed later (section 5.10). For live cell analysis, DAPI positive events were excluded. The markers and the gating strategy used are explained in the first section of results and are thoroughly detailed in Belenguer et al., 2020, 2021.

5.2. Characterization of cortex astrocytes

During the dissection of the SEZs, a piece of cortex was kept and processed exactly as explained for the SEZs in the previous section (5.1). $DAPI^-$ $CD45^-$ $CD31^-$ $TER119^-$ $O4^-$ $GLAST^+$ cells were considered astrocytes.

5.3. Identification of immune cells in the SEZ

To characterize immune cells, adult mice were transcardially perfused with saline solution (0.09% NaCl) with 10 U/ml of heparin for 10 min. The SEZ of 4 to 6 mice were dissected and pooled. This time, cell suspensions were prepared by mechanical digestion on ice using a dounce homogenizer (Li et al., 2019). Then, they were filtered (40 µm nylon filter), centrifuged (300x*g*, 10 min) and resuspended in blocking buffer (HBSS 1x, HEPES 1 mM, EDTA 20 mM and BSA 0.5% in distilled water) containing antibody constant region receptor (FcR) blocking reagent 1x (Miltenyi, 130-092-575). After 15 min, primary antibodies were added and incubated for 30 min on ice. Finally, cells were washed and analyzed by flow cytometry. DAPI positive events were excluded from the analysis.

5.4. Analysis of NSC cultures

Cells were harvested, centrifuged (300x*g*, 10 min), and resuspended in blocking buffer (HBSS 1x, HEPES 1 mM, EDTA 20 mM and BSA 0.5% in distilled water) containing fluorescent-labeled primary antibodies. Neurospheres were at the same time disaggregated mechanically by pipetting up and down for 20 - 25 times. Then, they were incubated for 30 min on ice. Finally, 5 ml of blocking buffer were added and cells were spun down. After resuspension in blocking buffer, cells were analyzed by flow cytometry. For live cell analysis, DAPI positive events were excluded.

5.5. Characterization of splenocytes and JEDI T cells

Spleens were perfused with blocking buffer (PBS containing 2% FCS and 2 mM EDTA), as explained for JEDI T cell isolation. Then, cell suspensions were centrifuged (500x*g*, 5 min) and resuspended in 2 ml of Red Blood Cell Lysing Buffer Hybri-Max (Sigma, R7757) to get rid of erythrocytes (RBCs). After 2-3 min incubation, more buffer was added and cells were pelleted again (500x*g*, 5 min). Then, cells were incubated with FcR blocking reagent (Miltenyi, 130-092-575). After 15 min, primary antibodies diluted in blocking buffer were added and cells were incubated for 30 min on ice. Finally, cells were washed by adding more buffer, centrifuging and resuspending, and samples were then analyzed by flow cytometry. For the characterization of purified JEDI T cells, they were centrifuged after isolation and resuspended in buffer containing antibodies. The process was then the same as for splenocytes.

5.6. Characterization of whole blood

Blood collection always coincided with the end of an experiment, and therefore mice were sacrificed by cervical dislocation for other reasons. Right after the sacrifice, the heart was exposed and a cut was done in its left ventricle. 100 µl of blood were collected with a pipette, and transferred to an eppendorf tube containing 25 µl of 0.4% heparin. Samples were diluted with blocking buffer (PBS containing 2% FCS and 2 mM EDTA), centrifuged (300x*g*, 10 min) and carefully resuspended and incubated with FcR blocking reagent (Miltenyi, 130-092-575).

After 15 min, primary antibodies were added in blocking buffer and cells were incubated for 30 min on ice. Cells were finally washed, resuspended (all in the same blocking buffer) and analyzed by flow cytometry.

5.7. Intracellular flow cytometry

If extracellular staining was also performed, primary antibodies for this purpose were incubated and washed prior to fixation. Then, pellets were resuspended in 100 µl of Fixation and Permeabilization Solution (BD, 554722). Fixed cells were spun down (300x*g*, 10 min) and resuspended in blocking buffer (HBSS 1x, HEPES 1 mM, EDTA 20 mM and BSA 0.5% in distilled water) containing 10% saponin (saponin blocking buffer). An additional washing step with the same buffer was performed and pellets were finally resuspended in saponin blocking buffer and fluorescent-labeled primary antibodies for intracellular staining. After 30 min of incubation at 4 °C, cells were washed twice with saponin blocking buffer and finally resuspended in blocking buffer without saponin. Cells were then analyzed by flow cytometry.

5.8. Determination of autophagy rate

Autophagy was assessed with the Autophagy Assay Kit (Red) (Abcam, ab270790) as indicated by the manufacturer. Briefly, NSCs were incubated for 30 min with 100 µl of Autophagy Probe 1x diluted in blocking buffer (HBSS 1x, HEPES 1 mM, EDTA 20 mM and BSA 0.5% in distilled water). Then, cells were washed, resuspended and analyzed by flow cytometry. This probe could be excited with multiple lasers and seen with several detectors. Nevertheless, the 640 nm laser and the 670/14 detector were selected as they provided the best resolution.

5.9. Data processing and quantification of protein expression

Flow cytometry data was analyzed with Flowjo, version 10.8.1. Median fluorescence intensity (MFI) was used to compare protein expression between samples or populations. MFI values were normalized by subtracting their autofluorescence, which was considered as the MFI of the corresponding fluorescence minus one (FMO) control. For intracellular staining, autofluorescence

was determined by using isotype controls. Normalized MFI values were plotted and used for statistical analysis.

5.10. Cytometer configuration

All experiments involving flow cytometry were analyzed with a LSR-Fortessa cytometer (Becton Dickinson) with 350, 405, 488, 561 and 640 nm lasers with the following configuration:

Laser (nm)	Detectors					
355	740/35	450/40	379/28			
405	780/60	710/50	660/20	610/20	525/50	450/50
488	695/40	530/30	488/10			
561	780/60	670/30	610/20	586/15		
640	780/60	730/45	670/14			

5.11. Antibodies

The biotinylated or fluorescent-labeled primary antibodies that were used in flow cytometry are the following, both for *in vivo* and *in vitro* experiments.

Antigen	Supplier	Clone	Fluorophores
CD11b	Miltenyi	M1/70.15.11.5	FITC
CD11c	BD	HL3	PerCP-Cy5.5
CD19	BD	1D3	BV605
CD24	BD	M1/69	PerCP-Cy5.5
CD3	Miltenyi	REA641	FITC / PE
CD31	BD	390	BUV395 / BV421
CD4	BD	104	BUV737
CD40	Biolegend	3/23	PE
CD44	BD	IM7	PerCP-Cy5.5
CD45	BD	30-F11	BUV395 / BV421
CD45.1	BD	A20	BV650
CD62L	BD	MEL-14	APC-Cy7
CD80	Biolegend	16-10A1	PerCP-Cy5.5
CD86	BD	GL1	BV650

CD8	Miltenyi	53-6.7	PE-Vio770
CD9	Miltenyi	MZ3	APC-Vio770
CD99	R&D	Polyclonal	PE
GLAST	Miltenyi	ACSA-1	PE / APC / biotin-BUV737
H2Kb/Db	Miltenyi	REA932	APC / VioBlue / PE-Vio770
IFNGR2	Miltenyi	REA381	PE
O4	R&D	O4	AF350 / AF405
PD-L1	BD	MIH5	BV421 / BV650
PD-L2	BD	TY25	BUV395
TCRβ	BD	H57-597	BV421
TER119	BD	TER-119	BUV395 / BV421
β2M	BD	S19.8	BUV737

6. Cell culture and in vitro procedures

6.1. Establishment of primary NSC cultures

Cultures of adult SEZ NSCs were obtained from 2 to 4-months-old mice. Dissected SEZs (as explained for whole-mount immunofluorescence) were minced and enzymatically digested with 12U papain (Worthington, LS003120) in a solution containing 0.2 mg/ml EDTA (Sigma, E6511) and 0.2 mg/ml L-cysteine hydrochloride (Sigma, C8277) in Earle's Balanced Salt Solution (EBSS) (Gibco, 24010-043). Digestion was performed for 30 min at 37 °C. Then, culture media was added and samples centrifuged at 100x*g* for 3 min. After discarding the supernatant, the tissue was mechanically dissociated in 1 ml of media by pipetting up and down to get a homogeneous cell suspension. Next, 10 ml of medium were added and samples were centrifuged (300x*g*, 10 min). Pellets were finally resuspended in media and cells seeded in 8 wells of a 48 well plate (15,000 cells/cm^2 approximately). NSCs were then incubated for 7-10 days at 37 °C in a 5% CO2 humidified incubator. In these conditions, differentiated cells die and NSCs proliferate and form floating neurospheres. A detailed protocol can be found in Belenguer et al., 2016 (Belenguer et al., 2016).

NSCs culture media was prepared as follows:

Reagent	Final concentration	Supplier	Cat. No.
DMEM-F12	1x	Gibco	13210-074
L-Glutamine	2 mM	Gibco	50320-081
Heparin sodium salt	0.7 U/ml	Sigma	H3149
Sodium bicarbonate	0.1%	Biowest	L0680-500
HEPES	5 mM	Biowest	L0180-100
Antibiotic/Antimycotic	1x	Gibco	15240-062
Apo-transferrin	0.1 mg/ml	Sigma	T2252
Bovine Insulin	5 µg/ml	Sigma	I6634
Putrescine	16 µg/ml	Sigma	T7505
Progesterone	0.2 nM	Sigma	P6149
Sodium selenite	30 nM	Sigma	S9133
BSA	50 µM	Sigma	B4287
EGF	20 ng/ml	Gibco	53003-018
bFGF	10 ng/ml	Sigma	F0291

Only when cell culture media was used for growing cells, not for washing or harvesting, EGF and basic fibroblast growth factor (bFGF) were added. This applies for the establishment of primary cultures and also for their subculture and expansion.

6.2. Subculture and bulk expansion of NSCs

Neurospheres need to be disaggregated and subcultured before they get too big, as cells in their core will suffer from oxygen and nutrient deprivation. Therefore, neurospheres were subcultured every 5 to 7 days. Besides, NSCs *in vitro* were only used for experiments before passage 7, as we have previously observed cell stress and telomere shortening later on (Ferrón et al., 2004).

For splitting, neurospheres were harvested and centrifuged at 100x*g* for 7 min. Then, spheres were enzymatically dissociated with 200 µl of Accutase solution (Sigma, A6964) for 10 min at RT. Digestion was stopped by adding cell culture media, and cells were mechanically dissociated by pipetting up and down. Then, more medium was added, cell suspensions were centrifuged (300x*g*, 10 min) and cells were resuspended in cell culture media supplemented with EGF and bFGF. Cell

concentration was measured with an automatic ADAM cell counter, and NSCs were seeded at 10,000 cells/cm^2. NSCs were kept at 37 °C in a 5% CO2 humidified incubator. A detailed protocol can be found in Belenguer et al., 2016.

6.3. Co-cultures of NSCs and T cells

For the co-culture of NSCs and JEDI T cells, 50,000 NSCs/well were seeded in 24-well plates using conventional NSCs media. The next day, 120,000 JEDI T cells were seeded on transwell inserts (0.4 µm of pore size) in X-VIVO 15 Serum-free Hematopoietic Cell Medium (Lonza). Many of these JEDI T cells were not naïve, as they were isolated from the spleen of C57BL/6JxB10D2 mice previously injected with JEDI T cells and LV.EGFP using the EasySep Mouse CD8$^+$ T Cell Isolation Kit (Stem Cell). Murine IFNγ 100 ng/ml (Preprotech, 315-05), murine IL-2 2.5 ng/ml (Miltenyi, 130-120-332), dynabeads anti-CD3/CD28 (ThermoFisher, 11456D) at a 1:1 ratio with T cells and/or anti-IFNγ blocking antibody 20 µg/ml (BioXCell, BE0055) were added together with the T cell suspension. Samples were collected for analysis 72 h later.

6.4. Plasmid amplification, gene knockdown and overexpression

Plasmids encoding short hairpin RNAs (shRNAs) or the protein of interest (CD99) were used for this purpose. For plasmid amplification, electrocompetent E. coli DH5α cells were transformed with 100 ng of plasmid DNA in 1 µl of nuclease-free water by incubating them in a thermoblock at 42 °C for 45 s. Then, they were seeded on plates with LB-agar medium containing ampicillin or kanamycin, depending on the plasmid. After overnight incubation at 37 °C, single colonies were picked and seeded in 200 ml of liquid LB with the proper antibiotic in an Erlenmeyer flask. They were incubated at 37 °C with agitation overnight. Bacterial pellets were collected after centrifugation (3,500x*g*, 15 min, 4 °C) and plasmids were purified using the Genopure Plasmid Maxi Kit (Roche, 3143422001) following the instructions provided by the manufacturer. Plasmid DNA was stored at -20 °C.

For the nucleofection of cells, 7 µg of plasmid DNA and of 2.5 million NSCs were used with a mouse neural SC nucleofector kit (Lonza, vpg-1004) following the manufacturer's instructions. Nucleofections were carried out with an Amaxa Nucleofector II (Lonza) using the following plasmids: shRNA CD99 TRCN0000077078

pLKO.1-CMV-tGFP (Sigma) for *Cd99* knock-down and CD99 Lentiviral cDNA ORF Clone, Mouse, C-GFPSpark tag (Abytek, MG50520-ACGLN) for CD99 overexpression. A pLKO.1-puro non-target shRNA control plasmid was also used for the electroporation of control cells.

6.5. Kinetic assay of MHCI export

To assess the rate of MHCI export to the cell membrane, NSCs *in vitro* were harvested, pelleted (300x*g*, 10 min) and resuspended in 100 µl of blocking buffer (HBSS 1x, HEPES 1 mM, EDTA 20 mM and BSA 0.5% in distilled water) containing 8 µg/ml of anti H2Kb/Db antibody conjugated to APC (clone REA932, Miltenyi, 130-115-587). After 45 min of incubation on ice, cells were washed and resuspended in blocking buffer. The same clone of anti H2Kb/Db antibody conjugated to VioBlue (clone REA932, Miltenyi, 130-115-592) was added at a concentration of 0.5 µg/ml. After antibody addition, samples were analyzed immediately (0 min time point) and then every 10 min. Cells were kept at RT in the dark between measurements. $DAPI^+$ cells were excluded from the analysis. Both CD99-$EGFP^+$ cells and $EGFP^-$ control cells were within the same tube, ensuring equal antibody concentrations and time points between experimental groups.

6.6. Treatments

Unless stated otherwise, treatments *in vitro* were done for 24 h. IFNγ 100 ng/ml (Preprotech, 315-05), tumor necrosis factor α (TNFα) 10 ng/ml (R&D, 410-MT-010) were used from aqueous stock solutions. Forskolin (Selleckchem, S2449), IBMX (Stemcell, 72762), Rapamycin (Selleckchem, S1039), Bafilomycin A1 (Invivogen, tlrl-baf1), Bortezomib (Tocris, 7282), Brefeldin A (Medchemexpress, HY-16592), Rhosin (Tocris, 5003) and EHT 1864 (Tocris, 3872) were dissolved in DMSO, and this was used for treating control cells. No more than 0.1% DMSO was present in NSCs culture media. For starvation, NSCs were cultured in PBS for 4h.

7. Molecular methods

7.1. Analysis of gene expression

For the quantification of gene expression, RNA extraction and RT-qPCR expression analysis were performed. RNA from SEZ homogenates and NSC cultures was extracted and purified with the RNeasy Plus Mini or Micro Kits (Qiagen, 74104 or 74034) following the manufacturer's guidelines. Then, RNA concentration was quantified using a nanodrop 2000 (Thermofisher, ND2000) and 0.3-1 µg were reverse transcribed using the PrimeScript RT reagent kit (Takara, RR037A) in the presence of 50 pmol random hexamers and 25 pmol oligo-dT primer (final volume of 20 µl). Complementary DNA (cDNA) was then diluted in RNase-free water.

Gene expression was analyzed by reverse transcription quantitative PCR (RT-qPCR) in a Step One Plus detection system (Applied Biosystems) using 5-15 ng of cDNA and predesigned TaqMan probes in a final reaction volume of 10 µl. The Premix Ex Taq Master Mix (Takara, RR390) was used with its standard amplification program for 45 cycles, with a common annealing and extension step at 60 °C. Expression levels were determined by relative quantification using both *Gapdh* and *Actb* as housekeeping endogenous controls. The TaqMan probes that were used are the following:

Gen	Reference		
Actb	Mm02619580_g1	*Ifng*	Mm01168134_m1
Cd274	Mm03048248_m1	*Irf1*	Mm01288580_m1
Gapdh	Mm99999915_g1	*Nlrc5*	Mm01243039_m1
H2K1/D1	Mm04208017_mH	*S100b*	Mm00485897_m1
		Serpinb9	Mm00777163_m1

7.2. Co-immunoprecipitation and western blotting

Neurospheres were treated with IFNγ for 3 days to maximize the expression of MHCI. Then, cells were washed with PBS containing Complete mini protease inhibitor cocktail (Roche, 11836153001) and lysed with 1 ml of NP-40 lysis buffer (10 mM TrisHCl pH 8.0, 150 mM NaCl, 1% Nonidet P40, 10% glycerol, DNasa 1x, SDS 0.2%, 1 mM $NaVO_3$, 1 mM NaF, 1 mM PMSF and Complet mini 1x). After vigorous

vortexing and 30 min of incubation on ice, samples were centrifuged at maximum speed (20817x*g*) for 15 min at 4 °C. Supernatants were then transferred to low-binding 1.5 ml eppendorf tubes and were incubated with 50 µl of protein G dynabeads (Thermofisher, 10003D) for 30 min on a rotating wheel at 4 °C for pre-clearing. After beads were magnetically removed, 50 µl of each sample (which was their 5%) were separated and incubated at 98 °C for 5 min with western blot sample buffer 1x (62.5 mM Tris-HCl pH 6.8, 10% glycerol, 1% SDS, 50 mM DTT and 0.02% bromophenol blue), and then stored at -20 °C as input samples. The rest of the precleared lysates were separated in two equal samples and incubated overnight at 4 °C with 5 µg of either goat anti-mouse CD99 antibody (R&D, AF3905) or control antibody (R&D AB-108-C) on a rotating wheel in a total volume of 1 ml (more NP-40 was added). The following day, 50 µl of protein G dynabeads were added to the samples and incubated for 20 min at 4 °C on the wheel, and then washed 4 times with NP-40 buffer (the same as for the lysis, but now containing 300 mM NaCl). Beads were finally incubated at 98 °C for 5 min with western blot sample buffer, and then removed with a magnet.

Samples were loaded into a 12% polyacrylamide electrophoresis gel (SDS-PAGE), subjected to electrophoretic separation and then transferred onto a nitrocellulose membrane using the Trans-Blot Turbo Transfer System (Bio-Rad). Potential nonspecific interactions were first blocked with 5% milk in TBS-T (0.1% Tween-20 in tris-buffered saline) for 1 h at RT. Then, membranes were incubated with mouse anti-mouse H2Kb (BD, 562832) or goat anti-mouse CD99 (R&D, AF3905) in blocking buffer (TBS-T with 5% milk), overnight at 4 °C. After thoroughly washing with TBS-T (4 times for 5-10 min), nitrocellulose membranes were incubated with horseradish peroxidase (HRP)-conjugated antibodies for 1 h at RT, and developed with either Western Lightning Plus-ECL (PerkinElmer, NEL103001EA) or SuperSignalTM West Femto Maximum Sensitivity Substrate (Thermo Scientific, 34095). Images were acquired in a Mini HD 9 chemiluminescence imaging system (Uvitec, Cambridge).

8. RNA-seq and sequence alignments

Heatmaps show row Z-scores that were calculated using RNA-seq normalised gene expression data. They were generated either using the ComplexHeatmap (Gu et al., 2016) and ggplot2 (Wickham, 2016) packages in R or GraphPad Prism Software, version 8.0.2.

Multiple sequence alignment of DNA was performed with the web tool Clustal Omega from the EMBL-EBI. Sequences were obtained from the NCBI database.

9. Statistical analysis

Statistical tests were carried out in the GraphPad Prism Software, version 8.0.2. Analyses of significant differences were assessed using unpaired (mainly for *in vivo* experiments) or paired (mainly for *in vitro* experiments where the same cultures were exposed to different conditions) two-tailed Student's t-tests or one-way ANOVA with Tukey post-hoc tests when appropriate. For RT-qPCR data, the statistical analysis was performed considering ddCt values. p-values lower than 0.05 were considered as statistically significant and referred as *p<0.05, **p<0.01, ***p<0.001 or ****p<0.0001 for t-tests, and $^{\#}$p<0.05, $^{\#\#}$p<0.01, $^{\#\#\#}$p<0.001 or $^{\#\#\#\#}$p<0.0001 for one-way ANOVA followed by Tukey multiple comparisons tests. For the comparison of MHCI export kinetics, the statistical analysis was performed using a mixed-effects model that allows the inclusion of variables as random effects. It assumed that MFIs follow a normal distribution that depends on time, EGFP positivity and the sample, and the kinetics had linearity (values at 80 min were excluded as the kinetics reached saturation and loss of linearity at that point). The *lmer* function from the *lme4* R package was used to obtain the estimates of the model by quadratic approximation using bobyqa optimizer. To assess statistical significance of the fixed effects, a Satterthwaite t-test was carried out using the *lmerTest* function from the *lmerTest* package. P values are indicated as *p<0.05, **p<0.01, ***p<0.001. Data are always presented as mean ± standard deviation (SD). The number of biological replicates (independent cultures or animals) (n) is indicated in the figure legends and often represented as dots in the graphs.

RESULTS

1. T cells do not affect neurogenic cells in steady state

1.1. The absence of lymphocytes does not affect neurogenesis

As explained in the introduction, previous studies reported that both $CD4^+$ and $CD8^+$ T cells can affect the neurogenic output in homeostasis in the dentate gyrus and the SEZ (Ziv et al., 2006). Moreover, an increased presence of $CD8^+$ T cells has been detected by single cell RNA-seq in the SEZ of old mice, where they reduce NSC proliferation by releasing IFNγ (Dulken et al., 2019). In this framework, we wanted to assess whether the absence of T lymphocytes has an impact on the neurogenic populations in the SEZ by analyzing *Rag1*$^{-/-}$ mice, which completely lack B and T lymphocytes, as Rag1 and Rag2 proteins are both essential for somatic recombination of TCR and immunoglobulin genes (Mombaerts et al., 1992). To analyze the neurogenic lineage in the absence of *Rag1*, we decided to use our recently established protocol for cell classification by flow cytometry (Belenguer et al., 2020, 2021). Briefly, SEZ dissociates were gated by size and cellular complexity to discard cell debris, myelin, dead cells as well as ependymal cells and neurons (Murayama, 2002). Then, $CD45^+$ (immune cells, mainly microglia), $CD31^+$ (endothelial), $TER119^+$ (RBCs) and $O4^+$ (oligodendrocytes) cells were negatively selected in all experiments **(Figure 1A)**. The remaining lineage-negative (Lin^-) cells were then labeled using fluorescent antibodies to GLAST and CD24 and fluorescent EGF to label the EGFR, a receptor associated with all proliferative populations of the neurogenic lineage (Codega et al., 2014) **(Figure 1B)**. CD24 is reportedly restricted to NBs and ependymal cells (Pastrana et al., 2009) and the highest CD24 levels co-distribute with PSA-NCAM, a well-known NB marker, both in the SEZ and the OB (Belenguer et al., 2020; Llorens-Bobadilla et al., 2015). The $GLAST^-$ $CD24^{high}$ fraction are NBs, which represent almost 70% of all SEZ cells, that can be subsequently subdivided into $EGFR^+$ and $EGFR^{low/-}$ pools of proliferating ENBs and non-proliferating migrating LNBs, respectively **(Figure 1C)**. $GLAST^-$ $CD24^{-/low}$ $EGFR^+$ and $GLAST^+$ $CD24^{high}$ $EGFR^+$ cells correspond to NPCs and represent around 5-6% of all cells in the SEZ **(Figure 1D)**. Within the $GLAST^+$ $CD24^{-/low}$ fraction, cells with low levels of CD9 are considered mature non-neurogenic astrocytes whereas $CD9^{high}$ NSCs can be classified into different states by GLAST intensity and fluorescent EGF binding: $GLAST^{high}$ $CD24^{-/low}$ $CD9^{high}$ $EGFR^{-/low}$ qNSCs and $GLAST^{low}$ $CD24^{-/low}$ $CD9^{high}$ $EGFR^{-/low}$ pNSCs are quiescent whereas $GLAST^{low}$ $CD24^{-/low}$ $CD9^{high}$ $EGFR^+$ aNSCs are proliferative (Belenguer et al., 2020, 2021) **(Figure 1E)**.

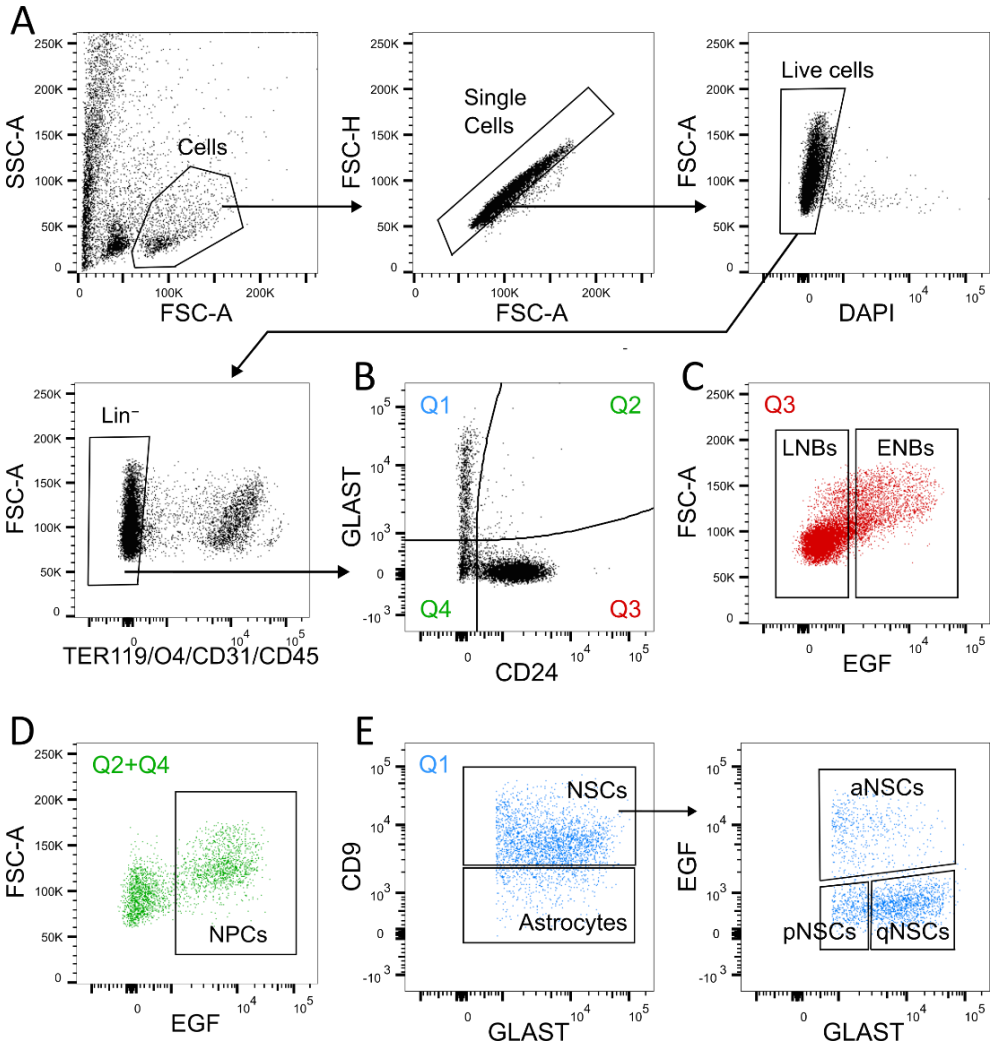

Figure 1. Gating strategy for the classification of SEZ neurogenic cells by multiparameter flow cytometry. A) Selection of neurogenic live cells. B) Cell classification based on the levels of GLAST and CD24, in Q1, Q2, Q3 and Q4. C) Subclassification of the events from Q3 in ENBs and LNBs depending on EGF binding. D) Selection of NPCs from Q2 and Q3 by EGF positivity. E) Identification of NSCs and non-neurogenic astrocytes from Q1 by CD9 expression, and categorization in quiescent, primed and activated NSCs.

Rag1 wild-type and heterozygous mice exhibited normal numbers of B (CD19$^+$) and T (CD3$^+$) lymphocytes in the spleen **(Figure 2A)**. Among splenocytes, *Rag1*$^{+/-}$ mice exhibited normal wild-type proportions of CD4$^+$ and CD8$^+$ cells **(Figure 2B)** and, therefore, they were used as control mice. Analysis of *Rag1* null two-months-old mice with our cytometry marker panel, in comparison to heterozygous mice, revealed normal proportions of the different cell types in the SEZ neurogenic lineage in the absence of lymphocytes **(Figure 2C)**. Therefore, it seems clear that nonspecific T cells do not substantially affect neurogenic cells in the young adult and healthy SEZ.

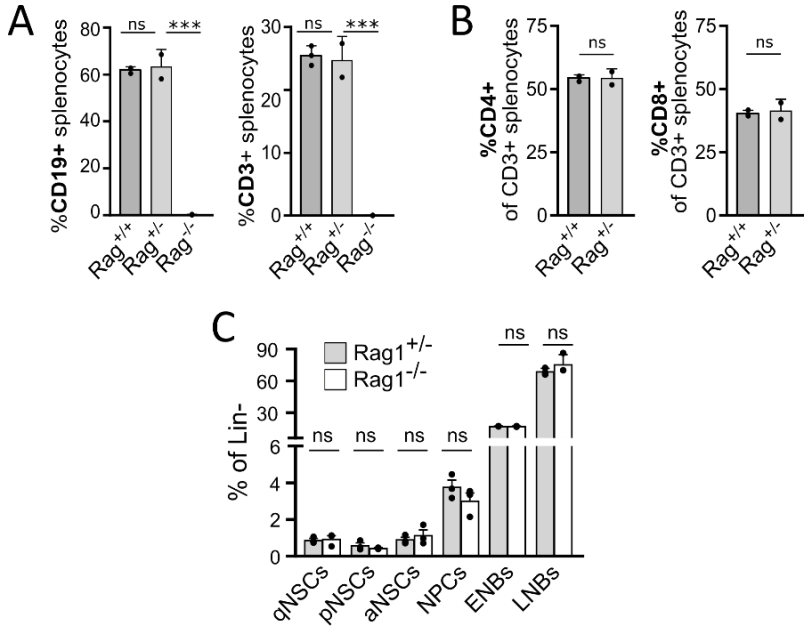

Figure 2. The absence of lymphocytes does not affect the distribution of neurogenic cell populations in the SEZ. A) Percentage of B (CD19$^+$) and T (CD3$^+$) cells in the spleen, measured by flow cytometry (n=2-3). B) Percentage of CD4$^+$ and CD8$^+$ cells among CD3$^+$ cells (T lymphocytes) in the spleen, measured by FACS. D) Characterization of SEZ neurogenic cells in Rag1$^{+/-}$ and Rag1$^{-/-}$ mice by flow cytometry (n=3). Graphs represent mean ± SD. Statistical analysis by Student's t-tests (p values are referred as ns>0.05 or ***p<0.001).

1.2. The steady-state SEZ might contain scarce T cells

Despite being a controversial matter, different studies have described the presence of $CD4^+$ and $CD8^+$ T cells in the healthy brain parenchyma (Pasciuto et al., 2020; Smolders et al., 2018; Song et al., 2016; Xie et al., 2015). Interestingly, $CD3^+$ cells have been described around the walls of the ventricles, adjacent to neurogenic niches (Ziv et al., 2006), and the resolving power of single cell deep RNA-sequencing has allowed the detection of rare T cells in the healthy SEZ of old mice (Dulken et al., 2019). Flow cytometry has great sensitivity and allows the pooling of SEZs from different mice, increasing the capacity to detect events of very low frequency. We applied this technique and tried to identify T cells in the SEZ of young adult healthy mice. We thoroughly perfused animals with saline solution and heparin to minimize blood contamination, dissected the SEZ, homogenized the tissue and pooled the cell suspensions obtained from the SEZs of 6 mice. $CD4^+$ T cells ($CD45^{high}$ $CD11b^-$ $TCR\beta^+$ $CD4^+$), $CD8^+$ T cells ($CD45^{high}$ $CD11b^-$ $TCR\beta^+$ $CD8^+$) and RBCs ($TER119^+$) were stained. Despite performing a prolonged perfusion, remaining RBCs were detected in the samples. A few T cells were also found in the SEZ of these mice **(Figure 3A)** which, relative to RBCs, were clearly enriched compared to peripheral blood **(Figure 3B)**.

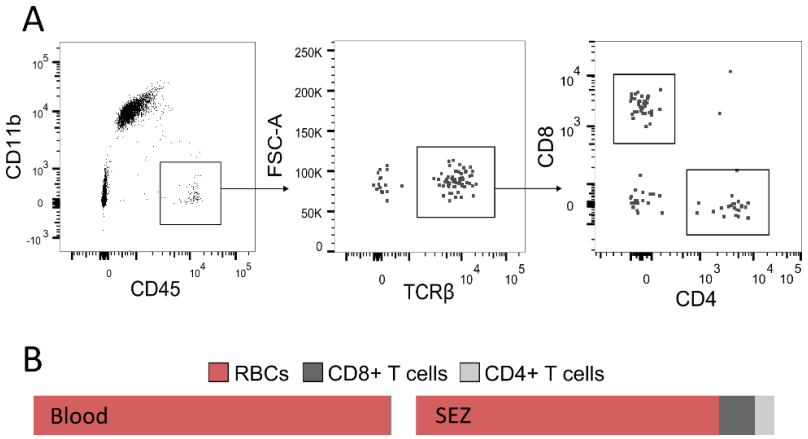

Figure 3. T cells are rare in the healthy SEZ of young adult mice. A) Dot plots showing flow cytometry data analyzing T cells in the SEZs of 6 2-months-old mice after perfusion with saline and heparin. B) Proportion of T cells ($CD45^{high}$ $CD11b^-$ FSC^{low} $TCR\beta^+$) and RBCs ($TER119^+$) in the SEZ and in peripheral blood. Plots show a representative experiment pooling the samples of 6 mice, but the whole process was performed three different times with similar results.

This suggests that residual contamination with blood does not account for all of the T cells that were found. However, the lymphocytes detected could have been attached to blood vessels or brain interfaces and thus resisted perfusion. In any case, it seems that T cells might be present in the SEZ, but they are extremely rare. This does not mean they do not have the potential to establish specific cell-cell interactions in the proper circumstances. In fact, previously activated T cells can enter the brain parenchyma (Engelhardt and Ransohoff, 2012; Mundt et al., 2019a; Schläger et al., 2016) and neoantigens can potentially appear in NSCs (Lee et al., 2018) as in any other cell type and drain into SLOs (Engelhardt et al., 2017; Mastorakos and McGavern, 2019; Papadopoulos et al., 2020).

2. Quiescent but not activated NSCs evade cellular immunity

2.1. Immune surveillance in the brain can be studied by using JEDI T cells

We next set out to evaluate whether NSCs and their progeny can be surveilled by activated $CD8^+$ T cells. The appearance of neoantigens is a stochastic process that happens with very low frequency and, therefore, in order to study and measure CTL-mediated killing, we need systems where many activated CTLs can encounter cells that express their specific antigen-MHCI. Although different models have been created for this purpose, most of them rely on the same idea. This is, transferring monoclonal $CD8^+$ T cells, all with the same TCR, into mice expressing their specific antigen-MHCI complex (Bertrand, 2014; Cho et al., 2020). In the same manner, we decided to test whether NSCs in the adult SEZ could be susceptible to T cell surveillance by using a previously reported protocol that evaluates the interaction between EGFP or GFP-expressing cells and $CD8^+$ T cells (Agudo et al., 2015). The technology is based on the use of EGFP-specific $CD8^+$ T lymphocytes isolated from JEDI mice. This mouse strain was generated by somatic nuclear transfer using $EGFP_{200\text{-}208}$-specific T lymphocytes, isolated from the F1 progeny of BALB/c and C57BL/6 mice vaccinated with EGFP, as nuclear donors (Agudo et al., 2015). All $CD8^+$ T cells in these mice carry a TCR that specifically recognizes the corresponding GFP/EGFP epitope if presented on H2Kd, whose coding allele is present in a number of mouse strains, including BALB/c or C57BL/6 strains B6D2 and B10D2 (Agudo et al., 2015, 2018). From now on, we will refer to these EGFP-specific $CD8^+$ T cells as

JEDI T cells. Adoptive transfer of JEDI T cells in a mouse has to be combined with vaccination with GFP/EGFP to activate the transferred cells. In this way, naïve JEDI T cells are first activated by DCs in lymph nodes and, potentially, can thereafter attack any EGFP/GFP-expressing cell in the body (Agudo et al., 2015, 2018; Baldominos et al., 2022).

We first decided to corroborate that the combination of the adoptive transfer of JEDI T cells with vaccination with in-house generated lentiviruses engineered to encode EGFP (LV.EGFP) resulted in the efficient activation of JEDI T cells. Highly pure suspensions of naïve JEDI T cells were obtained from the spleens of JEDI mice by negative magnetic cell sorting to exclude those cells expressing CD4, CD11b, CD11c, CD19, CD44, CD45R/B220, CD49b, TCRγ/δ or TER119. Next, by i.v. injection in the retro-orbital sinus, we transferred $5{\cdot}10^6$ JEDI T cells and $2{\cdot}10^8$ TU/mice LV.EGFP into two-months-old wild-type C57BL/6-B10D2 mice **(Figure 4A)**. A sign of efficient activation was a 3 to 4-fold increase in spleen size and weight 7 days after the injection **(Figure 4B, C)**. Moreover, almost all JEDI T cells recovered from the spleen of the transferred mice were activated, as they were $CD44^+$ $CD62L^-$, contrary to splenocytes immediately isolated from the JEDI mice (which are considered as day 0) **(Figure 4D)**. Because activation of JEDI T cells is key in these experiments and virus production and titration may exhibit some variability, we also tried a lower dosage of $0.5{\cdot}10^8$ (0.25x) TU/mice and found that JEDI T cells were also fully activated, with a significant increase in spleen weight **(Figure 4E)** and almost 100% of them in the spleen being $CD44^+$ $CD62L^-$ one week after the injection **(Figure 4F)**, meaning that small variabilities in virus handling do not affect the results. As an additional control, we then decided to analyze the cell populations of the SEZ neurogenic lineage by flow cytometry in wild-type C57BL/6-B10D2 mice, bearing no EGFP cells, injected with JEDI T cells and LV.EGFP. We confirmed that activated CTLs had no effect on the neurogenic populations of the SEZ in the absence of $EGFP^+$ cells **(Figure 4G)**. Therefore, we decided to use uninjected mice as controls for the rest of the experiments.

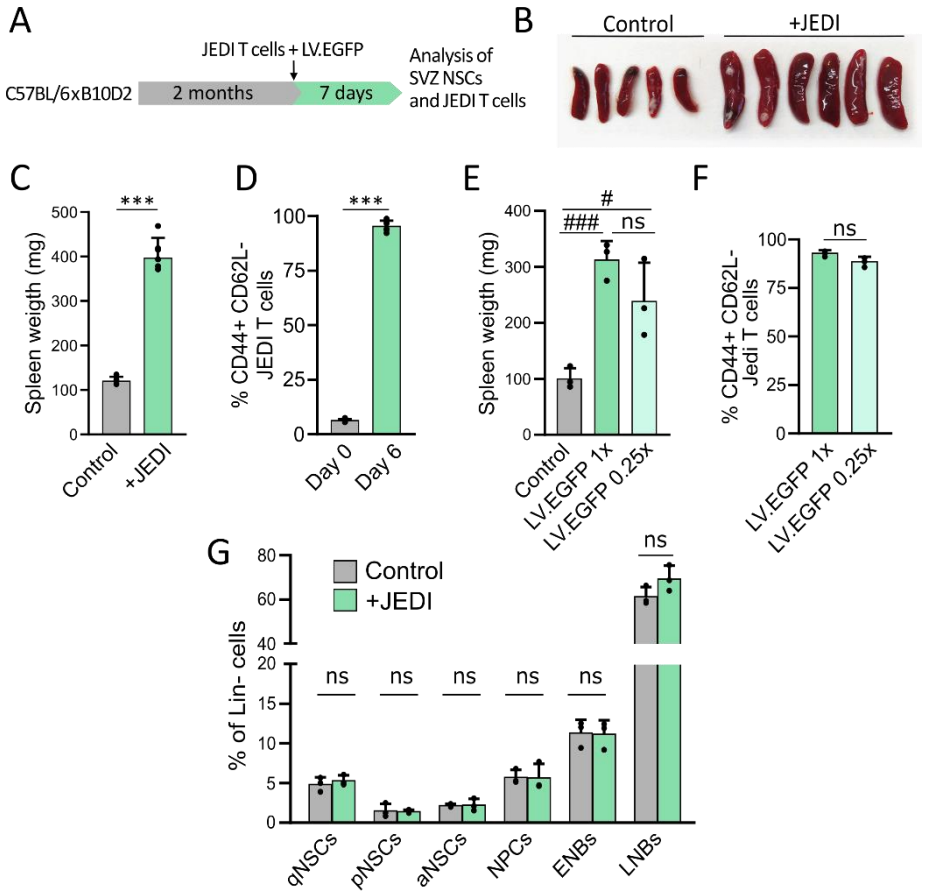

Figure 4. JEDI T cells are activated *in vivo*. A) Basic experimental workflow for the assessment of CTL-mediated killing capacity using JEDI T cells. B) Picture of the spleens of injected mice (n=6) and their controls (n=5) 7 days after the injection of JEDI T cells and LV.EGFP. C) Weight of the spleens shown in B. D) Proportion of activated JEDI T cells ($CD44^+$ $CD62L^-$) in the spleen of receptor mice (n=6), measured by flow cytometry. E) Weight of the spleens a week after the injection of JEDI T cells and 1x or 0.25x LV.EGFP dosage (n=3). F) Characterization of JEDI T cells ($CD45.1^+$ $TCR\beta^+$ $CD8^+$) in the spleen of the mice in E by flow cytometry (n=3). G) Characterization by FACS of the neurogenic populations in the SEZ of mice injected with JEDI T cells and LV.EGFP or in uninjected controls (n=3). Graphs represent mean ± SD. Statistical analysis was carried out by Student's t-tests (p values are referred as ns>0.05 or ***p<0.001) or one-way ANOVA followed by Tukey multiple comparisons tests (p values are indicated as ns>0.05, $^{\#}$p<0.05 or $^{\#\#\#}$p<0.001).

2.2. JEDI T cells do not kill quiescent NSCs

We next set out to analyze the effect of injecting JEDI T cells into mice expressing EGFP in the SEZ neurogenic lineage. To do that, we used the R26mTmG mouse strain, a Cre-dependent double-fluorescent reporter line which constitutively expresses a floxed membrane-targeted tandem dimer Tomato (TdTomato) (mT) reporter in the R26R locus. This can be excised by Cre-mediated recombination to unleash the expression of a membrane-targeted GFP (mG) also present in the knock-in construct (Muzumdar et al., 2007). Breeding of this strain with a hGfap-Cre mouse line produces recombination of the reporter in postnatal SEZ $GFAP^+$ NSCs and all their descending progeny, as well as in astrocytes (Zhuo et al., 2001). As expected, this strategy generated mice expressing GFP, but not TdTomato, in almost all cells of the SEZ neurogenic lineage and astrocytes **(Figure 5A, B)**. R26mTmG;hGfap-Cre mice were crossed with B10D2 mice as JEDI T cells only recognize $EGFP_{200\text{-}208}$ when it is presented by H2Kd. The F1 progeny was injected at two months of age with $10{\cdot}10^6$/mouse JEDI T cells together with $2{\cdot}10^8$ TU/mouse of LV.EGFP and we waited for 10 days so the immune response could fully develop **(Figure 5C)**. We then monitored the activation of the JEDI T cells ($CD45.1^+$, $CD8^+$) present in the SEZ by measuring CD44 expression **(Figure 5D)**. To confirm that JEDI T cells do infiltrate the SEZ, $CD45.1^+$ cell extravasation was detected by immunofluorescence in SEZ whole-mounts **(Figure 5E)**. We also observed images of JEDI CTLs in close contact with $EGFP^+$ cells **(Figure 5F)**.

The total count of $EGFP^+$ cells in SEZ dissociates by flow cytometry was clearly reduced in the JEDI-injected mice **(Figure 6A)**, indicating that JEDI T cells were actually capable of killing EGFP-expressing cells. Interestingly, not all neurogenic populations were affected similarly. Cell phenotyping by flow cytometry indicated that, while aNSCs and their progeny were clearly reduced, the number of qNSCs and pNSCs did not change at all **(Figure 6B)**. The reduction in NPCs and NBs could be either a direct consequence of JEDI T cell-mediated killing or an indirect effect derived from the reduction in aNSCs. However, this data does indicate that aNSCs are susceptible to CTL-mediated killing whereas the two populations of quiescent NSCs (q and p) are resistant to CTLs. As previously described in the periphery, quiescent NSCs evade surveillance by CTLs (Agudo et al., 2018). In line with this, images obtained by immunofluorescence showed that many of the EGFP-expressing cells in the SEZ that were in contact with JEDI T cells were positive for

the proliferation-related antigen Ki67 **(Figure 6C)**. Almost 40% of all infiltrating JEDI T cells were clearly contacting Ki67$^+$ cells. Subependymal EGFP$^+$ Ki67$^+$ cells correspond to aNSCs, NPCs and ENBs and, as we had previously characterized the SEZ of these mice by flow cytometry, we know that these populations represent approximately 10% of EGFP-expressing cells within the SEZ of these animals. We could also observe consistently that these JEDI T cells were larger and Ki67+ **(Figure 6C)**, both signs of activation. The data together suggest that JEDI T cells were preferentially attracted to proliferating neurogenic cells or stayed longer after contacting them compared to resting NSCs or LNBs.

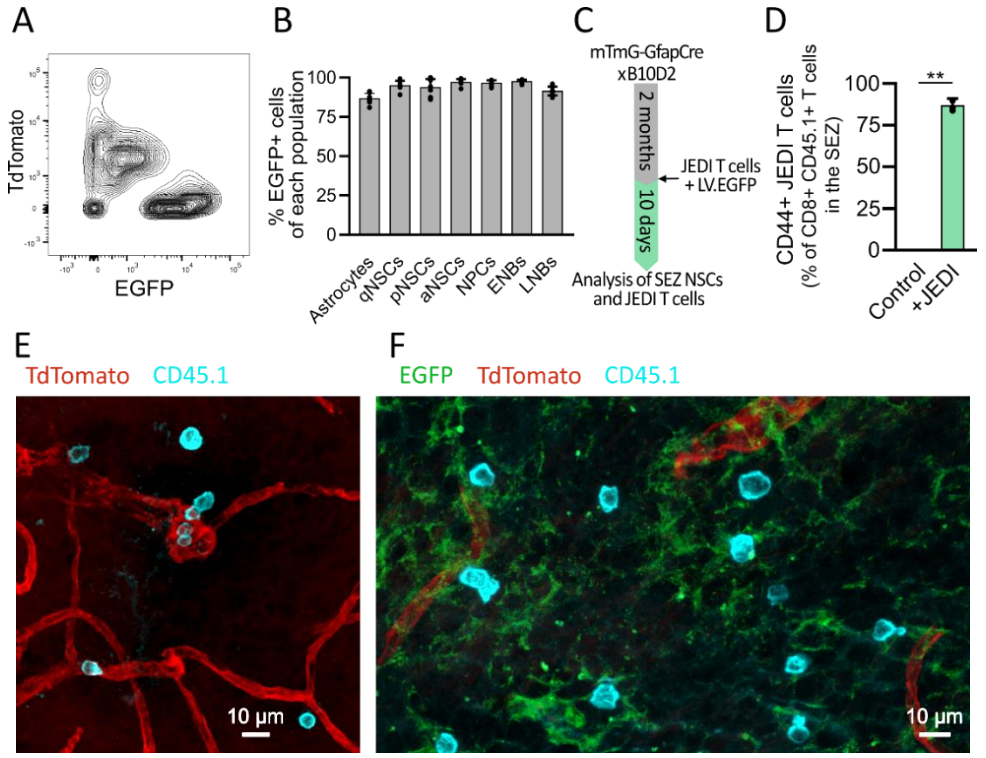

Figure 5. JEDI T cells infiltrate the SEZ and contact EGFP$^+$ cells in the mTmG-GfapCre model. A) Contour plot showing the expression of EGFP and TdTomato in SEZ cells from R26mTmG;hGfap-Cre mice. B) Percentage of EGFP$^+$ cells among SEZ astrocytes and neurogenic populations (n=8). C) Experimental workflow for the assessment of T cell killing capacity. D) Percentage of CD44$^+$ JEDI T cells (CD45.1$^+$ CD8$^+$) in the SEZ of injected and uninjected mice (n=3). E, F) immunofluorescence of SEZ whole-mounts of mice injected as indicated in C. CD45.1 (cyan), TdTomato (red) and EGFP (green) are shown. Graphs represent mean ± SD. Statistical analysis by Student's t-tests (p value is referred as **p<0.01).

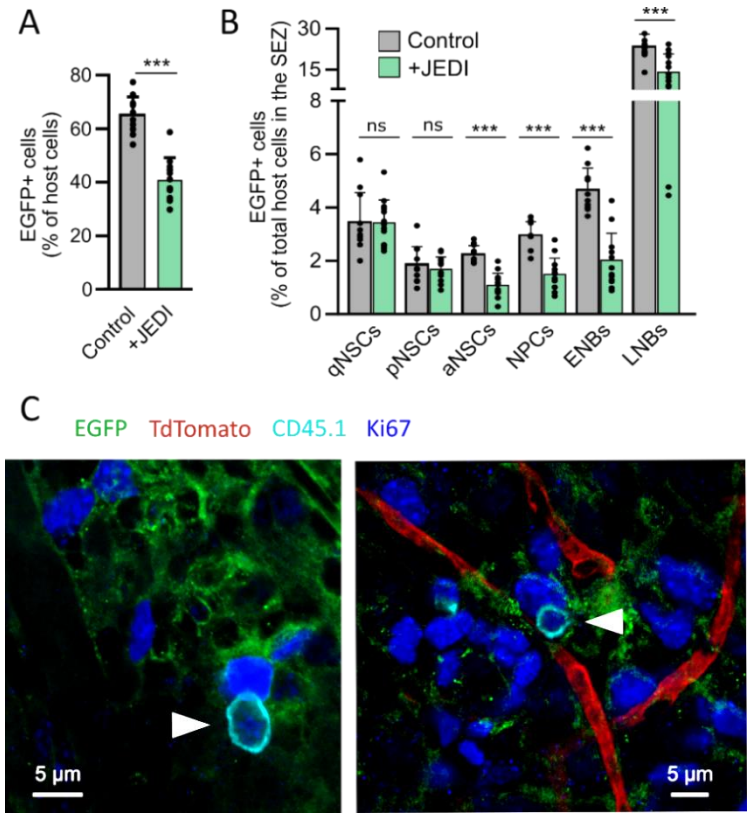

Figure 6. Quiescent NSCs resist JEDI T cell-mediated killing in the R26mTmG;hGfap-Cre model. A) Total EGFP⁺ cells in the SEZ of injected (+JEDI) (n=13) and uninjected (control) mice (n=11). B) Percentage of EGFP⁺ cells among each neurogenic population, relative to all cells isolated from the SEZ (except from EGFP⁻ TdTomato⁻ cells that were essentially transferred cells). n=13 in the injected group and n=11 in the control group. C) Immunofluorescence of SEZ whole-mounts of mice from the injected group. CD45.1 (cyan) marks JEDI T cells (white arrows), Ki67 (dark blue) stains positive in proliferating cells, TdTomato (red) is expressed by the endothelium, and EGFP (green) marks neurogenic cells and astrocytes. Graphs represent mean ± SD. Statistical analysis by Student's t-tests (p values are referred as ns>0.05 or ***p<0.001).

In proliferating populations of the SEZ lineage, the JEDI T cells did not eliminate all EGFP-expressing cells indicating more resistance to JEDI T cell-mediated killing than in the periphery, where virtually no EGFP$^+$ cells survived in similar conditions (Agudo et al., 2015, 2018). In order to test whether a partial response to T cells is characteristic of a healthy brain environment and not something specific of the SEZ microenvironment, we took advantage of the fact that astrocytes are EGFP$^+$ in the brain of R26mTmG;hGfap-Cre mice and analyzed the effects of JEDI T cells in the cerebral cortex. We could recover JEDI T cells from the cortex, although in lower proportions than in the SEZ **(Figure 7A)**. A fraction of EGFP-expressing cortical astrocytes were lost in the animals exposed to JEDI T cells, although around half of them still survived **(Figure 7B)**.

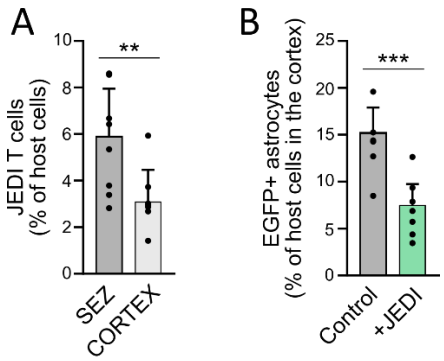

Figure 7. JEDI T cells do not completely eliminate EGFP$^+$ cells in the brain. A) Infiltration of JEDI T cells (EGFP$^-$ TdTomato$^-$ CD45.1$^+$) in the SEZ (n=8) and the cortex (n=7) of R26mTmG;hGfap-Cre mice previously injected with LV.EGFP, relative to total host cells (EGFP$^+$ or TdTomato$^+$) within the tissue, measured by FACS. B) EGFP$^+$ astrocytes (CD45/O4/CD31/Ter119$^-$ GLAST$^+$) in mTmG-GfapCre mice previously injected with JEDI T cells and LV.EGFP (n=7) or in uninjected controls (n=6). Graphs represent mean ± SD. Statistical analysis were performed by Student's t-tests (p values are referred **p<0.01 or ***p<0.001).

This is in contrast with previous studies reporting a complete elimination of EGFP-expressing cells by JEDI T cells. For instance, infiltrating JEDI T lymphocytes, which were the 3% of cells, were able to completely eliminate EGFP$^+$ SCs in hair follicles, which initially represented the 6% of cells in the tissue. The same happened in the skeletal muscle, where JEDI T cells represented 9% of cells and yet they could

eliminate all EGFP$^+$ ones, which constituted the 5% of total cells (Agudo et al., 2018). In our case, infiltrating JEDI T cells were approximately 6% and 3% of cells in the SEZ and the cortex, respectively, whereas around 75% of all cells within the SEZ and 30% within the cortex were EGFP$^+$. Therefore, a possible explanation for the partial killing effect of JEDI T cells could be that the numbers of those who get access to the brain were not enough to eliminate all the target cells. Complete elimination of cells inside the brain by JEDI T cells had already been shown in CX3CR1-EGFP knock-in mice, in which all microglial cells express EGFP, but under conditions of irradiation-induced neuroinflammation (Agudo et al., 2015).

We, therefore, decided to use a second model of EGFP expression in neurogenic cells which yields fewer positive cells. C57BL/6 and B10D2 mice were crossed, and their F1 progeny electroporated *in utero* at E15.5 **(Figure 8A)**. A transposon carrying an EGFP cDNA (PB-CAG-EGFP) and a transposase-encoding cDNA controlled by the Glast promoter (GLAST-Transp) for its activation in GLAST$^+$ NSCs were introduced in the lateral ventricles of the embryos. By doing so, we transduced cells that line these cavities, which include NSCs. Therefore, cells incorporating both plasmids integrate the reporter and become, together with all their cell progeny, EGFP$^+$ as observed by flow cytometry **(Figure 8B)** and immunocytochemistry **(Figure 8C)** in fetally-electroporated mice at two months of age. This time, a dosage of $5{\cdot}10^6$ naïve JEDI T cells in each receptor mouse was enough to kill most EGFP$^+$ neurogenic cells in the SEZ after 10 days **(Figure 8D)**, suggesting that the limited trafficking of T cells in the brain may need to be considered when evaluating immune surveillance. Interestingly, although JEDI T cells eliminated most EGFP-expressing cells from most neurogenic populations, they were, again, unable to kill qNSCs **(Figure 8E)**. The results together indicate that quiescent SCs escape T cell surveillance also in the CNS.

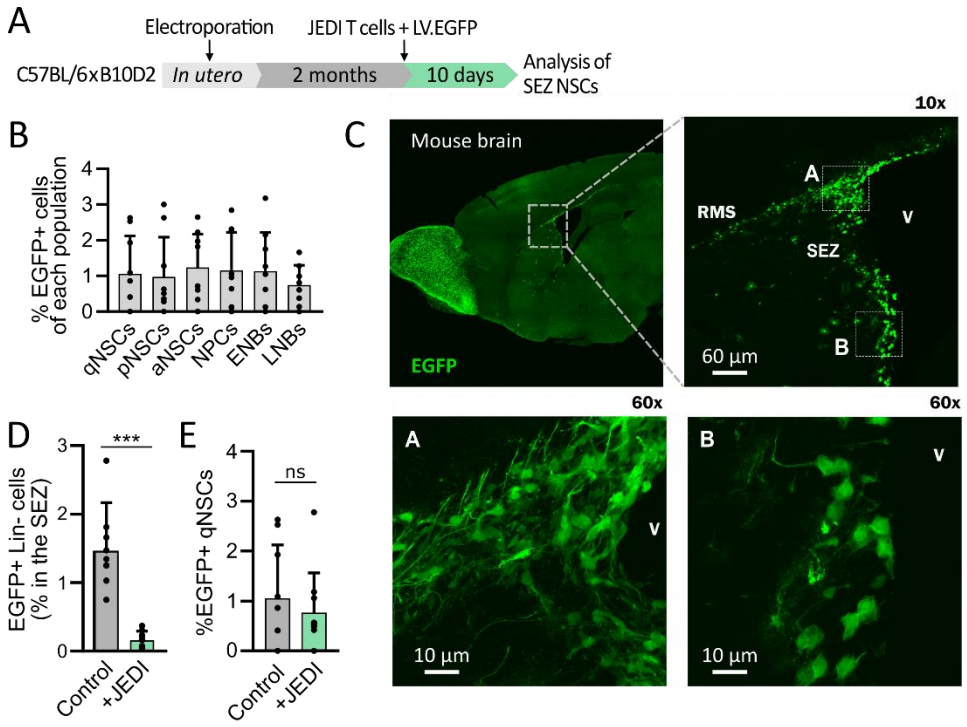

Figure 8. Quiescent NSCs resist JEDI T cell-mediated killing in a model of *in utero* electroporation. A) Experimental workflow for the assessment of T cell killing capacity in a model of *in utero* electroporation. B) Percentage of EGFP$^+$ cells within each neurogenic population in the SEZ in 2-months-old mice after electroporation *in utero* (n=9). C) Immunofluorescence showing EGFP$^+$ (green) cells in the SEZ in mice electroporated as in B. The lateral ventricle is indicated as "V". D) Proportion of neurogenic (Lin$^-$) EGFP$^+$ cells in the SEZ (n=9 in the control group and n=10 in the injected group). E) Percentage of EGFP$^+$ qNSCs, as measured by flow cytometry 10 days after the adoptive transfer of JEDI T cells and LV.EGFP (n=9-10). Graphs represent mean ± SD. Statistical analysis by Student's t-tests (p values are referred as ns>0.05 or ***p<0.001).

3. A dynamic balance between opposing signals correlates with immune evasion

3.1. MHCI is differentially induced in quiescent and activated NSCs

CTL-mediated killing requires presentation of intracellular antigens loaded into the antigen-binding groove of MHCI surface molecules. MHCI is generally expressed by all nucleated cells outside the brain, although recent reports have indicated that, in some tissues, resting SCs do not exhibit detectable surface levels of MHCI due to NLRC5-dependent transcriptional regulation (Agudo et al., 2018). Although MHCI has been detected by immunocytochemistry in brain Nestin^{+} cells during fetal development (Chacon and Boulanger, 2013), MHCI subunits have only been detected at the messenger RNA (mRNA) level in adult NSCs (Lin et al., 2021; Liu et al., 2015, 2013). The surprising lack of information on MHCI in NSCs at the protein level prompted us to analyze by flow cytometry the membrane levels of the MHCI subunits H2Kb and H2Db α-chains (the classical HCs expressed in C57BL/6 mice), both recognized by the same antibody, and β2M in the different neurogenic populations of the SEZ. We could not detect surface levels of any of these MHCI components in cells of the neurogenic lineage, while microglial cells, which were used as controls, stained positive **(Figure 9A)**. This indicates that NSCs and their progeny do not present antigens under resting conditions. However, MHCI genes can be induced by IRF transcription factors, which are activated by IFNs, and by NF-kB, whose activity can be triggered by TNFα (Kobayashi and Van Den Elsen, 2012). IFNγ is the main cytokine produced by CTLs and a potent inducer of antigen presentation (Abbas et al., 2016; Castro et al., 2018; Kobayashi and Van Den Elsen, 2012), and TNFα is produced during inflammatory situations and has been described to activate NSCs while favoring the maintenance of the qNSC pool (Belenguer et al., 2020). Therefore, we treated NSCs *in vitro*, which did not express MHCI constitutively, with both cytokines to see whether they had an effect on MHCI levels. While TNFα did not affect antigen presentation, IFNγ strikingly up-regulated the levels of MHCI subunits H2Kb/Db and β2M **(Figure 9B)**. As expected, we could confirm a transcriptional induction of *Irf1* (an IFNγ target gene), *Nlrc5* (a positive regulator of MHCI), and the MHCI genes *H2-K1* and *H2-D1* (detected together by the Taqman probe) in response to IFNγ by RT-qPCR **(Figure 9C)**.

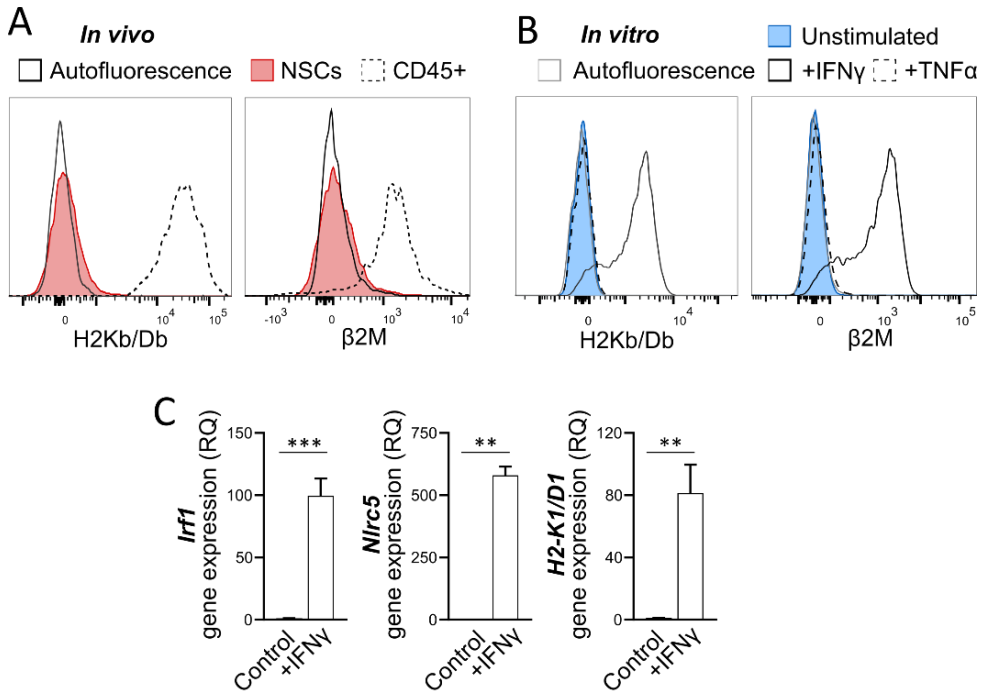

Figure 9. NSCs do not express MHCI in resting conditions but can induce it in response to IFNγ. A) Histograms obtained by flow cytometry showing the expression of the indicated MHCI subunits in NSCs and CD45+ cells in the SEZ. B) The same as in A for NSCs *in vitro* unstimulated or treated with IFNγ or TNFα for 24h. All plots in A and B show the concatenation of 5 biological replicates. Autofluorescence is the FMO control. B) Relative gene expression data measured by RT-qPCR of NSCs treated with IFNγ as in B (n=3). Graphs show mean ± SD. Statistical analysis by Student's t-tests (p values are referred as **p<0.01 or ***p<0.001).

Next, we tried to induce MHCI expression also *in vivo*. The i.p. injection of LPS induces systemic inflammation affecting the SEZ, where TNFα is highly up-regulated (Belenguer et al., 2020). Although at a lower level, *Ifng* is also induced in the SEZ in this model **(Figure 10A)**, and NSCs have receptors for IFNγ **(Figure 10B**; and Dulken et al., 2019**)**. However, LPS did not induce the expression of MHCI in NSCs **(Figure 10C)**. Also, an increase in IFNγ has been described in the SEZ of old mice (Dulken et al., 2019), but we could barely see MHCI expression in NSCs from 18-months-old mice either **(Figure 10D)**.

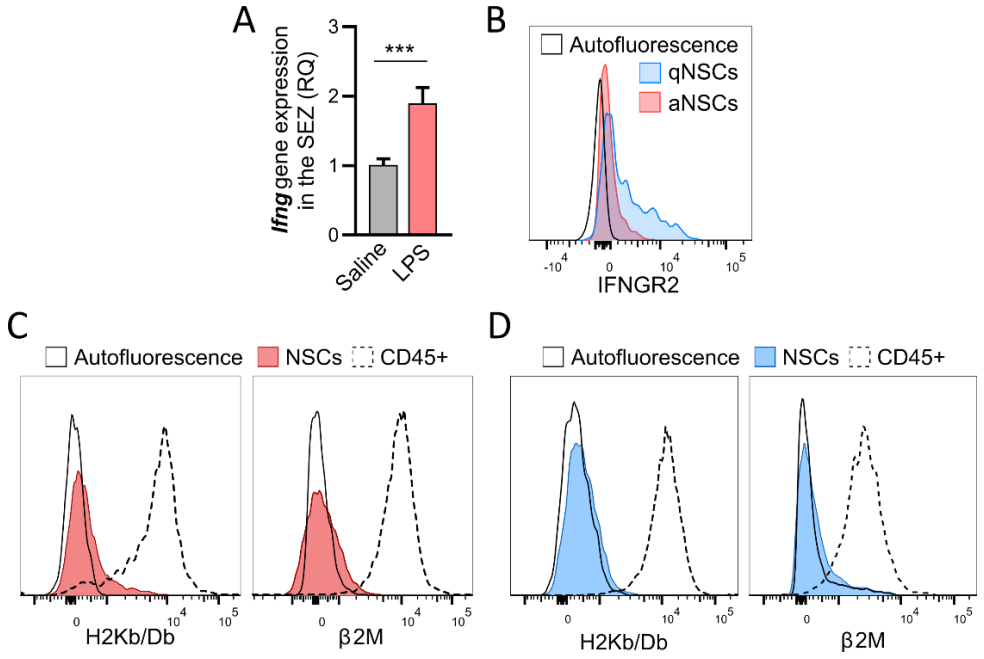

Figure 10. NSCs *in vivo* do not induce MHCI with LPS or with aging. A) *Ifng* relative gene expression measured by RT-qPCR in the SEZ of mice treated with LPS i.p. (5 mg/kg) for 24 h (n=5). Graph represents the mean ± SD. Statistical analysis by Student's t-tests (p value is referred as ***p<0.001). B) Histograms showing the expression of IFNGR2 measured by FACS in NSCs *in vivo*. C) Histograms obtained by flow cytometry showing the expression of MHCI in NSCs directly isolated from wild-type mice treated with LPS as in A. D) Expression of the indicated proteins in NSCs of 18-months-old C57BL/6 mice in homeostatic conditions. All histograms in B, C and D show the concatenation of 5 biological replicates. Autofluorescence is the FMO.

Nevertheless, the increase in IFNγ in the SEZ with age and after the injection of LPS is probably much smaller than during a T-cell mediated immune response. Therefore, to try to reconcile the absence of functional MHCI with the loss of EGFP$^+$ cells after the exposure to JEDI T cells *in vivo*, we evaluated H2Kb/Db levels in R26mTmG;hGfap-Cre mice after the injection of JEDI T cells and LV.EGFP. This time, *Ifng* and *Irf1* were induced much more strongly than with LPS **(Figure 11A)**, and we found that all cells of the lineage exhibited surface MHCI molecules. Interestingly, the levels *per* cell differed among populations: the highest expression was found in aNSCs while quiescent NSCs exhibited much lower levels **(Figure 11B)**. To get a clearer idea of the potential relevance of MHCI levels in these conditions, we

compared the levels of MHCI in NSCs and astrocytes from the SEZ as well as in cortical astrocytes (CD45$^-$ TER119$^-$ CD31$^-$ O4$^-$ GLAST$^+$), with those of splenic CD4$^+$ (CD45$^+$ CD3$^+$ CD4$^+$) and CD8$^+$ (CD45$^+$ CD3$^+$ CD8$^+$) T cells, and splenic DCs (CD45$^+$ CD11c$^+$ CD8$^+$), both basally and during a T cell-mediated immune response. In the second condition, the surface level of MHCI in aNSCs was higher than in T lymphocytes, and even relatively comparable with that of DCs **(Figura 11C)**.

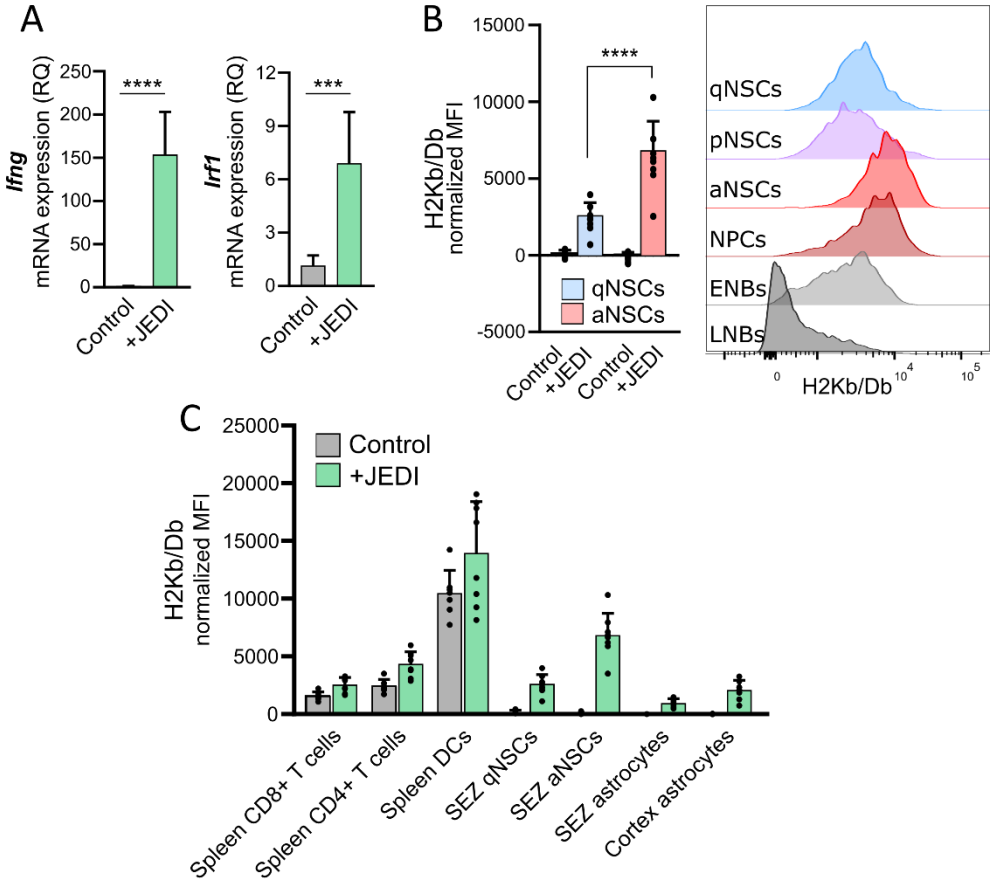

Figure 11. aNSCs up-regulate MHCI more than qNSCs when exposed to JEDI T cells *in vivo* in R26mTmG;hGfap-Cre mice. A) *Ifng* and *Irf1* relative gene expression measured by RT-qPCR in the SEZ of mice injected with JEDI T cells and LV.EGFP or in uninjected controls (n=8). B) H2Kb/Db expression measured by flow cytometry in NSCs and their progeny. Histograms show the concatenation of 8 biological replicates and only represent the +JEDI group. C) H2Kb/Db expression measured by FACS in the indicated cell types in the same conditions as in A and B (n=7/8). Graphs represent mean ± SD. Statistical analysis by Student's t-tests (p values are referred as ***p<0.001 or ****p<0.0001).

CTLs can induce the expression of MHCI genes by a number of mechanisms (Castro et al., 2018). In order to test the possibility that the expression was induced by the presence of activated JEDI T cells in the SEZ, we injected them into CX3CR1-EGFP C57BL/6-B10D2 mice and evaluated the levels of MHCI in cells of the neurogenic lineage **(Figura 12A)**. This time, microglia, instead of NSCs, were the specific target of JEDI T cells in the SEZ, but the levels of antigen presentation increased in the cells of the EGFP-negative neurogenic lineage. As we already observed in R26mTmG;hGfap-Cre mice, aNSCs induced MHCI expression much more than qNSCs **(Figure 12B)**. The results suggested that CTLs were likely inducing MHCI molecules through cytokine release, as *Ifng* and *Irf1* were highly induced in the SEZ **(Figure 12C)**.

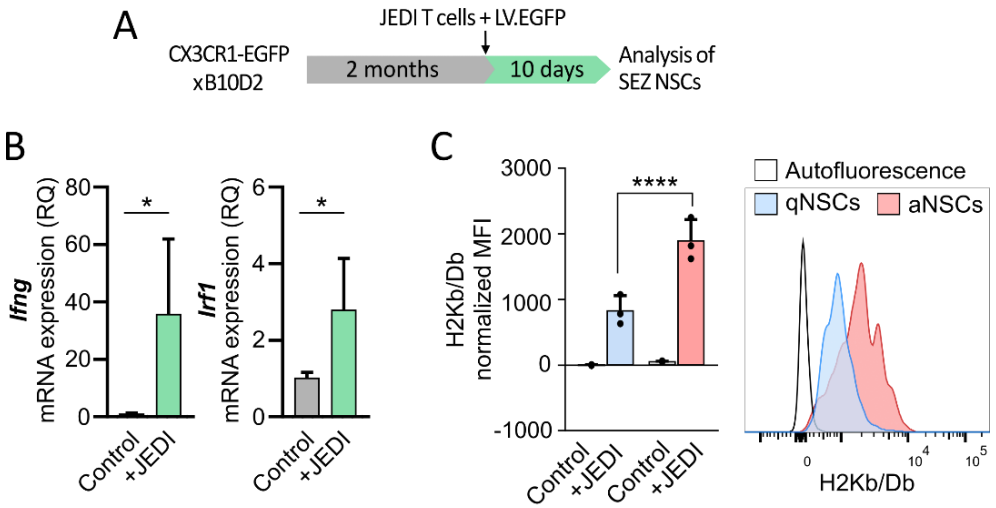

Figure 12. aNSCs up-regulate MHCI more than qNSCs when exposed to JEDI T cells *in vivo* in the Cx3Cr1-EGFP model. A) Experimental design. B) *Ifng* and *Irf1* relative gene expression measured by RT-qPCR in the SEZ of mice injected with JEDI T cells and LV.EGFP or in uninjected controls (n=4). C) H2Kb/Db expression measured by flow cytometry (n=4 for controls and n=3 in injected mice) in NSCs from the same mice of A and B. Histograms show the concatenation of all biological replicates and only the +JEDI group. Graphs represent mean ± SD. Statistical analysis were performed by Student's t-tests (p values are referred as *p<0.05 or ****p<0.0001).

3.2. Additional mechanisms protect qNSCs

Lower levels of MHCI in the membrane of qNSCs alone are unlikely to fully explain their resistance to CTL-mediated killing. The interaction between a CTL and a cell exposing its cognate antigen-MHCI can result in killing or not, depending on the balance between co-stimulatory and co-inhibitory signals provided by the APC. Moreover, additional mechanisms such as the expression of specific serpins, which can inhibit granzymes, can contribute to the survival of the target cell. As a first approach to uncover potential additional mechanisms that could underlie the different susceptibility of qNSCs and the rest of the lineage we interrogated our bulk RNA-seq datasets of the different neurogenic populations of the SEZ (Belenguer et al., 2020). First of all, to see whether qNSCs had general transcriptomic differences when compared with the rest of the lineage, we assessed the expression of the genes included in the GOs ``*Regulation of T cell activation"* and "*T cell mediated immunity"*. Interestingly, quiescent NSCs (qNSCs and pNSCs) show a very differentiated transcriptome in these categories when compared to other neurogenic populations **(Figure 13)**.

Next, we focused specifically on those genes potentially modulating the interaction between neurogenic cells exposing MHCI and CTLs by concentrating our analysis on transcripts encoding ligands of immune checkpoints or co-inhibitors (most co-stimulators are absent in the dataset, indicating that they are not expressed significantly) **(Figure 14A)**, chemokines **(Figure 14B)** and serpin proteases **(Figure 14C)**. To sum up, most co-inhibitory ligands, including PD-L1 (encoded by *Cd274*), and the enzyme SERPINB9 (a well characterized intracellular inhibitor of granzyme B) are mainly expressed in qNSCs. Besides, the chemokine CXCL10, which directs CTLs in peripheral immune responses, is up-regulated in aNSCs. To confirm the expression of SERPINB9 in qNSCs at the protein level, we electroporated mice in utero (E15.5) with an episomal plasmid expressing EGFP under the control of a general promoter (CAG::EGFP). Cells lining the lateral ventricle incorporate the episomal plasmid, which will be diluted upon cell divisions. In the adult mouse brain, only cells that have not divided or that have divided only a few times will retain the plasmid and will remain fluorescent. As expected, we have confirmed that in the SEZ, only qNSC, together with ependymal cells, will be fluorescently labeled, and these cell types can be distinguished by their position and morphology. In this framework, SERPINB9 protein expression was identified in qNSCs in steady

state conditions **(Figure 14D)**. SERPINB9 staining appears as a dotted pattern. However, we confirmed that it was specific as a similar look is seen when analyzing splenic T cells, and no fluorescence is detected in cell-free areas (data not shown). This suggests that, apart from up-regulating MHCI to a lesser extent than aNSCs, qNSCs are shielded from CTLs by multiple mechanisms that act at different levels: they are less likely to be recognized by CTLs as they induce less MHCI, but even if they are spotted, co-inhibitory receptors could prevent the release of cytotoxic proteins and these could be inhibited by serpins.

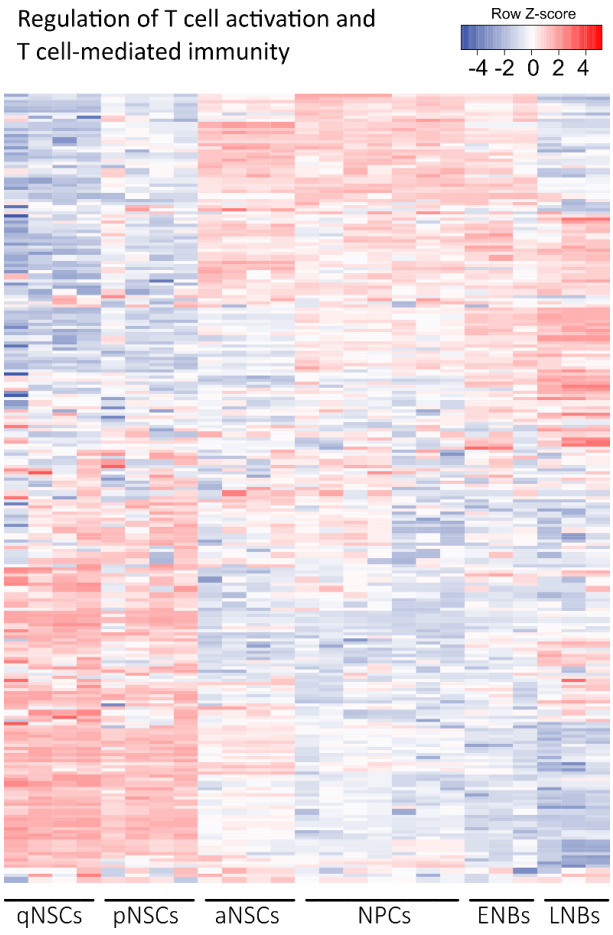

Figure 13. Quiescent NSCs show a distinct transcriptome with regard to T cell interaction. Heatmap showing RNA-seq gene expression data (row Z-scores calculated from normalized expression) of the different SEZ neurogenic populations considering the genes included in the GOs "*Regulation of T cell activation*" and "*Regulation of T cell-mediated immunity*".

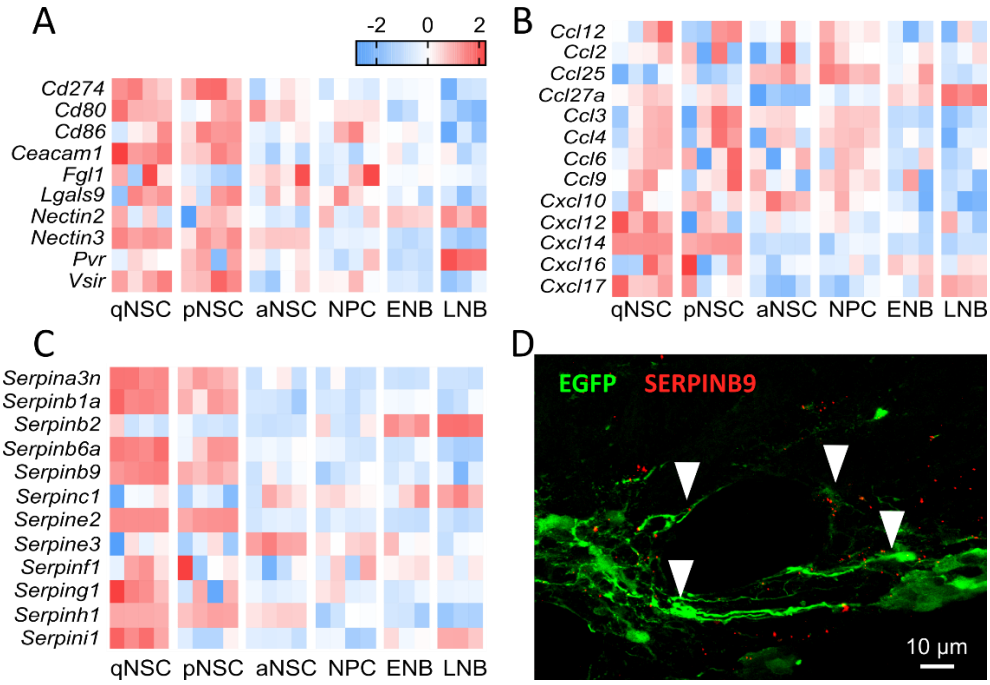

Figure 14. Different mechanisms can explain the resistance of qNSCs to CD8⁺ T cells. RNA-seq data of the neurogenic populations in the SEZ. The heatmaps show row z-scores and include A) ligands of immune checkpoints, B) Chemokines and C) Serpin proteases. D) Immunofluorescence of a representative SEZ section of mice electroporated *in utero* with CAG::EGFP (green fluorescence marks qNSCs), showing SERPINB9 staining (red) in steady-state conditions. The white arrows point to qNSCs (EGFP⁺).

Next, we assessed protein expression levels of a selection of costimulators and ligands of immune checkpoints (CD40, CD80, CD86, PD-L1 and PD-L2) in SEZ NSCs *in vivo*, both in steady-state **(Figure 15A)** and in inflammatory conditions 24 h after the i.p. injection of LPS **(Figure 15B)**. None of them could be detected by flow cytometry on the cell surface. Similarly, none of these molecules could be detected in unstimulated NSCs *in vitro*. In contrast, and similarly to what happened with MHCI subunits, PD-L1 levels were strikingly increased when exposing NSCs *in vitro* to IFNγ, but not TNFα **(Figure 15C)**.

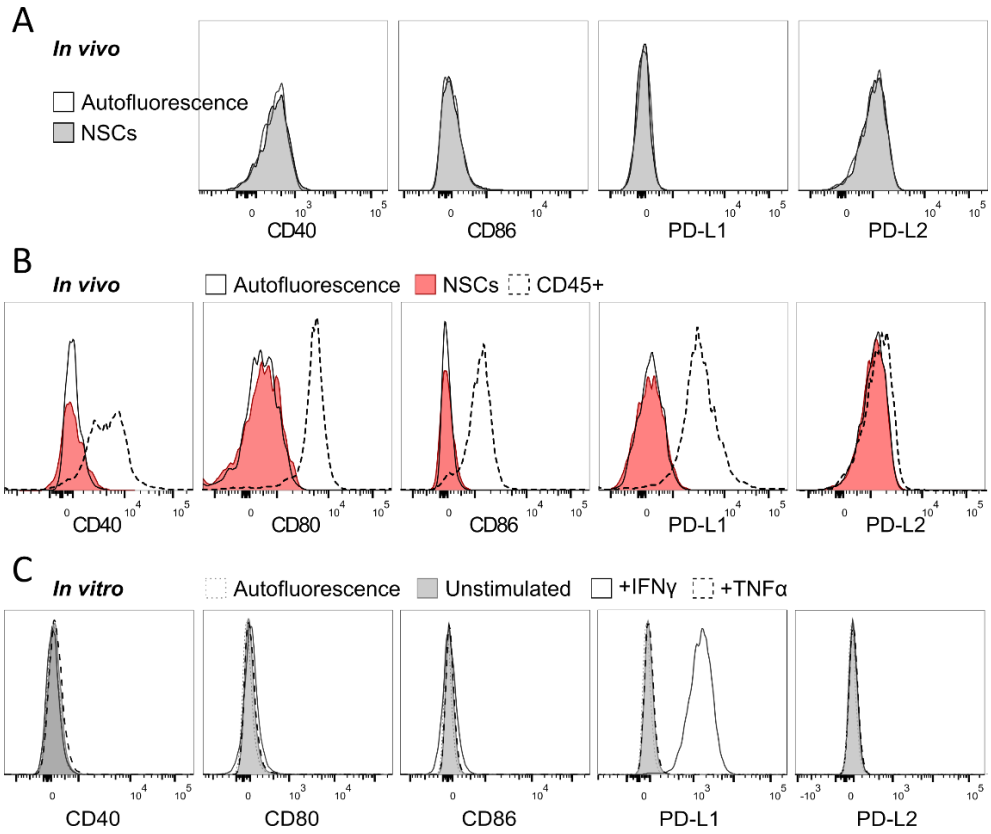

Figure 15. Unstimulated NSCs do not express ligands of immune checkpoints or costimulators, but can induce PD-L1 in response to IFNγ. A) Expression of the indicated markers in NSCs *in vivo* measured by flow cytometry. B) The same as in A 24 h after the administration of LPS i.p. (5 mg/kg). C) Expression of the indicated markers in NSCs *in vitro* measured by FACS in basal conditions or after being exposed to IFNγ or TNFα for 24 h. All histograms in A, B and C show the concatenation of 5 biological replicates. Autofluorescence is the FMO.

On the other hand, PD-1 (the receptor for PD-L1) is increased in $CD8^+$ T cells infiltrating the SEZ of old mice (Dulken et al., 2019) and is probably the best characterized immune checkpoint affecting CTL function outside SLOs (Chen and Flies, 2013; He and Xu, 2020). Therefore, we selected it as a prototypical molecule determining the balance between stimulatory signals (mainly MHCI) and inhibitory mechanisms (including PD-L1) in CTLs interacting with NSCs. We have previously seen that the transfer of JEDI T cells together with LV.EGFP into the F1 of B10D2 and R26mTmG;hGfap-Cre mice produces a great increase in IFNγ in the SEZ. Thus,

we used this model again to analyze PD-L1 expression in the neurogenic lineage *in vivo* by flow cytometry. Remarkably, the induction of PD-L1 was maximal in qNSCs, much lower in aNSCs, and decreased progressively through the lineage to almost disappear in LNBs **(Figure 16A)**. In response to IFNγ the trend in PD-L1 levels has an inverse correlation to MHCI expression in NSCs **(Figure 16B)**. This suggests that the fate of a NSC engaging the TCR of a CTL could be determined by a finely tuned balance between activating and inhibitory signals rather than by individual mechanisms, and differential expression of MHCI and PD-L1 could displace the balance to promote the killing of aNSCs and immune evasion in qNSCs.

3.3. CTLs determine the immunogenicity of NSCs by releasing IFNγ

Our data indicated a correlation between the presence of CTLs, the increase in IFNγ-dependent signaling and the induction of MHCI and PD-L1 surface levels. Also, we have previously seen that NSCs up-regulate MHCI even when activated CTLs are infiltrating the SEZ but are not attacking them (as in the CX3CR1-EGFP model). To demonstrate that NSCs respond to IFNγ released by $CD8^+$ T cells, we turned to our *in vitro* assay of neurospheres. We isolated splenic $CD8^+$ T cells from mice previously injected with JEDI T cells and LV.EGFP, and cultured them on transwell inserts (pore size of 0.4 μm) in wells already containing neurospheres **(Figure 17A)**. When T cells were restimulated with IL-2 and anti-CD3/CD28 beads, NSCs up-regulated the transcription of *Irf1*, *H2-K1/D1*, *Cd274* and *Serpinb9*, as well as MHCI and PD-L1 protein expression on the cell surface. More interestingly, an antibody neutralizing IFNγ completely suppressed these changes **(Figure 17B, C)**, indicating that JEDI T cells can make NSCs visible to the immune system by releasing IFNγ.

Together, our data indicate that NSCs are endowed with a number of coordinated mechanisms for their interaction with CTLs that are differentially regulated in quiescent *vs*. activated NSCs. The results suggest more complicated mechanisms than at the periphery, where immune evasion of quiescent SCs is based on down-regulation of MHCI (Agudo et al., 2018).

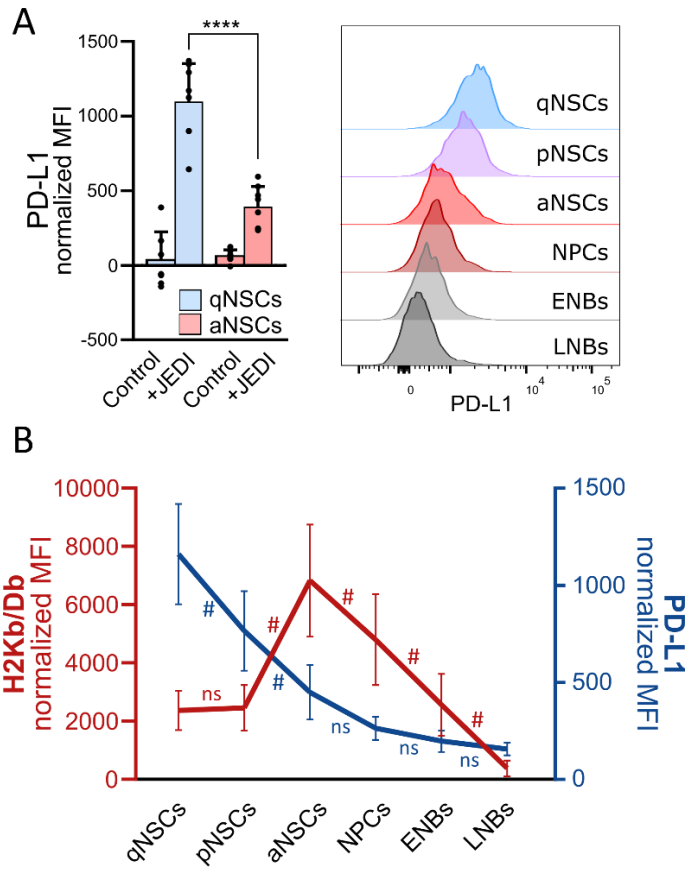

Figure 16. qNSCs up-regulate PD-L1 more than aNSCs when exposed to JEDI T cells *in vivo* in R26mTmG;hGfap-Cre mice. A) PD-L1 expression measured by flow cytometry in NSCs and their progeny (n=8). Histograms show the concatenation of 8 biological replicates and only the +JEDI group. B) Comparison of the changes in H2Kb/Db and PD-L1 expression along the lineage in the context of a T cell-mediated immune response in the SEZ, based on the data presented in the figures 11B and 16A (n=8). Graphs represent mean ± SD. Statistical analysis by Student's t-tests (p value is referred as ****p<0.0001) or one-way ANOVA followed by Tukey multiple comparisons tests (p values are indicated as ns>0.05, $^{\#}$p<0.05).

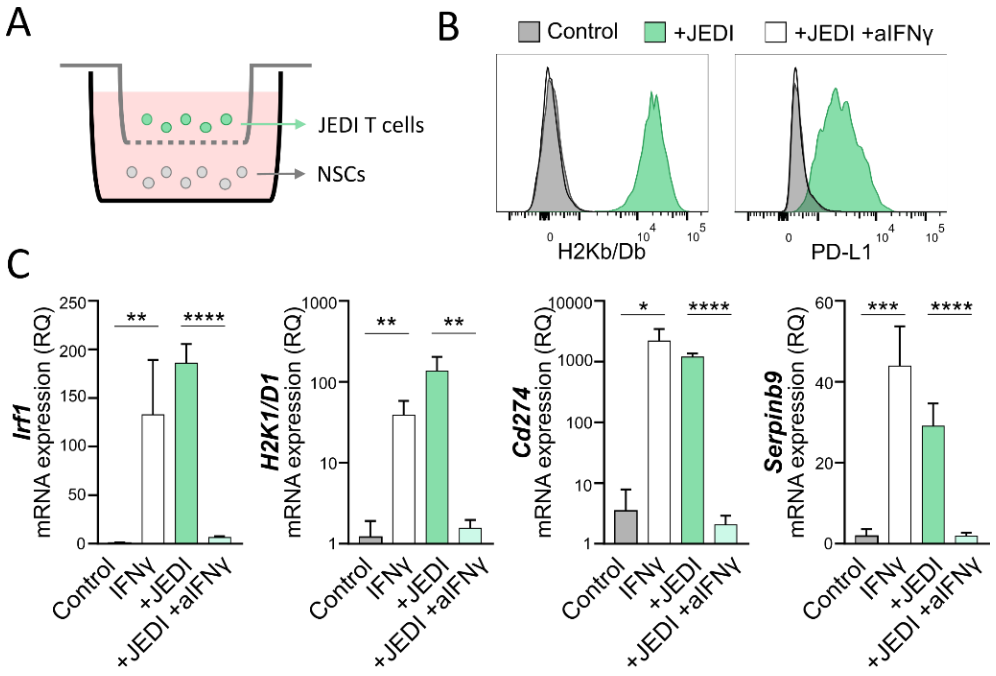

Figure 17. Activated CTLs make NSCs up-regulate antigen presentation and other immune mediators by releasing IFNγ. A) Co-culture system. JEDI T cells were isolated by negative magnetic sorting of total $CD8^+$ T cells from the spleens of R26mTmG;hGfap-Cre mice, a week after they were injected together with LV.EGFP. B) Histograms showing the expression of PD-L1 and H2Kb/Db measured by FACS. The concatenation of 5 biological replicates is plotted. C) Relative gene expression of the indicated genes in NSCs exposed to IFNγ or to JEDI T cells cultured with IL-2, beads anti-CD3/CD28 and +/- IFNγ blocking antibody (aIFNγ) (n=5). Graphs represent mean ± SD. Statistical analysis by Student's t-tests (p values: *p<0.05, **p<0.01, ***p<0.001 or ****p<0.0001).

4. Post-translational mechanisms control antigen presentation

4.1. Post-transcriptional changes explain the differences in MHCI

Immune evasion of quiescent SCs outside the brain has been shown to be regulated at the transcriptional level, as resting cells down-regulate NLCR5, the key transactivator of MHC class I genes (Agudo et al., 2018). We, therefore, decided to explore the possibility that a similar mechanism would be operating in NSCs. To get a general overview of MHCI gene expression throughout the neurogenic lineage, we explored again our bulk RNA-seq datasets (Belenguer et al., 2020) and assessed the expression of MHCI-related genes including those coding for: A) protein degrading enzymes that generate the peptides that are to be presented **(Figure 18A)**, B) antigen transporters to the ER and proteins involved in the assembly of functional antigen-MHCI complexes **(Figure 18B)**, C) structural components of the MHCI complex **(Figure 18C)** and D) transcriptional regulators of MHCI genes **(Figure 18D)**. Despite the lack of MCHI protein at the membrane in all SEZ neurogenic populations, as shown before, we could observe the up-regulated expression of genes coding for HCs and β2M, as well as TAPs, especially in quiescent NSCs. Despite the expression of MHCI structural elements, the transactivator *Nlrc5* and most other genes determining the transcription of MHCI genes were down-regulated in qNSCs, as described in the periphery. Therefore, contrary to what was reported in peripheral SCs (Agudo et al., 2018), the levels of NLRC5 did not correlate with MHCI gene expression in steady-state NSCs. NLRC5 lacks a known DNA-binding domain and relies on transcription factors that associate with MHCI genes promoters to perform its function as MHCI genes transactivator (Meissner et al., 2010). Indeed, induction of MHCI genes by IFNγ requires the formation of transactivating complexes in *cis*-regulatory elements of their promoters termed W/S, X1, X2 and Y-box motifs, which are occupied the X1-box binding trimeric RFX protein complex (composed of RFX5, RFXAP and RFXANK/RFXB) (Meissner et al., 2012), members of the X2-box binding CREB/ATF1 family of transcription factors (Gobin et al., 2001), and the Y-box binding NF-Y protein (composed of NF-YA, NF-YB and NF-YC) (Boss and Jensen, 2003). Together with NLRC5 they form a macromolecular nucleoprotein complex called the MHC enhanceosome (Gobin et al., 2001). Among these transcription factors, only *Rfx5* and *Rfxap* mRNAs were differentially up-regulated in qNSCs. Further studies will be required to understand the fine regulation of MHCI genes in NSCs and derived progeny.

However, we decided to focus on our observation that mRNA expression for MHCI structural components did not appear to correlate with their protein surface levels detected by FACS. Because this discrepancy suggested potential regulation by post-transcriptional processes, we decided to test whether these could be operating in SEZ NSCs.

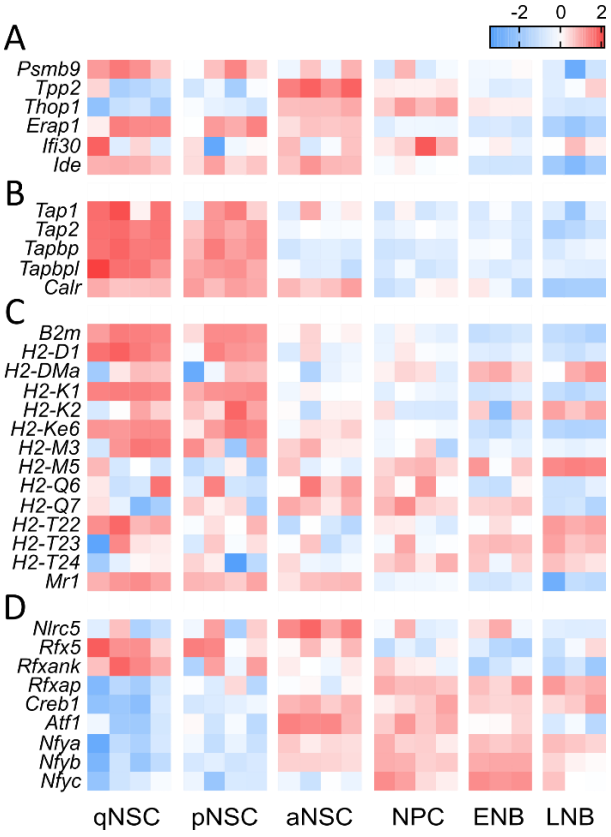

Figure 18. The expression MHCI genes and their transcriptional inducers do not correlate in SEZ neurogenic cells. RNA-seq data of the neurogenic populations in the SEZ. The heatmaps show row z-scores and include MHCI genes involved in antigen generation (A), antigen transport to the ER and complex assembly (B), structural components of the MHCI complex (C) and transcriptional regulators of MHCI genes (D).

As a first approach to test whether post-transcriptional mechanisms could be regulating the antigen-presentation machinery in SEZ cells and explain the differences among different NSCs, we decided to measure surface *vs*. intracellular levels of MHCI in NSCs. To do so, we used NSCs *in vitro* and performed flow cytometry. The incubation with the primary antibody was carried out either before

or after fixation and permeabilization to detect either surface or total H2Kb/Db, respectively. The data indicate that unstimulated neurosphere cells have low levels of HC protein that is located intracellularly. In response to IFNγ, its expression increases considerably and, furthermore, the protein is all found at the cell surface **(Figure 19)**. The data suggested that transcriptional up-regulation in response to IFNγ is coupled to a differential regulation of protein levels at the plasma membrane.

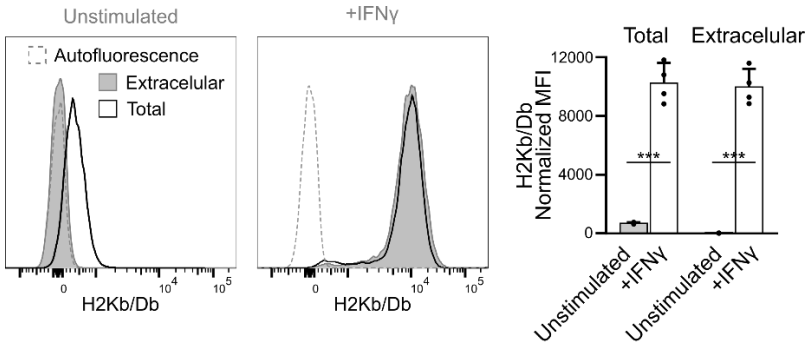

Figure 19. Unstimulated NSCs have low levels of intracellular MHCI. Histograms showing the expression of extracellular and total (extracellular + intracellular) H2Kb/Db in NSCs *in vitro* in basal conditions (unstimulated) or treated with IFNγ (100 ng/ml, 24 h) measured by FACS, and their quantifications. Histograms show the concatenation of 4 biological replicates. Bar plots represent mean ± SD. Statistical analysis by Student's t-tests (p values: ***p<0.001).

Different post-translational mechanisms have been described to regulate antigen presentation, including MHCI recycling/degradation and translation/trafficking to the membrane.

4.2. Protein degradation

Antigen presentation is a complex process that requires the dynamic interaction between different organelles from the secretory and endocytic pathways. Protein degradation plays a role in antigen presentation at two different levels: 1) the

balance between membrane protein recycling and degradation by the lysosome determines the levels of MHCI at the cell surface and 2) protein degradation by the proteasome determines the generation of peptides to be loaded into MHCI complexes at the ER, a requirement for subsequent trafficking to the cell surface.

Like other membrane proteins, MHCI molecules are continuously removed from the cell surface through the formation of endocytic vesicles that fuse to endosomes, followed by intracellular degradation at the lysosome or recycling back to the cell surface. However, the molecular mechanisms allowing this process in non-professional APCs are yet poorly understood. In addition, the recycling of MHCI to the plasma membrane seems to be a complex process that also includes antigen recycling (Montealegre and Van Endert, 2019). We decided to focus on degradation at the lysosomes as quiescent NSCs have been reported to have a large lysosomal compartment that is key to preserve their capacity for activation (Leeman et al., 2018). Moreover, our bulk RNA-seq datasets (Belenguer et al., 2020) also support the possibility of a higher autophagic rate in qNSCs *in vivo* as they have increased expression of most genes associated with autophagy activation **(Figure 20A)** and lysosomal biogenesis **(Figure 20B)** (Bordi et al., 2021). In fact, autophagy can target membrane proteins for lysosomal degradation (Pavel and Rubinsztein, 2017) and has been shown to reduce the surface exposure of MHCI in certain types of cancer cells. When that happens, the antigen presentation machinery accumulates within autophagosomes and lysosomes and cells can escape immune surveillance (Yamamoto et al., 2020).

In order to test whether protein degradation in the lysosomes plays a role in the regulation of MHCI surface levels in NSCs, we decided to use a pharmacological approach in neurospheres. We treated NSCs *in vitro* with Bafilomycin A1, which causes the alkalinization of the lysosomal lumen by inhibiting the ability of the vacuolar H^+-ATPase (V-ATPase) to transfer protons into the lysosome, and found enhanced induction of MHCI produced by IFNγ. We also tried up-regulating the autophagy-related lysosomal function by suppressing the activity of the mammalian target of rapamycin (mTORC1) by its allosteric inhibitor Rapamycin or by starvation. This time, MHCI membrane levels got reduced **(Figure 20C, D)**. Both Bafilomycin A1 and Rapamycin modulated autophagy as expected, as indicated by a commercially available probe **(Figure 20E)** which consists of a cationic amphiphilic tracer that provides bright fluorescence upon incorporation into autophagosomes and autophagolysosomes.

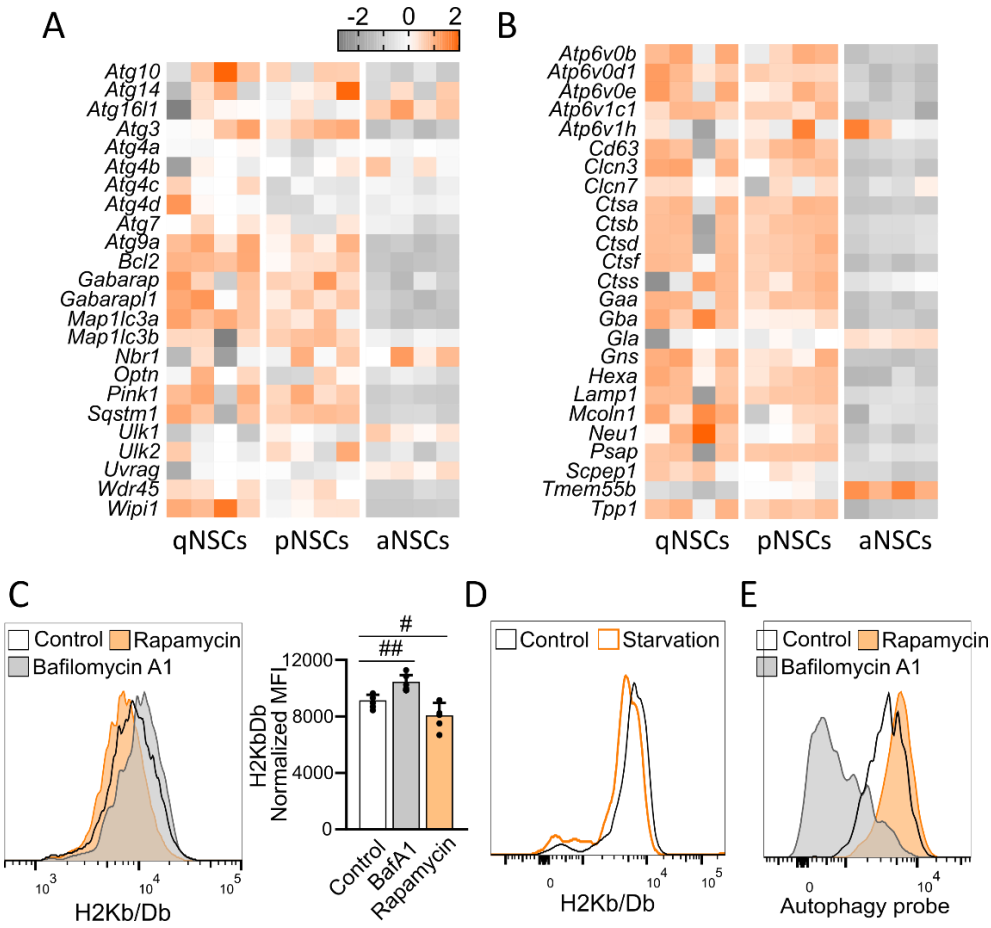

Figure 20. Autophagy modulates MHCI expression in NSCs. RNA-seq data of the neurogenic populations in the SEZ. The heatmaps show row z-scores and include genes involved in autophagy activation (A) and lysosomal biogenesis (B). C) Histograms showing the expression of H2Kb/Db in NSCs *in vitro* stimulated with IFNγ and treated with Bafilomycin A1 (100 nM), Rapamycin (2 µM) or their vehicle (DMSO) in the control condition for 24 h, and their quantifications (n=5). Histograms show the concatenation of 5 biological replicates. D) The same as in C, in NSCs subjected to 4 h of nutrient deprivation (maintained in PBS). E) Autophagy rate measured by flow cytometry with a commercial probe in NSCs treated as in C. Graphs represent mean ± SD. Statistical analysis by one-way ANOVA followed by Tukey multiple comparisons tests (p values are indicated as $^{\#}p<0.05$ or $^{\#\#}p<0.01$).

On the other hand, proteasomal activity, which is essential to generate the peptides that are loaded into MHCI complexes, was reported to be reduced in qNSCs

compared to aNSCs (Leeman et al., 2018). Besides, our RNA-seq data (Belenguer et al., 2020) shows that most genes related to proteasome activity (KEGG pathway mmu03050) are indeed clearly up-regulated in aNSCs **(Figure 21A)**. Interestingly, the proteasome inhibitor Bortezomib completely prevented the induction of MHCI produced by IFNγ on the surface of NSCs **(Figure 21B)**, whereas other proteins such as GLAST and CD133 reached the plasma membrane normally and even accumulated **(Figure 21C)**. Therefore, differences in protein turnover could be playing a role in the differential regulation of antigen presentation in NSCs.

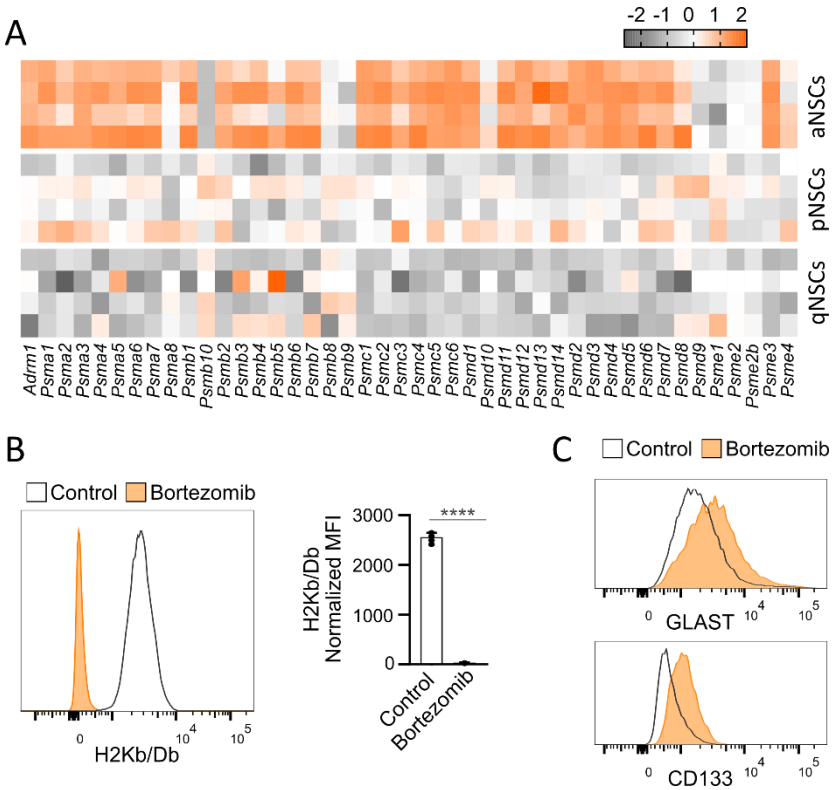

Figure 21. Proteasomal degradation determines MHCI expression in NSCs. A) RNA-seq data of the neurogenic populations in the SEZ. The heatmaps show row z-scores and include genes involved in proteasomal activity (KEGG pathway mmu03050). B) Histogram showing the expression of H2Kb/Db in NSCs *in vitro* stimulated with IFNγ and treated with Bortezomib (100 nM) or its vehicle (DMSO) in the control condition and their quantification (n=5). C) Expression of GLAST and CD133 in the same conditions of B. Histograms show the concatenation of 5 biological replicates. The bar plot represents mean ± SD. Statistical analysis by Student's t-tests (p value: ****p<0.0001).

4.3. Intracellular trafficking: CD99

We next decided to investigate mechanisms implicated in the targeting of surface molecules to the plasma membrane. Antigen-MHCI complexes assemble in the ER, travel to the Golgi compartment and are then exported to the cell membrane within vesicles generated in the TGN (Neefjes et al., 2011). First of all, we wanted to test whether intracellular vesicles containing MHCI complexes could be stored inside NSCs, ready to fuse and increase antigen exposure in response to the proper stimuli. A similar mechanism was reported to regulate the surface levels of the neurotrophin receptor TrkB in CNS neurons: this is stored in intracellular vesicles and can be rapidly translocated to the cell membrane when the concentration of cyclic AMP increases and induces the fusion of these vesicles (Meyer-Franke et al., 1998). In order to test this idea, we increased the levels of cyclic AMP in NSCs *in vitro* by treating them simultaneously with Forskolin, an activator of the adenylate cyclase which increases its synthesis, and IBMX, an inhibitor of phosphodiesterases that inhibits its degradation. However, we could not see any change in MHCI surface expression after 1 or 24 h **(Figure 22)**.

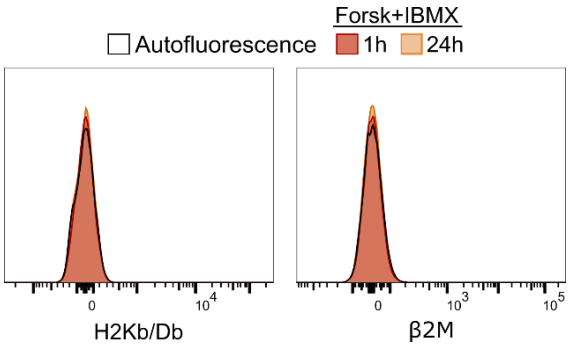

Figure 22. The elevation of cyclic AMP levels does not trigger MHCI surface expression in unstimulated NSCs. Surface expression of the indicated proteins in NSCs *in vitro* treated with Forskolin (Forsk) (5 µM) and IBMX (0.1 mM) for 1 or 24 h, compared to the autofluorescence.

In contrast, Brefeldin A1, an inhibitor of protein transport from the ER to the Golgi apparatus that induces coat protein redistribution and breakdown of the Golgi stack, completely suppressed the IFNγ-mediated up-regulation of MHCI at the surface of NSCs *in vitro* **(Figure 23)**, suggesting that regulated sorting may play a role.

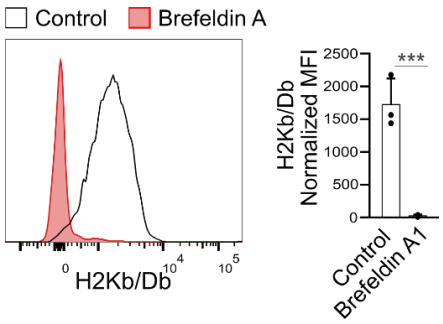

Figure 23. The inhibition of protein transport from the Golgi to the ER prevents MHCI surface expression. Histogram showing the expression of H2Kb/Db in the cell surface of NSCs *in vitro* treated with IFNγ and Brefeldin A1 (1 µM) or DMSO (control) for 24 h, and the quantifications (n=3). Histograms show the concatenation of all replicates. Graphs represent mean ± SD. Statistical analysis by Student's t-tests (p value is referred as ***p<0.001)

In the past, MHCI molecules were thought to rapidly arrive at the cell surface after leaving the ER, by default pathway without the need of additional signals. However, it is already known that the export of MHCI to the plasma membrane can be determined by ER-Golgi and post-Golgi traffic control (Sohn et al., 2001). For example, some viral proteins hijack the cellular trafficking mechanisms to avoid antigen presentation and CTL-mediated killing (Pereira and DaSilva, 2016). On the other hand, MHCI molecules are retained by the chaperon tapasin in the ER are released upon peptide binding. However, some viral infections can trigger the expression of MHC retention molecules, and retain antigen-MHC complexes in the ER. Other viral proteins exit the ER upon binding to MHCI, but reroute the newly synthesized MHCI complexes to intracellular sites of proteolysis such as lysosomes (Gruhler and Früh, 2000). MHCI components lack a trafficking signal in their protein sequence, suggesting that MHCI may bind to cargo receptors the identity of which remains elusive (Dancourt and Barlowe, 2010; Donaldson and Williams, 2009). As mentioned in the Introduction, although the transmembrane protein BAP31 cycles between the ER and the Golgi and can bind to MHCI in human and mouse cells, it does not appear to regulate its surface levels (Ladasky et al., 2006).

A second protein, known as CD99, has been described to regulate MHCI trafficking in human thymocytes. CD99 is a ubiquitous transmembrane protein that has been

shown to regulate the intracellular transport of MHCI, MHCII and TCR molecules during the positive selection of thymocytes (Brémond et al., 2009; Choi et al., 1998; Sohn et al., 2001) and to be involved in the formation of immune synapses (Pata et al., 2011). However, that has only been studied in human cells of the lymphocyte lineage, and few parallelisms have been explored between human and mouse CD99 proteins (Pasello et al., 2018). Interestingly, CD99 is expressed in neural tissues (Ambros et al., 1991) and CD99 protein can be detected at the plasma membrane of NSCs *in vitro* **(Figure 24A)**. Human CD99 is a highly O-glycosylated small protein of only 32 kDa, with a unique structure that has no resemblance to any protein family known. Its coding gene is located in the pseudoautosomal region of the human X and Y chromosomes (Goodfellow et al., 1986). The mouse CD99 homolog gene, which is very poorly characterized, has been shown to code for a protein 45% identical in its sequence to human CD99, which is involved in lymphocyte recruitment into inflamed tissue *in vivo* (Bixel et al., 2004). However, potentially similar activities in MHC trafficking have not been described in the mouse. Importantly, we also found CD99 and H2Kb to be physically associated in our NSCs **(Figure 24B)**, showing that both proteins also interact in murine cells, and that human and mouse CD99 might have essential roles in common. This finding further supports a potential role of CD99 enabling the transport of MHCI to the plasma membrane in SEZ NSCs. Additionally, we compared the sequences of the human and mouse gene transcripts to analyze similarities. The alignments also show the sequences that we use to overexpress (which is the exact murine sequence) or to knock-down CD99 in mouse cells **(Figure 24C)**.

We next decided to test whether the levels of CD99 could play a role in the trafficking and presentation of MHCI complexes. Our results clearly indicate that CD99 levels correlate with the capacity of NSCs to induce antigen presentation: reducing CD99 by delivering a shRNA targeting its transcript attenuates the increase in surface β2M and H2Kb/Db **(Figure 25A)**, but not PDL1 **(Figure 25B)**, in response to IFNγ. Conversely, CD99 overexpression enhances MHCI expression **(Figure 25C)**.

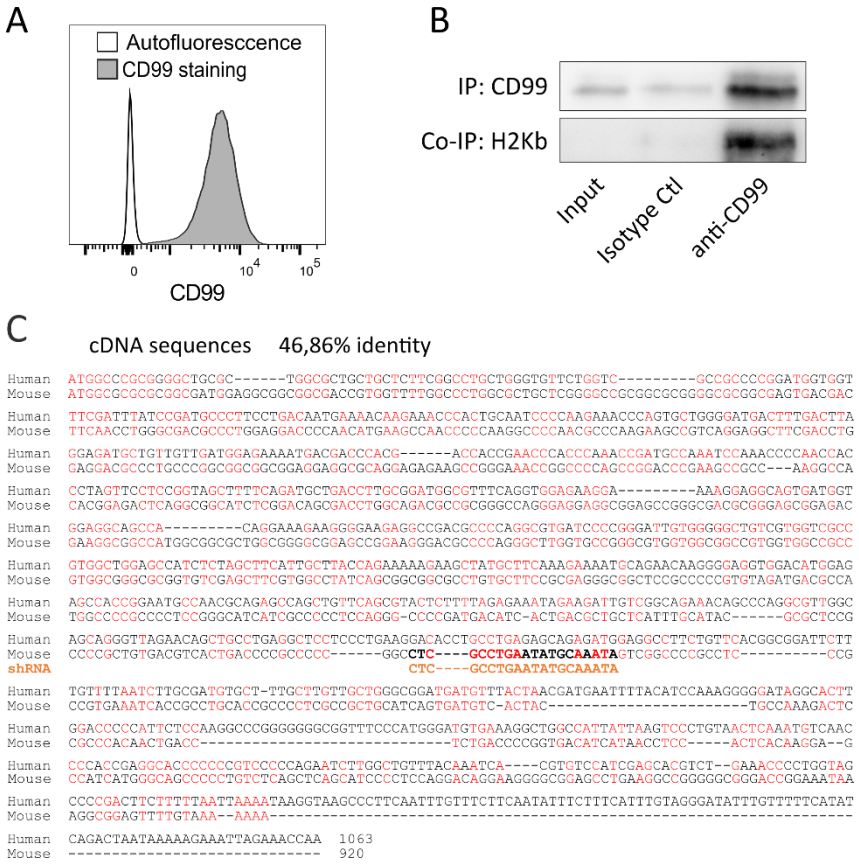

Figure 24. CD99 could play a role in the regulation of antigen presentation in NSCs. A) Histogram showing the expression of CD99 in untreated NSCs *in vitro* measured by flow cytometry (n=4). The concatenation of 4 biological replicates is shown. B) Western blot showing the co-immunoprecipitation of H2Kb with CD99. Input and immunoprecipitates obtained with anti-CD99 antibody and with its isotype control are compared. A representative blot among 3 biological replicates is shown. C) Alignment of the cDNA sequences of human and mouse Cd99 transcripts, and the shRNA that will be used in this study. Conserved nucleotides are highlighted in red.

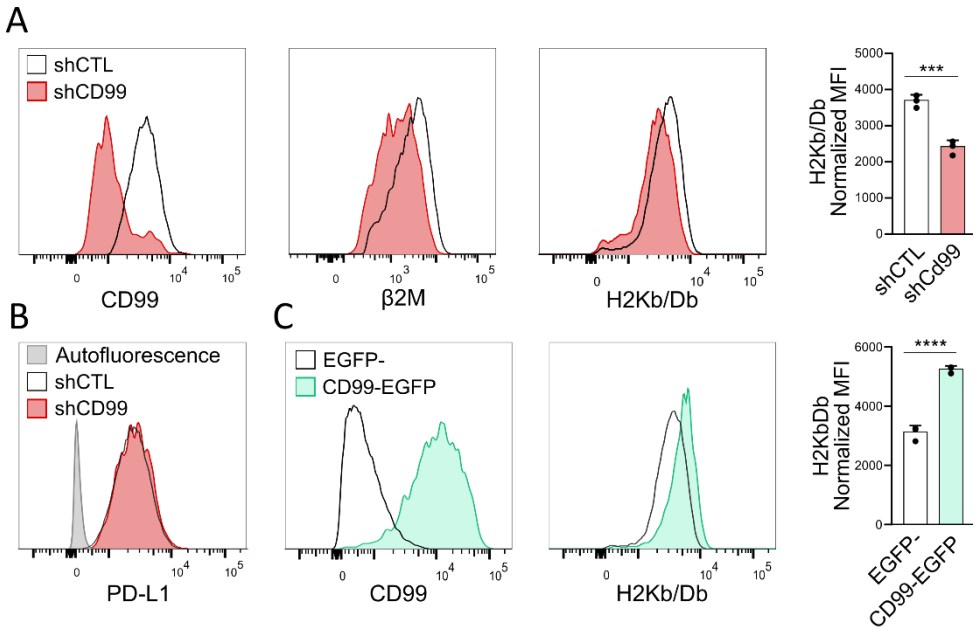

Figure 25. CD99 expression correlates with the surface levels of MHCI. A) Histograms showing the protein expression at the cell surface of CD99, β2M and H2Kb/Db in NSCs that included a plasmid encoding shCd99 or a control shRNA (shCTL) and treated with IFNγ, measured by flow cytometry (n=4). The quantifications for H2Kb/Db are also included. B) PD-L1 expression measured by flow cytometry in the same conditions of A. C) The same as in A, but in NSCs nucleofected with a plasmid encoding CD99-EGFP, compared to the cells that did not include the plasmid (n=4). All histograms show the concatenation of 4 biological replicates. Bar plots show mean ± SD. Statistical analysis by Student's t-tests (p values are referred as ***p<0.001 or ****p<0.0001).

We could detect differentially regulated expression of the *Cd99* (or *Mic2*) gene in NSC populations. In fact, aNSCs express much more CD99 transcript and protein than qNSCs *in vivo* **(Figure 26A, B)**, which might explain, at least in part, why aNSCs can expose more MHCI at their surface than their quiescent counterparts. Contrary to antigen presentation, CD99 levels are not regulated by IFNγ **(Figure 26C)**. These results indicate that CD99 plays a role in antigen presentation in adult mouse NSCs.

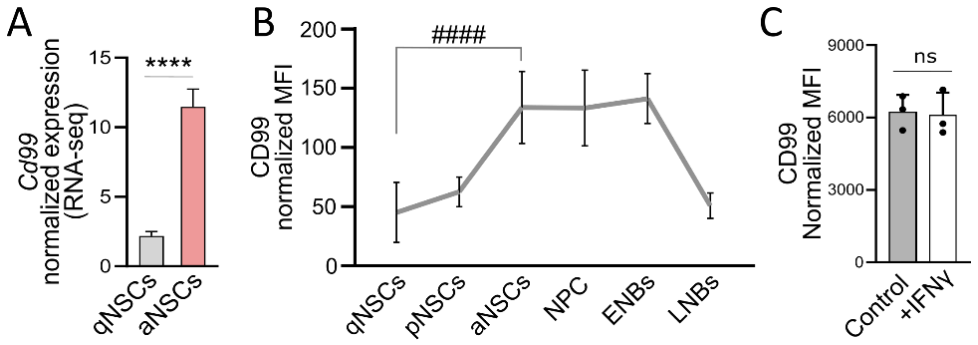

Figure 26. CD99 could explain the differences in antigen presentation between activated and quiescent NSCs. A) Gene expression of *Cd99* in NSCs *in vivo* (RNA-seq data) (n=4). B) Expression at the surface of CD99 protein in SEZ neurogenic cells *in vivo* measured by flow cytometry (n=6). C) Expression of CD99 measured by flow cytometry in NSCs *in vitro* unstimulated (control) or treated with IFNγ for 24 h (n=3). Bar plots show mean ± SD. Statistical analysis by Student's t-tests (p values: ns>0.05 or ****p<0.0001) or one-way ANOVA followed by Tukey multiple comparisons tests (p value: ####p<0.0001).

Several observations support a role for CD99 regulating the intracellular transport of MHCI in NSCs. First, reduced levels of CD99 resulted in MHCI accumulation inside NSCs in response to IFNγ **(Figure 27A)**, while decreasing at the cell surface. Second, we incubated NSCs *in vitro* with a fluorescently-labeled antibody against H2Kb/Db at a very high concentration to block surface MHCI molecules. Then, we washed it and added a different antibody, from the same clone but conjugated to a different fluorophore, and measured its binding to the cell surface every 10 min. Differences in the speed of MFI increase between cells within the same sample suggested that overexpressing CD99 boosts the velocity of MHCI export to the plasma membrane **(Figure 27B)**.

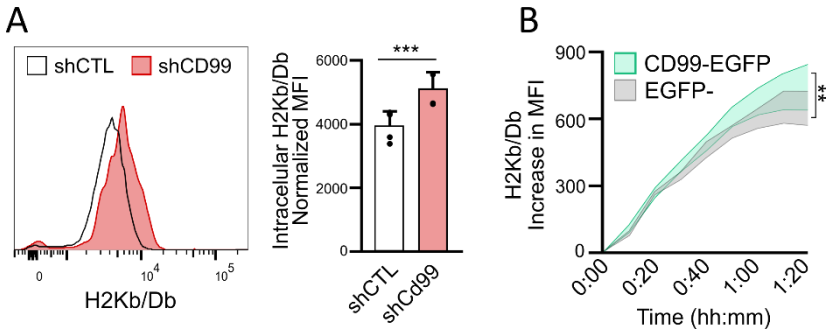

Figure 27. CD99 is involved in the intracellular transport of MHCI. A) Histograms showing the intracellular expression of H2Kb/Db in NSCs exposed to IFNγ that included a plasmid encoding a shRNA targeting *Cd99* or a control shRNA (shCTL). Histograms show the concatenation of all replicates, and their quantification is also included (n=4). For intracellular protein detection, extracellular H2Kb/Db was first stained with a fluorescently-labeled antibody and, after washing and fixation, the same clone of antibody conjugated to a different fluorophore was used to detect the intracellular protein. Statistical analysis by Student's t-tests (p value: ***p<0.001). B) Kinetics of MHCI transport to the cell surface in NSCs nucleofected with CD99-EGFP compared to the cells from the same cultures that did not include the plasmid (EGFP⁻), previously treated with IFNγ for 24h (n=3). The details about the statistical analysis can be found in the methodology section. Statistical significance was calculated with a Satterthwaite t-test. P value: **p<0.01.

Additional elements are probably necessary to link antigen-MHCI complexes and the intracellular transport machinery. In this framework, a role of CD99 binding MHCI on one side and p230/golgin-245, which participates in regulatory transport from the TGN, has been reported in human lymphoid cells (Brémond et al., 2009; Pata et al., 2011). In addition, vesicular transport inside a cell is orchestrated by molecular motors, and small GTPases from the Rho and Rac families have been suggested as downstream effectors of CD99 (Kim et al., 1998; Sohn et al., 2001). We tried inhibiting them with Rhosin, a chemical inhibitor of Rho GTPases, and with EHT 1864, which inhibits GTPases from the Rac family. While Rhosin had no effect, EHT 1864 completely prevented the induction of MHCI in response to IFNγ **(Figure 28)**, suggesting the implication of Rac GTPases.

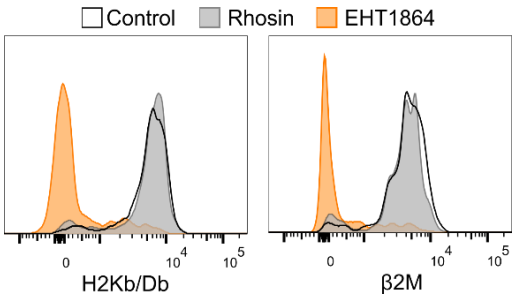

Figure 28. The inhibition of Rac GTPases blocks the induction of MHCI at the surface of NCSs. Histograms showing the expression of the indicated proteins in the cell surface of NSCs *in vitro* exposed to IFNγ and treated with DMSO (control), Rhosin (50 µM) or EHT 1864 (20 µM) for 24 h. Histograms show the concatenation of 4 biological replicates.

4.4. CD99 makes qNSCs vulnerable to CTLs

Our results suggested that the susceptibility of NSCs to CTL-mediated killing seems to depend on both MHCI expression and the induction of co-inhibitory mechanisms such as PD-L1, which have inverse expression patterns along the neurogenic lineage. To test whether a balance between these signals determines the susceptibility of NSCs to CTLs, we decided to assess whether a modification of CD99 levels would render qNSCs differentially exposed to CTLs. C57BL/6 and B10D2 mice were crossed and their F1 progeny electroporated *in utero* at E15.5, by introduction into the lateral ventricles of an episomal plasmid carrying a Egfp cDNA fused to mouse Cd99. The construct was used to both overexpress CD99 and make NSCs the target of JEDI T cells. As cell proliferation dilutes episomal plasmids, only qNSCs, which are already present fetally, will carry the plasmid into adulthood. In addition, we also introduced a transposon carrying a red fluorescencent protein (RFP) cDNA (PB-CAG-RFP) and a transposase-encoding cDNA controlled by the Glast promoter (GLAST-Transp) for its activation in GLAST$^+$ NSCs. Doing so, we integrated RFP, which is not recognized by JEDI T cells (Agudo et al., 2015), in NSCs and their progeny so we could trace whether there was electroporation in case there were no EGFP$^+$ cells in the adult SEZ. Electroporated mice were i.v. injected at 2 months of age with JEDI T cells and LV.EGFP as usual, and neurogenic cells were analyzed by FACS 10 days later. As expected, most EGFP$^+$ NSCs in uninjected mice were qNSCs, with some pNSCs **(Figure 29A)**, and there was a strong infiltration of lymphocytes (FSC^{low} CD45^{high}) within the SEZ of injected mice **(Figure 29B)**. NSCs

that had retained the Cd99-Egfp construct were low in number but they exhibited much higher levels of surface H2Kb/Db **(Figure 29C)**. The number of RFP$^+$ qNSCs was similar in injected and uninjected animals **(Figure 29D)**, indicating minor differences in electroporation efficacy and lack of effects of JEDI T cell administration, as expected. In contrast, the same animals showed a clear reduction in EGFP$^+$ qNSCs when they received the JEDI T cells **(Figure 29E)**, contrary to what was seen in the previous models of EGFP-expressing NSCs. The data suggests that CD99 overexpression was sufficient to render qNSCs vulnerable to JEDI T cells.

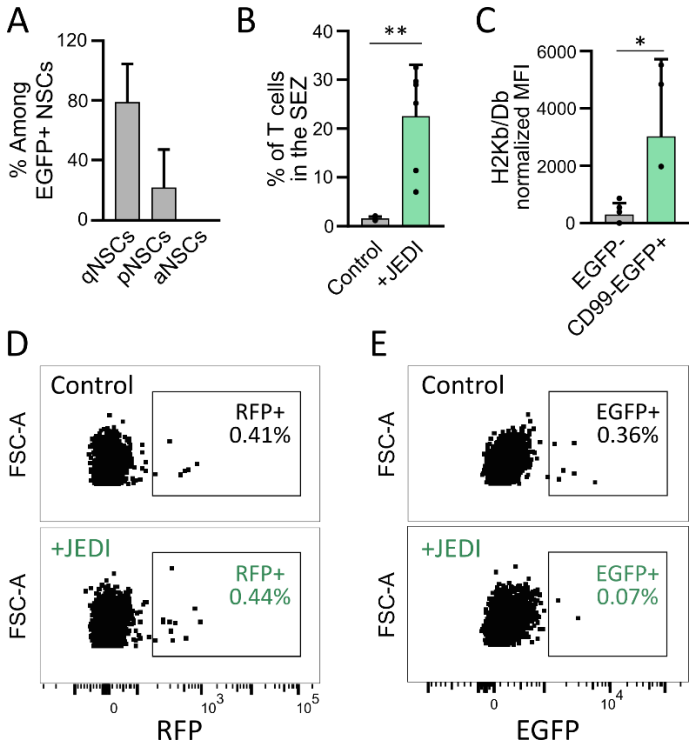

Figure 29. The overexpression of CD99 seems enough to make qNSCs vulnerable to JEDI T cells. A) Distribution of cell states of EGFP$^+$ NSCs in control (uninjected) mice, as determined by flow cytometry (n=3). B) Percentage of T cells (CD45^{high} FSC^{low}) within the SEZ of injected mice, detected by FACS. C) Quantification of H2Kb/Db expression in EGFP$^-$ and EGFP$^+$ quiescent NSCs (qNSCs and pNSCs) of injected mice (n=6 for EGFP$^-$, and n=3 for EGFP$^+$ as not all mice had EGFP$^+$ NSCs). D) Percentage of RFP$^+$ qNSCs in electroporated mice previously injected (+JEDI) or not (Control) with JEDI T cells and LV.EGFP (n=5 for control mice and n=6 for the injected group). E) Same as in D, for EGFP$^+$ cells. Dot plots show the concatenation of all samples. Graphs represent mean ± SD. Statistical analysis by Student's t-tests. P values are referred as *p<0.05 or **p<0.01.

DISCUSSION

The immune surveillance of the CNS has only started to be understood, and it is deeply determined by the anatomical barriers that separate the brain parenchyma, the blood and the CSF (Mastorakos and McGavern, 2019). The SEZ is a special region located right in the wall of the lateral ventricles, where NSCs contact the ventricular CSF and are intercalated among ependymal cells, which do not form tight junctions (Lim and Alvarez-Buylla, 2016; Obernier and Alvarez-Buylla, 2019). In this region, the ISF and the CSF are not separated by a restrictive barrier and there is easy exchange of antigens and other solutes. Moreover, the CSF contains immune cells, including T cells that traffic through the meninges and CSF-filled spaces (Engelhardt et al., 2017; Mastorakos and McGavern, 2019), which might have easier access to the SEZ than to other regions of the brain. Surprisingly, whether NSCs in the SEZ undergo immune surveillance had not been studied before, and it is of central importance as NSCs can be the cells-of-origin of primary GBM. Therefore, we used an adoptive transfer of specific $CD8^+$ T cells against EGFP (Agudo et al., 2015) into mice expressing EGFP in NSCs and their progeny, and analyzed CTL-mediated killing. Our results indicate that (A) immune surveillance by cytotoxic T cells takes place in the brain parenchyma, including the SEZ, (B) there is more resistance to the infiltration of T lymphocytes and to CTL-mediated killing in the brain than in peripheral organs, but T cells access the SEZ more easily than the cortex, (C) quiescent NSCs, in contrast to their proliferating progeny, are resistant to CTL-mediated killing, and (D) immune evasion of quiescent NSCs is based on a complex balance of different mechanisms, which include the post-transcriptional regulation of the antigen presentation machinery as well as the differential expression of immune checkpoints.

First, we tried to validate studies concluding a role of T cells supporting neurogenesis in healthy animals (Huang et al., 2010; Wolf et al., 2009b, 2009a; Zarif et al., 2018; Ziv et al., 2006). However, we could not see any differences in SEZ neurogenic cell populations between mice lacking lymphocytes (Rag1 *knock-out* mice) compared to their immunocompetent littermates. Interestingly, the same comparison was done to assess changes in cell proliferation within the SGZ (Wolf et al., 2009a), but the authors found a significant reduction in the number of cycling cells within the hippocampal neurogenic niche. The fact that they assessed hippocampal neurogenesis while we focused on the SEZ could explain, at least in part, those differences. However, a different study found that cell proliferation and neuron formation were diminished also in the SEZ in the absence of T cells (Ziv et

al., 2006). Therefore, the biggest differences between these studies and our experiments might not be in the experimental models but in the readout. The authors assessed cell proliferation by Ki67 or BrdU staining, and quantified neuron formation by identifying colocalization of these markers together with the neuronal markers doublecortin (DCX) or NeuN. This technical approach is of course informative, but has some limitations. First of all, different neurogenic populations are proliferative and coexist in neurogenic niches: aNSCs, NPCs and ENBs can be labelled with BrdU and Ki67 but cannot be distinguished. Second, additional cell types, for example microglia, reside within neurogenic niches, have proliferative capacity and could interfere with the quantification of cycling NSCs and neural progenitors. By flow cytometry we have seen that up to 20/25% of EdU^+ cells (1h pulse-chase) within the SEZ are not neurogenic (Lin+). Also, activated NSCs can return to quiescence and give rise to $BrdU^+$ non-proliferating cells. Hence, the proper characterization of the different cell states along the neurogenic lineage requires a more detailed assessment. We used a panel of 8 surface markers to identify by flow cytometry different subsets of NSCs, NPCs and NBs with much higher accuracy, and demonstrate that the absence of T cells does not affect the relative numbers of neurogenic cells within the SEZ. However, contrary to other authors, we did not assess hippocampal neurogenesis, neuron formation or the effect of T cell replenishment in immunodeficient mice.

At the same time, it is already widely accepted that T cells are constantly monitoring the CNS parenchyma in homeostasis and can initiate responses against CNS-derived antigens. However, the process of immune surveillance in the brain seems to be performed from the CNS interfaces. Only upon activation T cells infiltrate the parenchyma in substantial numbers and exert effector functions (Engelhardt et al., 2017; Louveau et al., 2015b; Mastorakos and McGavern, 2019). The SEZ is not separated from the CSF by highly restrictive barriers and might be more permissive to T cell trafficking. In line with this, the initial composition of immune cells in the CSF is determined by the permeability of the ependymal layer in the CP. This barrier contains tight junctions between ependymal cells and is therefore more restrictive than in the SEZ. Even in that case, the CP has a high density of leukocytes and the CSF contains a high variety of immune cells (Mastorakos and McGavern, 2019; Song et al., 2016). Moreover, the presence of $CD3^+$ cells, which are T lymphocytes, has been reported in the walls of the lateral ventricles (Ziv et al., 2006) and CTLs have been found in the SEZ of old mice (Dulken et al., 2019). Supporting these

observations, and in addition to different studies detecting scarce T cells within the brain parenchyma (Pasciuto et al., 2020; Smolders et al., 2018; Song et al., 2016; Xie et al., 2015), we detected T cells in the SEZ of young adult healthy mice. This observation needs validation by additional techniques and, in any case, T cell infiltration would not be necessary for immune surveillance, but proves that most of the central concepts regarding CNS immunity need to be revisited in the light of new data. In any case, the interaction between NSCs and T cells had not been studied in a context of an antigen-specific immune attack.

The interest to determine whether SCs are immunoprivileged entities started with studies in embryonic SCs and mesenchymal SCs (Agudo, 2021). Human ESCs were reported to express low levels of MHCI (Drukker et al., 2002), although it soon became clear that transplanted embryonic SCs trigger robust cellular and humoral immune responses and are rejected (Swijnenburg et al., 2008). Besides, the immunomodulatory properties of mesenchymal SCs are widely recognized: they can induce peripheral tolerance and inhibit $CD8^+$ T cell-mediated immune responses in different pathological contexts (Ghannam et al., 2010; Jain et al., 2020; Zhu et al., 2020). Among other mechanisms, they can act through the PD-1/PD-L1 pathway (Chen et al., 2018; Liu et al., 2021), by releasing prostaglandin E2 (Najar et al., 2010; Németh et al., 2009) and by inducing the activity of Tregs that in turn inhibit CTL function (Forbes and Rosenthal, 2014; Luz-Crawford et al., 2013; Neal et al., 2019; Pang et al., 2021; Sotoodehnejadnematalahi et al., 2021; Yang et al., 2018). Similarly, the transplantation of NSCs has been shown to suppress CNS inflammation, as they secrete prostaglandin E2 and capture extracellular succinate (Peruzzotti-Jametti et al., 2018). However, little focus has been given to the immune surveillance in healthy tissues. In part, this can be explained by the widely accepted assumption that all nucleated cells in mammals express MHCI, thereby expose antigens at their surface and are monitored by $CD8^+$ T cells that will kill them in case they express viral or abnormal proteins (Abbas et al., 2016). Therefore, the immune surveillance of all cells within healthy tissues was generally taken for granted, and it has been mostly studied in the context of established tumors as cancer cells often evade immunity. However, adult SCs are very long lived, can accumulate mutations for longer and have a higher tumorigenic potential than terminally differentiated cells (Ermolaeva et al., 2018; Lee et al., 2018; Tomasetti et al., 2017). At the same time, they are essential elements for homeostasis, as they are in charge of restoring tissues after injury and replacing cells in steady state

(Aurora and Olson, 2014; Rando and Jones, 2021). Therefore, SCs in adult tissues need to be closely monitored by the adaptive immune system, but also preserved in case of damage, even if they harbor immunogenic mutations. Consequently, tissues have evolved a number of strategies to preserve their precious pools of SCs in the face of harm. These include flooding the niche with anti-inflammatory mediators and upregulating the expression of immunosuppressive molecules such as IL-10, which is produced by Tregs in the vicinity of hematopoietic SCs (Fujisaki et al., 2011; Naik et al., 2018). Also, SEZ NSCs have been described to respond to TNFα by promoting the maintenance of their quiescent pool in inflammatory conditions (Belenguer et al., 2020). The epithelial tissues that line our body have developed particularly sophisticated means of protecting their SCs, and the hair follicle SC niche has long been described as a site of immune privilege (Agudo, 2021; Naik et al., 2018): it expresses low levels of immune-activating molecules and has high numbers of Tregs (Ali and Rosenblum, 2017; Ali et al., 2017; Christoph et al., 2000). Also, intestinal SCs rely on signals from innate lymphoid cells for protection from inflammation and injury (Aparicio-Domingo et al., 2015; Hanash et al., 2012). Interestingly, a recent study demonstrated that the immune susceptibility of SCs depends on their activity: on one hand, cycling SCs in different niches (intestine, ovary, mammary gland as well as muscle and hair follicle) display MHCI in their surface and can present neoantigens to CTLs that might kill them as a check for tumor formation. On the other hand, quiescent SCs, which are present in the hair follicle and in the muscle, suppress their antigen presentation machinery and, even if they have a high mutational burden, evade immune surveillance (Agudo et al., 2018). This can be understood from an evolutionary point of view, as the capacity to restore tissues after damage during reproductive age is a better selective advantage than avoiding malignancies, which are more frequent with aging (Campisi and D'Adda Di Fagagna, 2007). The differences between rapidly dividing and slowly cycling SCs might be explained by the fact that the first ones can be much more easily replaced by neighboring SCs if they are destroyed (Agudo et al., 2018). It seems, therefore, that immune surveillance can be considered a default property of most nucleated cells in peripheral tissues, with the exception of quiescent SCs that are so important for tissue homeostasis that are better mutated than eliminated. Conversely, our results suggest that the cells of the neurogenic lineage are immunologically dormant in resting conditions. However, cycling populations (mainly aNSCs and NPCs) can be "woken up" by patrolling T cells through IFNγ release.

Immune surveillance is necessarily associated with antigen presentation. Nevertheless, although MHCI expression has been detected by immunocytochemistry in brain Nestin$^+$ cells during fetal development (Chacon and Boulanger, 2013), its expression in adult NSCs had only been shown at the mRNA level (Lin et al., 2021; Liu et al., 2015, 2013). On the other hand, CD8$^+$ T cells with high IFNγ and PD-1 expression have been found in the SEZ of old mice (Dulken et al., 2019), and infiltrating T cells in the brain parenchyma seem to be enriched in PD-1 and CTLA-4 (Smolders et al., 2018). However, no PD-L1 had been detected in NSCs before. In the present work we use the adoptive transfer model of JEDI T cells into mice expressing EGFP in NSCs to demonstrate that CD8$^+$ T cells monitor the neurogenic lineage, can access the SEZ and are able to kill aNSCs, but not qNSCs. In contrast to peripheral tissues, antigen presentation is not a default characteristic of SEZ neurogenic cells, but can be triggered by infiltrating T cells. In line with this, we show that the expression at the protein level of both MHCI and PD-L1 is absent in resting neurogenic cells but can be triggered strikingly when these are exposed to IFNγ. In addition, our results show that the immune escape of qNSCs is not determined by a single mechanism but it is a robust property that can be explained by general phenotypic changes, including reduced antigen presentation in MHCI molecules, PD-L1 up-regulation and SERPINB9 expression. The capacity to induce these elements differs along the lineage, and it seems that aNSCs (and probably NPCs) might be the only quality checkpoint in the production of newborn neurons and glial cells in the SEZ: LNBs, even in the presence of IFNγ, do not express MHCI. Overall, our results support a model where the susceptibility of NSCs to CTL-mediated killing is determined by a tightly controlled balance between activation signals, essentially MHCI, and co-inhibitory mechanisms that can be exemplified in PD-L1 but probably include many other co-inhibitory ligands. T cell-activating cues are predominant in proliferating neurogenic cells and make them susceptible to CTLs, while co-inhibition could overcome activation in quiescent NSCs and make them resistant. Hence, substantial changes in the magnitude of activation or in the expression of inhibitory molecules can modify the equilibrium between opposing signals and change the fate of NSCs. It is interesting that IFNγ alone induces both MHCI and PD-L1 (among others) with different relative magnitudes depending on the cell state. Similarly, while IFNγ is essential for immune responses against tumors and promotes a great deal of anti-tumor mechanisms, it can also promote tumor growth and immune evasion depending on the tumor-specific context, the magnitude of the signal, and the microenvironment (Castro et al., 2018). As this CK

induces MHCI genes and Cd274 transcriptionally, their differential regulation in quiescent and cycling NSCs might be, at least in part, determined at other levels. In line with this, we found that the trafficking of antigen-MHCI complexes to the cell surface is regulated by CD99, as previously shown for human leukocytes (Brémond et al., 2009; Kim et al., 1998; Sohn et al., 2001). CD99 is a glycosylated transmembrane protein that seems to be involved in cell adhesion and migration, cell death, differentiation, intracellular protein trafficking, endocytosis and exocytosis. It also appears to play different roles in cancer progression, where it has been identified either as a requirement for cell malignancy or as an oncosuppressor (Pasello et al., 2018). In NSCs, CD99 expression is induced upon cell cycle entry and promotes differences in antigen presentation, even if MHCI genes are induced to the same extent in qNSCs and aNSCs by IFNγ. Further studies are needed to unravel what determines CD99 differential expression in NSCs and to explore whether post-translational mechanisms also regulate the surface level of PD-L1 in neurogenic cells. Additionally, we show that CD99 overexpression in qNSCs might be enough to make them vulnerable to $CD8^+$ T cells. It would be worth exploring whether Serpinb9 knock-down and/or Cd274 silencing or PD-L1/PD-1 blockade can also break the protective shield of qNSCs.

Characterizing the immune surveillance of NSCs is central to understand pathological processes that are mainly represented by primary GBM, as it has been demonstrated that SEZ NSCs are the cells-of-origin of these tumors, which is the most aggressive form of brain cancer (Jackson et al., 2019; Lee et al., 2018; Lim et al., 2018). To become malignant, NSCs need to accumulate mutations (Lee et al., 2018) and not be killed by CTLs in the process. However, whether NSCs need to actively evade immune surveillance or this process is just absent in the SEZ was unknown. In light of our data, it seems that GBM-initiating cells might be subjected to immune selective pressure from very early stages, which could partly account for the immunosuppressive properties of GBMs. In fact, these tumors are considered immunologically “cold” as less than 10% of patients respond to immunotherapy (Jackson et al., 2019) and have been extensively studied as a paradigm for cancer-associated immunosuppression. Despite rarely metastasizing to extracranial sites, circulating tumor cells have been detected in patients with GBM, and neoantigens are available for APCs both in the CNS and in the periphery (Lim et al., 2018). However, despite GBM being recognized by the immune system and being susceptible to immune attack, it has many means for eluding the

immunological pressure. First of all, GBMs impair systemic immunity, which significantly accounts for their lack of response to immunotherapy. Among other mechanisms, they can induce systemic immune tolerance to tumor antigens and promote the sequestration of T cells in the bone marrow (Chongsathidkiet et al., 2018; Jackson et al., 2019). Secondly, intrinsic mechanisms are also in place to inhibit tumor-infiltrating lymphocytes. Among them, immune checkpoint ligands such as PD-L1 can be released in extracellular vesicles (Ricklefs et al., 2018), mutations in JAK and STAT proteins as well as downregulation of MHC are relatively common in GBMs (Jackson et al., 2019; Lim et al., 2018), and loss of antigen presentation is associated with shorter survival (Yeung et al., 2013). Increasing evidence suggests that cancers are fueled by specialized cell populations that resemble normal adult SCs in their ability to maintain and propagate homeostasis and regeneration. To achieve this, tumor-initiating SCs must first overcome the immune surveillance that otherwise clears cancerous cells as they emerge. A recent study showed that the activation of immunoevasive pathways is produced in these tumor-initiating cells, and that tumoral adaptive immune resistance emerges already at this point (Miao et al., 2019). Moreover, it was shown that stem-like cancer cells have immunoevasive properties when they enter quiescence (Malladi et al., 2016). Also in GBM, GSCs or tumor cells with stem-cell like properties have been shown to resemble NSCs and be responsible for GBM resistance to therapy and relapse (Matarredona and Pastor, 2019). These cells have enhanced resistance to immunity and can also down-regulate MHCI (DeCordova et al., 2020; Yang et al., 2020). It would be really informative to validate our results in models of GBM initiation. Are the immunoevasive properties of GBM cells directly determined by their cycling activity? Are GBM-initiating cells more immunogenic when formed in immunodeficient animals? Is immunotherapy to GBM more effective when combined with CD99 up-regulation? Answering these questions might unveil the potential applicability of our findings in the tumoral context.

CONCLUSIONS

1. The brain parenchyma is subjected to immune surveillance. In particular, T cell infiltration is facilitated in the SEZ, where neurogenic cells can be eliminated by specific $CD8^+$ T cells.

2. Quiescent NSCs, contrary to their proliferating counterparts, evade adaptive immunity and cannot be killed by $CD8^+$ T cells. In fact, qNSCs are shielded from T lymphocytes by multiple mechanisms that include PD-L1 expression and limited antigen presentation through MHCI.

3. The relative proportion of activation signals, essentially antigen presentation, and inhibitory mechanisms that include PD-L1 expression, determines the susceptibility of NSCs to adaptive immunity. Besides, only when IFNγ is released by activated T cells, NSCs induce MHCI and/or reveal their immunoevasive potential.

4. Antigen presentation is determined, at least in part, by post-translational mechanisms that explain the differences between resting and cycling NSCs. Specifically, the transport of MHCI to the cell surface depends on the expression of CD99, which is more expressed in aNSCs than in qNSCs.

RESUMEN EN ESPAÑOL

INTRODUCCIÓN

El sistema inmunitario adaptativo: biología de linfocitos T

Las moléculas, células y tejidos que nos protegen de infecciones y reaccionan contra células propias dañadas o mutadas constituyen el sistema inmunitario (Abbas et al., 2016). La gran mayoría de las células inmunitarias derivan de células madre (SCs) hematopoyéticas de la médula ósea, que dan lugar a progenitores mieloides o linfoides. Este sistema tiene dos grandes ramas: la inmunidad innata y la adaptativa o específica (Abbas et al., 2016; Savino et al., 2005). La inmunidad innata es la primera línea de defensa contra cualquier agente invasor o antígeno extraño. Es desarrollada por barreras físicas y químicas (epitelios, sustancias antimicrobianas, etc.), células fagocíticas (esencialmente neutrófilos, células dendríticas (DCs), monocitos y macrófagos) y otras, además de proteínas sanguíneas como el sistema del complemento y otros mediadores de la inflamación (Abbas et al., 2016). Las células de la inmunidad innata pueden activar la inmunidad específica presentando antígenos a linfocitos T (Boehm and Swann, 2014). Las respuestas inmunitarias adaptativas pueden ser orquestadas por linfocitos o células B, que producen anticuerpos para marcar y bloquear moléculas o células peligrosas, y/o por linfocitos T αβ (linfocitos T de ahora en adelante), que reconocen antígenos presentados en la superficie de las células unidos al complejo mayor de histocompatibilidad (MHC) de tipo I o II, a través de su receptor de linfocitos T (TCR) (Abbas et al., 2016; Bonilla and Oettgen, 2010). Los dos tipos básicos de linfocitos T son los $CD4^+$ o colaboradores, y los $CD8^+$ o citotóxicos (CTLs). Los primeros secretan citocinas (CKs) que modulan a otras células, y los segundos detectan y eliminan células cancerosas o infectadas por virus (Abbas et al., 2016). Los linfocitos T solo reconocen antígenos presentados por células presentadoras de antígeno (APCs), cuando estas los sitúan en su superficie unidos a MHC de clase I (MHCI) o II (MHCII). MHCII es exclusivo de APCs profesionales, principalmente DCs, macrófagos y linfocitos B (Neefjes et al., 2011). En cambio, casi todas las células nucleadas en los mamíferos expresan MHCI y exponen una muestra representativa de sus antígenos intracelulares en superficie para que los linfocitos T puedan monitorizarlas (Chemali et al., 2011; Neefjes et al., 2011).

Hay miles de millones de especificidades diferentes de linfocitos T y por tanto muy pocos linfocitos T vírgenes (que nunca han sido activados) de cada una (Abbas et

al., 2016). Al mismo tiempo, un patógeno o célula defectuosa puede aparecer en cualquier parte del organismo y en cantidades minúsculas. En consecuencia, se debe maximizar la posibilidad de que estos sean reconocidos por una célula T específica, y aquí es donde los órganos linfoides secundarios (SLOs) son clave. Los linfocitos T vírgenes están en constante recirculación entre la sangre y SLOs (ganglios linfáticos, el bazo y los tejidos linfoides asociados a mucosas) en un proceso mediado por integrinas y quimiocinas (Abbas et al., 2016; Bonilla and Oettgen, 2010). Por otra parte, las DCs, que están presentes en casi todos los tejidos periféricos, incorporan constantemente material del medio y viajan a los SLOs donde presentan antígenos unidos a MHCI (presentación cruzada) y MHCII. Por tanto, tanto los linfocitos T como antígenos de todos los tejidos presentados por DCs se concentran en los ganglios linfáticos (Eisenbarth, 2019; Guermonprez et al., 2002). El mero reconocimiento de su complejo antígeno-MHC específico no es suficiente para activar una célula T vírgen: una segunda señal (o señal 2), principalmente el receptor CD28 en la célula T que se une a CD80 o CD86 en la APC (Chen and Flies, 2013; Guerder and Flavell, 1995), así como las CKs adecuadas (señal 3) son también necesarias (Curtsinger and Mescher, 2010). CD80 y CD86 tienen una elevada expresión en DCs, que también inducen la expresión de la señal 3 (y mejoran la señal 2) en condiciones inflamatorias (Abbas et al., 2016). Cuando los linfocitos T vírgenes se activan, proliferan para ampliar el clon y se diferencian a células efectoras o de memoria (Buchholz et al., 2016; Zhang and Bevan, 2011). Tras ello pueden abandonar los órganos linfoides y migran a los tejidos periféricos donde se necesitan, en un proceso mediado por diferentes moléculas de adhesión tanto en órganos linfoides como en los tejidos inflamados (Abbas et al., 2016; Ley et al., 2007). Los linfocitos T efectores y de memoria no necesitan coestimulación para activarse (Mahnke et al., 2013; Mueller et al., 2013), y tras solo recibir la señal 1 pueden atacar a las células diana. Para ello secretan gránulos cargados con proteínas citotóxicas (perforina y granzimas) que llegan específicamente a la célula diana, e inducen su apoptosis (Martínez-Lostao et al., 2015; Trapani and Smyth, 2002; Voskoboinik et al., 2006, 2015).

Además de la activación del TCR, otras señales pueden modular la función citotóxica de los CTLs efectores, siendo determinante el balance entre señales activadoras (MHC y coestimuladores como CD40) e inhibidoras (puntos de control inmunitarios). Se han descrito muchos puntos de control inmunitario que promueven la inhibición de los CTLs, siendo los mejor estudiados CTLA-4 y PD-1.

Los ligandos de CTLA-4 son las proteínas CD80 y CD86, mientras que PD-1 es activado por PD-L1 o PD-L2 (Van Coillie et al., 2020; Greenwald et al., 2005; Sun et al., 2018). Por otra parte, las APC pueden afectar a la localización de las CTLs efectoras en tejidos periféricos (guiadas por CXCL10 y CXCL9) (Griffith et al., 2014), o resistir a las granzimas expresando inhibidores de estas (el mejor caracterizado es SERPINB9 que inhibe la granzima B (Jiang et al., 2018)). Las respuestas inmunitarias están orquestadas por CKs, siendo el IFNγ la principal en respuestas inmunitarias específicas contra virus o células mutadas (Abbas et al., 2016). Es liberada en gran parte por los propios CTLs activados además de los linfocitos T $CD4^+$ de tipo Th1. Los receptores de IFNγ son heterodímeros transmembrana compuestos por IFNGR1 e IFNGR2 que al activarse promueven la activación de las proteínas JAK. Estas a su vez fosforilan los factores de transcripción STAT que tras ello regulan la expresión de cientos de genes (Castro et al., 2018; Negishi et al., 2018; Schoggins, 2019). Aunque el IFNγ es esencial para la activación y función de las CTLs también puede desarrollar funciones inmunosupresoras según el contexto tisular y la magnitud de su señal (Castro et al., 2018).

Inmunidad en el sistema nervioso central

El cerebro está separado de la periferia por un sistema especializado de barreras que determina sus interacciones con el sistema inmunitario. Desde el cráneo hacia el parénquima, tres capas llamadas meninges rodean el cerebro: la duramadre, la aracnoides y la piamadre (Engelhardt et al., 2017). La duramadre es una estructura fibrosa que contiene grandes senos venosos cuyos vasos sanguíneos son fenestrados. La aracnoides es una membrana avascular contigua a la duramadre y compuesta por dos capas de células epiteliales escamosas conectadas por uniones estrechas. Debajo de la aracnoides hay un espacio lleno de líquido cefalorraquídeo (CSF) llamado espacio subaracnoideo (SAS). Finalmente, la piamadre está compuesta por células epiteliales y una membrana basal sin uniones estrechas. Debajo de ella, la superficie del parénquima del CNS empieza con otra membrana basal y pies de astrocitos que forman la glía limitante. Las arteriolas que penetran en el parénquima cerebral desde el SAS y las vénulas que salen de él son seguidas en un principio por la glía limitante y la piamadre. En estas zonas, las membranas basales del endotelio y de la piamadre no están en contacto directo, generando así espacios perivasculares llenos de CSF entre ellas. Entre esos espacios y en el resto

del CSF hay libre circulación de solutos (Mastorakos and McGavern, 2019; Papadopoulos et al., 2020).

Por otra parte, la barrera hematoencefálica (BBB) es una suma de mecanismos que controlan el intercambio de solutos y células entre la sangre y el SNC. Está compuesta por células endoteliales y membrana basal, pericitos, glía limitante y microglía, que en conjunto restringen el movimiento de la mayoría de las sustancias hacia el SNC (Mastorakos and McGavern, 2019). La glía limitante y las membranas basales son la barrera más restrictiva y por tanto determinante en el intercambio de fluido, solutos y células entre el CSF y líquido intersticial cerebral (ISF) (Engelhardt et al., 2017; Mastorakos and McGavern, 2019; Papadopoulos et al., 2020). Curiosamente, el CSF y las regiones limítrofes del cerebro (ventrículos, plexo coroideo y meninges) están pobladas por una considerable variedad de células inmunitarias, incluidas DCs, macrófagos y linfocitos T, y muestran una reactividad inmunitaria similar a la de la mayoría de órganos (Mundt et al., 2019b, 2019a).

La formación de ISF cerebral se lleva a cabo a través de la entrada de CSF, la extravasación vascular o el metabolismo. Al mismo tiempo se equilibra con la salida de líquido, que arrastra las sustancias de deshecho del parénquima, al CSF (Iliff et al., 2012; Mastorakos and McGavern, 2019; Papadopoulos et al., 2020). La glía limitante - piamadre es la interfaz más grande entre el ISF y el CSF y no es una barrera absoluta, pues los solutos se mueven a través de ella arrastrados por la salida de ISF, y quedan disponibles en el CSF (Engelhardt et al., 2017; Papadopoulos et al., 2020). De hecho, diferentes estudios demuestran que hay un extenso intercambio de solutos entre el ISF y el CSF, que incluye antígenos originados en el parénquima. El CSF, por su parte, drena hacia sangre venosa o vasos linfáticos en la duramadre y sus solutos pueden acceder a los ganglios linfáticos (Alves De Lima et al., 2020; Louveau et al., 2018; Papadopoulos et al., 2020). De este modo se pueden iniciar respuestas inmunitarias mediadas por linfocitos T específicos contra antígenos del parénquima cerebral (Louveau et al., 2015b; Mundt et al., 2019a). Una vez activadas, las células inmunitarias deben migrar a través de diversas barreras en un proceso bifásico para acceder al parénquima cerebral. Primero tienen que atravesar las células endoteliales y la membrana basal interna para acceder a los espacios perivasculares. Después deben atravesar la glía limitante y la membrana basal externa para acceder al parénquima (Engelhardt and Ransohoff, 2012; Mastorakos and McGavern, 2019). Si bien el primer paso no ofrece

resistencia al paso de linfocitos T activados, sea cual sea su especificidad, solo los linfocitos T cuya especificidad sea reconfirmada (tengan de nuevo activación de su TCR o señal 1) por APCs asociadas la periferia del CNS y que presentan antígenos derivados de este, podrán traspasar la glía limitante y acceder al parénquima para ejercer funciones efectoras (Mastorakos and McGavern, 2019; Mundt et al., 2019a). Aunque todavía quedan muchas preguntas por responder al respecto, ya es ampliamente aceptado que la aparición de células defectuosas en el CNS está vigilada estrechamente por el sistema inmunitario (Engelhardt et al., 2017; Mastorakos and McGavern, 2019; Papadopoulos et al., 2020; Ransohoff and Engelhardt, 2012).

Células madre adultas, tumorigénesis e inmunovigilancia

La mayoría de los tejidos de los mamíferos adultos contienen SCs adultas, esenciales para su homeostasis y regeneración. El cerebro no es una excepción, y las NSC generan nuevos astrocitos, oligodendrocitos y neuronas a lo largo de la vida. Estas se ubican en dos nichos neurogénicos principales, que son la zona subgranular (SGZ) en el hipocampo, y la zona subependimaria (SEZ, también conocida como zona ventricular-subventricular o V-SVZ) que es el nicho más grande. La SEZ está situada a lo largo de las paredes de los ventrículos laterales (Mirzadeh et al., 2008; Obernier and Alvarez-Buylla, 2019). Las NSC son astrocitos especializados con una morfología radial semejante a la de la glía radial embrionaria, a partir de la cual se originan durante el desarrollo embrionario medio (Chaker et al., 2016; Doetsch, 2003; Doetsch et al., 1999b; Fuentealba et al., 2015; Furutachi et al., 2015; Kriegstein and Alvarez-Buylla, 2009). Las NSCs extienden un proceso apical con un cilio primario que contacta el CSF, y en su extremo basal contactan con el plexo vascular a través de un largo proceso citoplasmático (Chaker et al., 2016; Fuentealba et al., 2012; Mirzadeh et al., 2008; Tavazoie et al., 2008). Esta morfología radial permite una interacción única con el CSF y los vasos sanguíneos que contribuyen a la regulación de las NSCs. Estas células, además, están expuestas a factores producidos por células vecinas, incluidas otras NSC, su progenie inmediata, células ependimarias, astrocitos, microglia y neuronas (Morante-Redolat and Porlan, 2019; Obernier and Alvarez-Buylla, 2019; Porlan et al., 2013; Silva-Vargas et al., 2016; Sirerol-Piquer et al., 2019).

En la SEZ coexisten NSCs en diferentes estados de activación. La mayoría de ellas están en quiescencia, un estado reversible y mantenido activamente caracterizado por la detención del ciclo celular, baja actividad metabólica, así como una reducción de la síntesis de RNA y proteínas (Urban et al., 2019). Cuando las NSCs se activan producen neuronas migratorias jóvenes (neuroblastos o NB) a través de la generación de células progenitoras neurales (NPCs) que se dividen rápidamente (Doetsch et al., 1997, 1999b). Las NPC se dividen simétricamente 3 o 4 veces antes de generar NBs. Estos, a su vez, pueden dividirse una o dos veces para amplificar la población (Calzolari et al., 2015; Ponti et al., 2013). Denominamos a la subpoblación de NBs en proliferación como NB tempranos (ENBs) y a los que están en migración como NB tardíos (LNBs). Los LNBs generados migran tangencialmente en cadenas hacia el bulbo olfatorio (OB), creando la corriente migratoria rostral (RMS) (Doetsch and Alvarez-Buylla, 1996; Lois et al., 1996), y allí se diferencian a interneuronas que se integran en circuitos neurales preexistentes (Lledo and Saghatelyan, 2005; Obernier and Alvarez-Buylla, 2019). La SEZ se encuentra en la interfaz entre el parénquima cerebral y el ventrículo lateral. La ausencia de uniones estrechas en la barrera ependimaria y la proximidad de las NSC con el CSF sugieren que la SEZ podría tener un fácil drenaje de antígenos al ventrículo y una infiltración de leucocitos incrementada (Bechmann et al., 2007; Engelhardt and Ransohoff, 2012; Jiménez et al., 2014; Wilson et al., 2010).

Tanto las SCs adultas como el sistema inmunitario evolucionaron para prevenir, mitigar y resolver las lesiones tisulares y no sorprende que estén en continua comunicación y puedan modularse entre sí. De hecho, las células inmunitarias son esenciales para crear el microambiente adecuado en los nichos de SCs (Aurora and Olson, 2014), y las SCs pueden atraer a células inmunitarias para mantener la homeostasis de los tejidos o hacer frente a situaciones de estrés (Naik et al., 2018). Al tener capacidad de autorrenovación, son las células proliferativas más longevas en los organismos multicelulares y, por tanto, tienen un riesgo aumentado de acumular mutaciones y volverse tumorigénicas (Ermolaeva et al., 2018; Tomasetti et al., 2017; Zindl and Chaplin, 2010). Las mutaciones somáticas pueden producirse por factores ambientales o errores de replicación del ADN (Blokzijl et al., 2016; Tomasetti et al., 2017), y pueden promover el desarrollo tumoral cuando favorecen una proliferación sostenida, evasión de los supresores tumorales, resistencia a la muerte celular, inmortalidad replicativa, angiogénesis y/o capacidad invasiva, así como resistencia a la destrucción inmunitaria, entre otros (Hanahan, 2022).

Específicamente, se ha demostrado que las células que originan los glioblastomas primario (GBM) son NSCs de la SEZ, tanto en ratones como en humanos (Alcantara Llaguno and Parada, 2021; Alcantara Llaguno et al., 2009, 2019; Lee et al., 2018), y se ha propuesto que estos tumores contienen pequeñas poblaciones de células cancerosas con propiedades similares a células madre (NSCs).

Tradicionalmente se pensaba que todas las células nucleadas de los mamíferos expresaban MHCI y exponían antígenos intracelulares a los CTLs. Sin embargo, recientemente se ha demostrado que este no es el caso de las SCs quiescentes en el músculo y el folículo piloso. Por contra, estas células dejan de expresar MHCI y evitan la vigilancia inmunológica, protegiéndose así para preservar el potencial regenerador del tejido en caso de daño. Por otro lado, la evasión inmunitaria de las SCs adultas puede favorecer su transformación neoplásica (Agudo et al., 2018).

OBJETIVOS

1. Determinar si existe inmunovigilancia en la SEZ, y si esta región tiene más permisividad a la infiltración de linfocitos T $CD8^+$ que otras partes del cerebro.

2. Determinar si las diferentes poblaciones neurogénicas de la SEZ tienen diferente grado de susceptibilidad a los linfocitos T $CD8^+$.

3. Determinar los mecanismos responsables de la diferente susceptibilidad de las poblaciones neurogénicas de la SEZ a los linfocitos T $CD8^+$.

METODOLOGÍA

Modelos animales. Los ratones fueron criados y alojados en el animalario de la *Universitat de València* (Servei Central de Suport a la Investigació Experimental, Burjassot) según las directrices de la Unión Europea. Salvo que se indique lo contrario se utilizaron ratones de 2 a 4 meses de edad de las cepas C57BL/6J (ratones *wild-type*), Rag1 *knock-out* (no tienen linfocitos), JEDI (fuente de linfocitos T JEDI), R26mTmG y hGfap-Cre para cruzarlos y generar ratones R26mTmG;hGfap-Cre (que expresan EGFP en las células neurogénicas y astrocitos), CX3CR1-EGFP (reportero de microglía) y B10D2 (aportan el alelo H2Kd, necesario para la histocompatibilidad con los linfocitos T JEDI).

Electroporación in utero. Ratonas preñadas en E15.5 fueron anestesiadas y se les aplicó la correspondiente analgesia. Se realizó una incisión en el abdomen para acceder al útero y extraerlo. Se introdujeron los plásmidos pertinentes en los ventrículos laterales de los embriones y se colocaron lateralmente electrodos de tipo fórceps alrededor de la cabeza. El electrodo positivo se orientó con la región ventrolateral del hemisferio inyectado y se aplicaron cinco pulsos de 50 V y 80 ms. El útero se colocó de nuevo en la cavidad abdominal y esta se cerró con suturas absorbibles.

Inyección de lipopolisacárido. El lipopolisacárido (LPS) (Sigma, L263) se inyectó por vía intraperitoneal (i.p.) en una dosis única de 5 mg/kg.

Aislamiento y transferencia de linfocitos T JEDI. Los linfocitos T JEDI vírgenes se aislaron mediante separación magnética de los bazos de ratones JEDI de 2 a 4 meses de edad. Para ello se utilizó el *EasySep Mouse Naïve CD8$^+$ T Cell Isolation Kit* (Stemcell, 19858) siguiendo las instrucciones del fabricante, pero usando el cóctel de anticuerpos y las partículas magnéticas a mitad de concentración. Las células obtenidas se resuspendieron en PBS y para su uso *in vivo* se inyectaron junto con lentivirus condificantes para EGFP (LV.EGFP) mediante inyección retroorbital intravenosa (i.v.). Para el cocultivo con NSCs, se aislaron linfocitos T CD8$^+$ totales utilizando el *EasySep Mouse CD8$^+$ T Cell Isolation Kit* (Stemcell, 19853).

Producción y titulación de lentivirus. Los LV.EGFP fueron generados en células HEK293T. Para ello estas fueron transfectadas con plásmido de envoltura CMV-

VSVG-PolyA, plásmidos de empaquetamiento CMV-GAG-POL-RRE y CMV-REV y plásmido de transferencia con el gen de interés (5'LTR-CMV-EGFP-LTR). Se cambió el medio de cultivo al día siguiente y se recogió el medio condicionado a las 48 y 72 h tras la transfección. Este se centrifugó (300x*g*, 5 min), filtró (0,45 µm), ultracentrifugó (90.000x*g*, 90 min) y resuspendió en PBS con 1% BSA. Las suspensiones de virus obtenidas a cada tiempo se agruparon y ultracentrifugaron nuevamente. Tras la resuspensión final se alicuotaron y ultracongelaron. La titulación se hizo en células HEK293T midiendo el %$EGFP^+$ obtenido con diferentes diluciones seriadas de virus.

Disección de la SEZ. Los ratones fueron sacrificados por dislocación cervical. La disección se realizó siguiendo los protocolos publicados por nuestro laboratorio (Belenguer et al., 2016, 2021).

Inmunofluorescencia. Cuando se necesitaban células vivas para otras técnicas, las SEZs extraídas se fijaron tras su disección por inmersión en paraformaldehído (PFA) al 4% y se hizo inmunofluorescencia en *whole mount*. En caso contrario, los ratones fueron perfundidos con PFA al 4% en tampón salino y se obtuvieron cortes de la SEZ. Tras lavar la muestra fijada con PBS se incubaron en una solución de bloqueo (PBS con suero al 10 % y TritonX-100 al 0,2 %). A continuación, se incubaron un día con los anticuerpos primarios correspondientes contra CD45.1 (BD, 563754), Ki67 (Abcam, ab15580), anti-SERPINB9 (Santa cruz, sc-390406) o EGFP/GFP (1:1000). Después de los correspondientes lavados, las muestras fueron incubadas con anticuerpos secundarios marcados fluorescentemente durante 1h, los núcleos se tiñeron con DRAQ5 o DAPI y las muestras se montaron con Fourmount-GT (Electron Microscopy Sciences, 17984-25) o FlourSave Reagent (Calbiochem, 345789). Las imágenes se adquirieron utilizando un microscopio confocal Olympus FV10i con láseres de 405, 458, 488 y 633 nm.

Fenotipado celular por citometría de flujo. Para el estudio de la SEZ el protocolo fue publicado recientemente por nuestro laboratorio y ahí se pueden consultar los detalles (Belenguer et al., 2021). El procesamiento de la corteza cerebral fue similar al de la SEZ. Para caracterizar las células inmunitarias en la SEZ, los ratones se perfundieron transcardiacamente previamente a la extracción del cerebro con solución salina (0,09 % NaCl) con 10 U/ml de heparina durante 10 min, y la disgregación tisular se hizo mecánicamente en frío. Por otra parte, el fenotipado de

NSCs en cultivo no requiere de disgregación enzimática (se hizo mecánicamente con la pipeta) ni disección, pero por lo demás fue igual. La autofagia se evaluó con el Autophagy Assay Kit (Red) (Abcam, ab270790). El marcaje de proteínas intracelulares se hizo utilizando una solución comercial de fijación y permeabilización (BD, 554722), siguiendo las instrucciones indicadas por su ficha técnica. Para el análisis de células inmunitarias periféricas, el tampón de bloqueo fue diferente (PBS con FCS al 2 % y EDTA a 2 mM). Por lo demás, las únicas diferencias fueron un paso adicional para el bloqueo de FcR (Miltenyi, 130-092-575) y, excepto en el caso del análisis de sangre entera, la lisis de eritrocitos (Sigma, R7757). Para extraer esplenocitos, los bazos se perfundieron con tampón usando una jeringuilla y las células sanguíneas se obtuvieron de sangre ventricular (fueron cogidas al final de otros experimentos). Los datos se analizaron con Flowjo y se utilizó la intensidad mediana de fluorescencia (MFI) para comparar la expresión de proteínas. Las MFI se normalizaron restando el valor de autofluorescencia.

Cultivos de NSC y cocultivos. Los detalles sobre el establecimiento de cultivos de NSCs y los medios de cultivo utilizados se pueden consultar en la metodología publicada por nuestro grupo (Belenguer et al., 2016). Para el cocultivo de NSC con linfocitos T JEDI se sembraron 50.000 NSCs/pocillo en placas de 24 pocillos. Al día siguiente se sembraron 120.000 linfocitos T JEDI en insertos Transwell (0,4 µm) en medio X-VIVOTM 15 (Lonza), y se matuvo el co-cultivo durante 3 días.

Silenciamiento de genes y sobreexpresión. Para la nucleofección de NSCs se utilizaron 7 µg de plásmido y 2,5 millones de NSC con un kit específico de NSCs murinas (Lonza, vpg-1004). Se utilizaron los siguientes plásmidos: shRNA CD99 TRCN0000077078 pLKO.1-CMV-tGFP (Sigma) para la eliminación de *Cd99* y CD99 Lentiviral cDNA ORF Clone, Mouse, C-GFPSpark® tag (Abytek, MG50520-ACGLN) para la sobreexpresión de CD99. También se usó un plásmido con shRNA control pLKO.1.

Ensayo cinético de exportación MHCI. Para evaluar la velocidad de salida de MHCI a la membrana celular, NSCs *in vitro* se incubaron con tampón de bloqueo conteniendo 8 µg/ml de anticuerpo anti H2Kb/Db conjugado con APC (Miltenyi, 130-115-587). Después de 45 min las células se lavaron y se añadió el mismo clon de anticuerpo anti H2Kb/Db conjugado con VioBlue (Miltenyi, 130-115-592) a una

concentración de 0,5 µg/ml. Las muestras se analizaron inmediatamente (tiempo de 0 min) y cada 10 min.

Tratamientos. Salvo que se indique lo contrario los tratamientos *in vitro* se realizaron durante 24 h. Se utilizaron IFNγ 100 ng/ml (Preprotech, 315-05), TNFα 10 ng/ml (R&D, 410-MT-010), forskolina (Selleckchem, S2449), IBMX (Stemcell, 72762), rapamicina (Selleckchem, S1039), bafilomicina A1 (Invivogen, tlrl-baf1), bortezomib (Tocris, 7282), brefeldina A (Medchemexpress, HY-16592), rhosin (Tocris, 5003) y EHT 1864 (Tocris, 3872). La privación de nutrientes se hizo en PBS durante 4h.

Análisis de la expresión génica. El RNA de homogeneizados de la SEZ y cultivos de NSCs se extrajo y purificó con los kits *RNeasy Plus Mini* o *Micro* (Qiagen, 74104 o 74034) y se cuantificó la concentración de ARN con un nanodrop 2000 (Thermofisher, ND2000). 0,3-1 µg de RNA se retrotranscribieron utilizando el kit *PrimeScript RT* (Takara, RR037A) y el DNA complementario obtenido (cDNA) se diluyó en agua libre de RNAsas. La expresión génica se analizó mediante PCR cuantitativa (RT-qPCR) con el sistema de detección *Step One Plus* (Applied Biosystems) utilizando 5-15 ng de cDNA, sondas TaqMan prediseñadas y la *Premix Ex Taq Master Mix* (Takara, RR390).

Co-inmunoprecipitación y western blot. Las NSCs (previamente tratadas con IFNγ) se lisaron con 1 ml de tampón NP-40 (TrisHCl 10 mM, pH 8,0, NaCl 150 mM, Nonidet P40 al 1 %, glicerol al 10 %, ADNasa 1x, SDS 0,2%, $NaVO_3$ 1 mM, NaF 1 mM, PMSF 1 mM y Complet mini 1x) y se centrifugaron a máxima velocidad (20817x*g,* 15min, 4°C). Los sobrenadantes se incubaron con partículas magnéticas (*dynabeads)* de proteína G (Thermofisher, 10003D) durante 30 min y posteriormente se retiraron con un imán. Los lisados se incubaron con anticuerpo anti-CD99 (R&D, AF3905) o control (R&D AB-108-C) en una rueda giratoria. Al día siguiente se añadieron 50 µl de *dynabeads* (proteína G) y se incubaron durante 20 min a 4 °C. Después las muestras se lavaron minuciosamente con tampón NP-40 (ahora con 300 NaCl mM). Finalmente se incubaron a 98°C durante 5 min con tampón de muestra de *western blot*, y las partículas magnéticas se eliminaron. Las muestras se cargaron en un gel de electroforesis de poliacrilamida al 12%, se realizó la separación electroforética de proteínas y se transfirieron a una membrana de nitrocelulosa usando el *Trans-Blot Turbo Transfer System* (Bio-Rad). Se bloqueó esta con leche al 5% en TBS-T y

posteriormente se incubó con anticuerpo anti-H2Kb (BD, 562832) o anti-CD99 (R&D, AF3905). Al día siguiente las membranas de nitrocelulosa se incubaron con anticuerpos secundarios conjugados con HRP y se revelaron con *SuperSignal West Femto* (Thermo Scientific, 34095).

RNA-seq. La comparación entre poblaciones se realizó generando *heatmps* utilizando los paquetes *ComplexHeatmap* (Gu et al., 2016) y ggplot2 (Wickham, 2016) en R o GraphPad Prism Software.

Análisis estadístico. Las pruebas estadísticas se realizaron en el software GraphPad Prism, versión 8.0.2 con pruebas t de Student o ANOVA de una vía seguida de test Tukey post-hoc.

RESULTADOS

La ausencia de linfocitos T no afecta a las proporciones de NSCs en estado basal

En primer lugar, quisimos evaluar si la ausencia de linfocitos T tiene un impacto en las poblaciones neurogénicas en la SEZ analizando ratones *Rag*$^{-/-}$ (Mombaerts et al., 1992), que carecen de linfocitos B y T, en comparación con ratones inmunocompetentes. Sin embargo, no observamos ningún cambio en las proporciones de poblaciones neurogénicas en la SEZ. Por otra parte, tratamos de identificar linfocitos T en la SEZ de ratones sanos adultos jóvenes. Para ello perfundimos minuciosamente a los animales con solución salina y heparina y analizamos la SEZ por citometría de flujo. Se encontraron unos pocos linfocitos T en la SEZ que, en relación con los glóbulos rojos, estaban claramente enriquecidos en comparación con sangre periférica. Si bien estos linfocitos podrían haber estado adheridos a vasos sanguíneos o interfaces cerebrales, parece que podría haber linfocitos T en la SEZ, aunque con una frecuencia extremadamente baja.

Las NSC quiescentes evaden la inmunidad celular específica

Decidimos probar si las NSCs de la SEZ adulta son susceptibles a la vigilancia mediada por linfocitos T mediante el uso de ratones JEDI, cuyos linfocitos T $CD8^+$ (T JEDI) expresan un TCR que reconoce específicamente un epítopo de GFP/EGFP. La transferencia de linfocitos T JEDI a un ratón debe combinarse con la vacunación con GFP/EGFP para activarlas, lo que decidimos hacer inyectando simultáneamente LV.EGFP. Para que las NSCs y su progenie expresaran EGFP y fueran por tanto atacadas por las T JEDI, generamos ratones R26mTmG;hGfap-Cre, que expresan TdTomato en todas las células, y EGFP en aquellas que expresan Gfap o provienen de otras que lo han hecho (lo que incluye las células neurogénicas y los astrocitos). Tras introducir linfocitos T JEDI y LV.EGFP en estos ratones observamos que, si bien las demás poblaciones neurogénicas fueron en buena parte eliminadas por las T JEDI, el número de NSCs quiescnetes no cambió. Así, aunque la reducción de NPCs y NBs podría ser una consecuencia directa de la muerte mediada por linfocitos T JEDI o un efecto indirecto derivado de la reducción de aNSC, las NSCs inactivas son resistentes a los CTLs.

A diferencia de lo que se ha visto en periferia (Agudo et al., 2015, 2018), las poblaciones en proliferación del linaje neurogénico no fueron eliminadas por completo. Para probar si una respuesta parcial a los linfocitos T es característica del cerebro sano, aprovechamos el hecho de que la mayoría de los astrocitos son $EGFP^+$ en ratones R26mTmG;hGfap-Cre y analizamos los efectos de los linfocitos T JEDI en la corteza cerebral. Por una parte, la infiltración de linfocitos T fue considerablemente mayor en la SEZ que en la corteza. Paralelamente, al igual que vio en la SEZ, alrededor de la mitad de astrocitos corticales sobrevivieron. Una posible explicación de esta muerte parcial podría ser que el número de Ts JEDI que acceden al cerebro no fue suficiente en relación con el número de células $EGFP^+$ en estos ratones. Por ello decidimos utilizar un segundo modelo de expresión de EGFP en células neurogénicas que produce menos células positivas. Por electroporación *in utero* en E15.5, se introdujeron en las NSCs un transposón que portaba un cDNA de EGFP (PB-CAG-EGFP) y un cDNA codificante de transposasa controlado por el promotor de Glast (GLAST-Transp). Así las NSCs adultas se convierten, junto con toda su progenie celular, en $EGFP^+$. Esta vez, los linfocitos T mataron a la mayoría de las células neurogénicas $EGFP^+$ en la SEZ. Aun así, fueron nuevamente incapaces de matar las NSC quiescentes.

Un equilibrio dinámico entre señales opuestas determina la evasión inmune

Para intentar explicar las diferencias observadas entre NSCs quiescentes y activadas evaluamos la presentación antigénica en el linaje neurogénico. Curiosamente, parece que las células neurogénicas no expresan MHCI en reposo, por lo que evaluamos los niveles de H2Kb/Db en ratones R26mTmG;hGfap-Cre tras la inyección de linfocitos T JEDI y LV. EGFP. Ello produce un gran incremento de IFNγ en la SEZ, lo que puede inducir MHCI. De hecho, en estas circunstancias todas las células del linaje exhibieron MHCI en su superficie. No obstante, los niveles fueron diferentes entre las poblaciones: la expresión más alta se encontró en aNSC mientras que las qNSC exhibieron niveles bastante inferiores.

Es poco probable que los niveles más bajos de MHCI en la membrana de qNSCs expliquen por sí solos la resistencia a los CTLs de estas células. Como primera aproximación para descubrir posibles mecanismos adicionales que expliquen la diferente susceptibilidad de las qNSCs y el resto del linaje, exploramos nuestros datos de RNA-seq (Belenguer et al., 2020). En primer lugar, las qNSCs muestran un transcriptoma muy diferente cuando se evalúan los genes incluidos en los GO *"Regulación de la activación de linfocitos T"* e "*Inmunidad mediada por linfocitos T".* Además, las qNSCs expresan en mucha mayor medida ligandos de puntos de control inmunitario, incluido PD-L1, y genes protectores frente a CTLs, como la enzima SERPINB9. Por otra parte, las aNSC tienen incrementada la expresión de CXCL10. La expresión de SERPINB9 a nivel de proteína fue validada por inmunofluorescencia, mientras que PD-L1 se induce mucho más en qNSCs que en aNSCs cuando linfocitos T JEDI activados infiltran la SEZ. Esto sugiere que el resultado de la interacción entre una NSC y un CTL activado específico contra ella podría depender de un equilibrio finamente ajustado entre señales activadoras e inhibidoras. Por otra parte, ensayos de cocultivos *in vitro* muestran que las NSCs, que no expresan MHCI ni PD-L1 en condiciones basales, inducen estas moléculas en presencia de CTLs activados de forma dependiente de IFNγ.

Mecanismos postraduccionales controlan la presentación de antígenos

Se ha demostrado que la evasión inmune de las células madre inactivas fuera del cerebro está regulada a nivel transcripcional, ya que las células en silencian NLCR5,

el transactivador clave de los genes MHCI (Agudo et al., 2018). Sin embargo, nuestros datos de RNA-seq muestran que la expresión de NLRC5 y MHCI sigue patrones no correlativos en las poblaciones neurogénicas. Eso nos llevó a centrarnos en mecanismos de regulación postranscripcionales. Ciertamente, se han descrito diferentes mecanismos, principalmente a nivel postraduccional, que pueden regular la presentación antigénica y que podrían estar actuando en las NSCs de la SEZ.

En primer lugar, la bibliografía existente (Leeman et al., 2018) y nuestros datos de RNA-seq (Belenguer et al., 2020) respaldan una tasa autofágica más alta en qNSCs, y se ha visto que esta puede reducir a la exposición de antígenos en superficie (Yamamoto et al., 2020). En consecuencia, el tratamiento de NSC en cultivo con Bafilomicina A1, un inhibidor de la autofagia, incrementó los niveles de MHCI en NSCs estimuladas con IFNγ, mientras que lo contrario ocurrió al inducir autofagia con rapamicina o mediante la privación de nutrientes. Por otro lado, la actividad proteasomal está disminuida en qNSCs (Leeman et al., 2018) como también se ve en nuestros datos de RNA-seq (Belenguer et al., 2020). Esta es necesaria para generar los péptidos que se cargan en los complejos MHCI, y el inhibidor proteasomal bortezomib impidió la inducción de MHCI producida por IFNγ en las NSCs.

Los complejos antígeno-MHCI se ensamblan en el RE, viajan al compartimento de Golgi y luego se exportan a la membrana celular dentro de las vesículas generadas en la red trans-golgi (TGN) (Neefjes et al., 2011). En consecuencia, la Brefeldina A1, un inhibidor del transporte de proteínas desde el RE hasta el aparato de Golgi, suprimió por completo la inducción de MHCI en la superficie celular mediada por IFNγ. Por otra parte, CD99 es una proteína transmembrana que se ha demostrado que regula el transporte intracelular de MHCI (Brémond et al., 2009; Kim et al., 1998; Sohn et al., 2001). CD99 se expresa en NSC *in vitro* y nuestros resultados indican que su expresión se correlaciona con la capacidad de inducir la presentación de antígenos en membrana afectando a su tráfico intracelular mediante la unión directa de CD99 a los complejos MHCI. Además, las aNSC expresan mucha más proteína y RNA mensajero de CD99 que las qNSC *in vivo*. Por último, parece que la sobreexpresión de CD99 en qNSCs *in vivo* hace que estas sean vulnerables a las células T JEDI activadas.

CONCLUSIONES

1. El parénquima cerebral está sujeto a vigilancia inmunitaria. En particular, la infiltración de linfocitos T está incrementada en la SEZ, donde las células neurogénicas pueden ser eliminadas por linfocitos T $CD8^+$ específicos.

2. Las NSCs quiescentes, a diferencia de las activadas, evaden la inmunidad específica y no pueden ser eliminadas por linfocitos T $CD8^+$. De hecho, las qNSCs están protegidas de los linfocitos T por múltiples mecanismos que incluyen la expresión de PD-L1 y una limitada capacidad de inducir MHCI.

3. La proporción relativa entre señales activadoras, esencialmente presentación antigénica, y mecanismos inhibidores como PD-L1, determina la susceptibilidad de las NSC a la inmunidad celular específica. Además, solo cuando los linfocitos T activados liberan IFNγ, las NSCs inducen MHCI y/o revelan su potencial inmunoevasivo.

4. La presentación de antígenos está determinada, al menos en parte, por mecanismos postraduccionales que explican las diferencias entre NSCs quiescentes y activadas. Específicamente, el transporte de MHCI a la superficie celular depende de CD99, cuya expresión es mayor en aNSCs que en qNSCs.

BIBLIOGRAPHY

Abbas, A.K., Lichtman, A.H., Pillai, S., Baker, D.L., and Baker, A. (2016). Cellular and Molecular Immunology (Elsevier).

Agudo, J. (2021). Immune privilege of skin stem cells: What do we know and what can we learn? Exp. Dermatol. *30*, 522–528.

Agudo, J., Ruzo, A., Park, E.S., Sweeney, R., Kana, V., Wu, M., Zhao, Y., Egli, D., Merad, M., and Brown, B.D. (2015). GFP-specific CD8 T cells enable targeted cell depletion and visualization of T-cell interactions. Nat. Biotechnol. *33*, 1287–1292.

Agudo, J., Park, E.S., Rose, S.A., Alibo, E., Sweeney, R., Dhainaut, M., Kobayashi, K.S., Sachidanandam, R., Baccarini, A., Merad, M., et al. (2018). Quiescent Tissue Stem Cells Evade Immune Surveillance. Immunity *48*, 271-285.e5.

Ajami, B., Bennett, J.L., Krieger, C., Tetzlaff, W., and Rossi, F.M.V. (2007). Local self-renewal can sustain CNS microglia maintenance and function throughout adult life. Nat. Neurosci. *10*, 1538–1543.

Ajami, B., Bennett, J.L., Krieger, C., McNagny, K.M., and Rossi, F.M.V. (2011). Infiltrating monocytes trigger EAE progression, but do not contribute to the resident microglia pool. Nat. Neurosci. *14*, 1142–1150.

Alcantara Llaguno, S., and Parada, L.F. (2021). Cancer stem cells in gliomas: evolving concepts and therapeutic implications. Curr. Opin. Neurol. *34*, 868–874.

Alcantara Llaguno, S., Chen, J., Kwon, C.H., Jackson, E.L., Li, Y., Burns, D.K., Alvarez-Buylla, A., and Parada, L.F. (2009). Malignant Astrocytomas Originate from Neural Stem/Progenitor Cells in a Somatic Tumor Suppressor Mouse Model. Cancer Cell *15*, 45–56.

Alcantara Llaguno, S., Sun, D., Pedraza, A.M., Vera, E., Wang, Z., Burns, D.K., and Parada, L.F. (2019). Cell-of-origin susceptibility to glioblastoma formation declines with neural lineage restriction. Nat. Neurosci. *22*, 545–555.

Alcantara Llaguno, S.R., Wang, Z., Sun, D., Chen, J., Xu, J., Kim, E., Hatanpaa, K.J., Raisanen, J.M., Burns, D.K., Johnson, J.E., et al. (2015). Adult Lineage-Restricted CNS Progenitors Specify Distinct Glioblastoma Subtypes. Cancer Cell *28*, 429–440.

Ali, N., and Rosenblum, M.D. (2017). Regulatory T cells in skin. Immunology *152*, 372–381.

Ali, N., Zirak, B., Rodriguez, R.S., Pauli, M.L., Truong, H.A., Lai, K., Ahn, R., Corbin, K., Lowe, M.M., Scharschmidt, T.C., et al. (2017). Regulatory T Cells in Skin Facilitate Epithelial Stem Cell Differentiation. Cell *169*, 1119-1129.e11.

Alves De Lima, K., Rustenhoven, J., and Kipnis, J. (2020). Meningeal Immunity and Its Function in Maintenance of the Central Nervous System in Health and Disease. Annu. Rev. Immunol. *38*, 597–620.

Ambros, I.M., Ambros, P.F., Strehl, S., Kovar, H., Gadner, H., and Salzer-Kuntschik, M. (1991). MIC2 Is a Specific Marker for Ewing's Sarcoma and Peripheral Primitive Neuroectodermal Tumors Evidence for a Common Histogenesis of Ewing's Sarcoma and Peripheral Primitive Neuroectodermal Tumors From MICZ Expression and Specific Chromosome Aberration. Cancer *67*, 1886–1893.

Aparicio-Domingo, P., Romera-Hernandez, M., Karrich, J.J., Cornelissen, F., Papazian, N., Lindenbergh-Kortleve, D.J., Butler, J.A., Boon, L., Coles, M.C., Samsom, J.N., et al. (2015). Type 3 innate lymphoid cells maintain intestinal epithelial stem cells after tissue damage. J. Exp. Med. *212*, 1783–1791.

Arvidsson, L., Covacu, R., Estrada, C.P., Sankavaram, S.R., Svensson, M., and Brundin, L. (2015). Long-distance effects of inflammation on differentiation of adult spinal cord neural stem/progenitor cells. J. Neuroimmunol. *288*, 47–55.

Arya, R., and Bassing, C.H. (2017). V(D)J Recombination Exploits DNA Damage Responses to Promote Immunity. Trends Genet. *33*, 479–489.

Aurora, A.B., and Olson, E.N. (2014). Immune Modulation of Stem Cells and Regeneration. Cell Stem Cell *15*, 14–25.

Bagchi, S., Yuan, R., and Engleman, E.G. (2021). Immune Checkpoint Inhibitors for the Treatment of Cancer: Clinical Impact and Mechanisms of Response and Resistance. Annu. Rev. Pathol. *16*, 223–249.

Baldominos, P., Barbera-Mourelle, A., Barreiro, O., Huang, Y., Wight, A., Cho, J.W., Zhao, X., Estivill, G., Adam, I., Sanchez, X., et al. (2022). Quiescent cancer cells resist T cell attack by forming an immunosuppressive niche. Cell *185*, 1694-1708.e19.

Barazzuol, L., Ju, L., and Jeggo, P.A. (2017). A coordinated DNA damage response promotes adult quiescent neural stem cell activation. PLOS Biol. *15*, e2001264.

Basak, O., Krieger, T.G., Muraro, M.J., Wiebrands, K., Stange, D.E., Frias-Aldeguer, J., Rivron, N.C., van de Wetering, M., van Es, J.H., van Oudenaarden, A., et al. (2018). Troy+ brain stem cells cycle through quiescence and regulate their number by sensing niche occupancy. Proc. Natl. Acad. Sci. U. S. A. *115*, E610–E619.

Bechmann, I., Galea, I., and Perry, V.H. (2007). What is the blood-brain barrier (not)? Trends Immunol. *28*, 5–11.

Belenguer, G., Domingo-Muelas, A., Ferrón, S.R., Morante-Redolat, J.M., and Fariñas, I. (2016). Isolation, culture and analysis of adult subependymal neural stem cells. Differentiation. *91*, 28–41.

Belenguer, G., Duart-Abadia, P., Jordán-Pla, A., Domingo-Muelas, A., Blasco-Chamarro, L., Ferrón, S.R., Morante-Redolat, J.M., and Fariñas, I. (2020). Adult Neural Stem Cells Are Alerted by Systemic Inflammation through TNF-α Receptor Signaling. Cell Stem Cell *28*, 285–299.

Belenguer, G., Duart-Abadia, P., Domingo-Muelas, A., Morante-Redolat, J.M., and Fariñas, I. (2021). Cell population analysis of the adult murine subependymal neurogenic lineage by flow cytometry. STAR Protoc. *2*.

Benham, A., Grommé, M., and Neefjes, J. (1998). Allelic Differences in the Relationship Between Proteasome Activity and MHC Class I Peptide Loading. J Immunol *161*, 83–89.

Bennett, F.C., Bennett, M.L., Yaqoob, F., Mulinyawe, S.B., Grant, G.A., Hayden Gephart, M., Plowey, E.D., and Barres, B.A. (2018). A Combination of Ontogeny and CNS Environment Establishes Microglial Identity. Neuron *98*, 1170-1183.e8.

Bertrand, H. (2014). Unraveling Autoimmunity with the Adoptive Transfer of T Cells from TCR-Transgenic Mice. Methods Mol. Biol. *1142*, 41–48.

Bhaduri, A., Di Lullo, E., Jung, D., Müller, S., Crouch, E.E., Espinosa, C.S., Ozawa, T., Alvarado, B., Spatazza, J., Cadwell, C.R., et al. (2020). Outer Radial Glia-like Cancer Stem Cells Contribute to Heterogeneity of Glioblastoma. Cell Stem Cell *26*, 48-63.e6.

Bixel, G., Kloep, S., Butz, S., Petri, B., Engelhardt, B., and Vestweber, D. (2004). Mouse CD99 participates in T-cell recruitment into inflamed skin. Blood *104*, 3205–3213.

Blanpain, C., and Fuchs, E. (2014). Plasticity of epithelial stem cells in tissue regeneration. Science (80-.). *344*.

Blokzijl, F., De Ligt, J., Jager, M., Sasselli, V., Roerink, S., Sasaki, N., Huch, M., Boymans, S., Kuijk, E., Prins, P., et al. (2016). Tissue-specific mutation accumulation in human adult stem cells during life. Nature *538*, 260–264.

Boehm, T., and Swann, J.B. (2014). Origin and Evolution of Adaptive Immunity. Annu Rev Anim Biosci *2*, 259–283.

Bonilla, F.A., and Oettgen, H.C. (2010). Adaptive immunity. J. Allergy Clin. Immunol. *125*.

Bordi, M., De Cegli, R., Testa, B., Nixon, R.A., Ballabio, A., and Cecconi, F. (2021). A gene toolbox for monitoring autophagy transcription. Cell Death Dis. *12*.

Boss, J.M., and Jensen, P.E. (2003). Transcriptional regulation of the MHC class II antigen presentation pathway. Curr. Opin. Immunol. *15*, 105–111.

Boyd, A.S., and Rodrigues, N.P. (2018). Stem Cells Cycle toward Immune Surveillance. Immunity *48*, 187–190.

Brémond, A., Meynet, O., Mahiddine, K., Coito, S., Tichet, M., Scotlandi, K., Breittmayer, J.-P., Gounon, P., Gleeson, P.A., Bernard, A., et al. (2009). Regulation of HLA class I surface expression requires CD99 and p230/golgin-245 interaction. Blood *113*, 347–357.

Brennan, C.W., Verhaak, R.G.W., McKenna, A., Campos, B., Noushmehr, H., Salama, S.R., Zheng, S., Chakravarty, D., Sanborn, J.Z., Berman, S.H., et al. (2013). The somatic genomic landscape of glioblastoma. Cell *155*, 462.

Buchholz, V.R., Schumacher, T.N.M., and Busch, D.H. (2016). T Cell Fate at the Single-Cell Level. Annu Rev Immunol *34*, 65–92.

Bustos-Morán, E., Blas-Rus, N., Martín-Cófreces, N.B., and Sánchez-Madrid, F. (2016). Orchestrating Lymphocyte Polarity in Cognate Immune Cell-Cell Interactions. Int. Rev. Cell Mol. Biol. *327*, 195–261.

Calzolari, F., Michel, J., Baumgart, E.V., Theis, F., Götz, M., and Ninkovic, J. (2015). Fast clonal expansion and limited neural stem cell self-renewal in the adult subependymal zone. Nat. Neurosci. *18*, 490–492.

Campisi, J., and D'Adda Di Fagagna, F. (2007). Cellular senescence: when bad things happen to good cells. Nat. Rev. Mol. Cell Biol. *8*, 729–740.

Carpenter, A.C., and Bosselut, R. (2010). Decision checkpoints in the thymus. Nat. Immunol. 2010 118 *11*, 666–673.

Castro, F., Cardoso, A.P., Gonçalves, R.M., Serre, K., and Oliveira, M.J. (2018). Interferon-gamma at the crossroads of tumor immune surveillance or evasion. Front. Immunol. *9*, 847.

Cebrián, C., Loike, J.D., and Sulzer, D. (2014a). Neuronal mhc-i expression and its implications in synaptic function, Axonal regeneration and parkinson's and other brain diseases. Front. Neuroanat. *8*, 1–9.

Cebrián, C., Zucca, F.A., Mauri, P., Steinbeck, J.A., Studer, L., Scherzer, C.R., Kanter, E., Budhu, S., Mandelbaum, J., Vonsattel, J.P., et al. (2014b). MHC-I expression renders catecholaminergic neurons susceptible to T-cell-mediated degeneration. Nat. Commun. *5*.

Chacon, M.A., and Boulanger, L.M. (2013). MHC class I protein is expressed by neurons and neural progenitors in mid-gestation mouse brain. Mol. Cell. Neurosci. *52*, 117–127.

Chaker, Z., Codega, P., and Doetsch, F. (2016). A mosaic world: puzzles revealed by adult neural stem cell heterogeneity. Wiley Interdiscip. Rev. Dev. Biol. *5*, 640–658.

Chapman, D.C., and Williams, D.B. (2010). ER quality control in the biogenesis of MHC class I molecules. Semin. Cell Dev. Biol. *21*, 512–519.

Chemali, M., Radtke, K., Desjardins, M., and English, L. (2011). Alternative pathways for MHC class I presentation: a new function for autophagy. Cell. Mol. Life Sci. *68*, 1533–1541.

Chen, L., and Flies, D.B. (2013). Molecular mechanisms of T cell co-stimulation and co-inhibition. Nat. Rev. Immunol. *13*, 227–242.

Chen, D., Tang, P., Liu, L., Wang, F., Xing, H., Sun, L., and Jiang, Z. (2018). Bone marrow-derived mesenchymal stem cells promote cell proliferation of multiple myeloma through inhibiting T cell immune responses via PD-1/PD-L1 pathway. Cell Cycle *17*, 858–867.

Cho, Y. Bin, Lee, I.G., Joo, Y.H., Hong, S.H., and Seo, Y.J. (2020). TCR Transgenic Mice: A Valuable Tool for Studying Viral Immunopathogenesis Mechanisms. Int. J. Mol. Sci. *21*, 1–12.

Choi, E.Y., Park, W.S., Jung, K.C., Kim, S.H., Kim, Y.Y., Lee, W.J., and Park, S.H. (1998). Engagement of CD99 induces up-regulation of TCR and MHC class I and II molecules on the surface of human thymocytes. J. Immunol. *161*, 749–754.

Chongsathidkiet, P., Jackson, C., Koyama, S., Loebel, F., Cui, X., Farber, S.H., Woroniecka, K., Elsamadicy, A.A., Dechant, C.A., Kemeny, H.R., et al. (2018). Sequestration of T cells in bone marrow in the setting of glioblastoma and other intracranial tumors. Nat. Med. *24*, 1459–1468.

Christoph, T., Müller-Röver, S., Audring, H., Tobin, D.J., Hermes, B., Cotsarelis, G., Rückert, R., and Paus, R. (2000). The human hair follicle immune system: cellular composition and immune privilege. Br. J. Dermatol. *142*, 862–873.

Codega, P., Silva-Vargas, V., Paul, A., Maldonado-Soto, A.R., DeLeo, A.M., Pastrana, E., and Doetsch, F. (2014). Prospective identification and purification of quiescent adult neural stem cells from their in vivo niche. Neuron *82*, 545–559.

Van Coillie, S., Wiernicki, B., and Xu, J. (2020). Molecular and Cellular Functions of CTLA-4. Adv. Exp. Med. Biol. *1248*, 7–32.

Covacu, R., Estrada, C.P., Arvidsson, L., Svensson, M., and Brundin, L. (2014). Change of fate commitment in adult neural progenitor cells subjected to chronic inflammation. J. Neurosci. *34*, 11571–11582.

Cresswell, P., Ackerman, A.L., Giodini, A., Peaper, D.R., and Wearsch, P.A. (2005). Mechanisms of MHC class I-restricted antigen processing and cross-presentation. Immunol. Rev. *207*, 145–157.

Curtsinger, J.M., and Mescher, M.F. (2010). Inflammatory cytokines as a third signal for T cell activation. Curr. Opin. Immunol. *22*, 333–340.

Dancourt, J., and Barlowe, C. (2010). Protein Sorting Receptors in the Early Secretory Pathway. Annu Rev Biochem *79*, 777–802.

Daynac, M., Chicheportiche, A., Pineda, J.R., Gauthier, L.R., Boussin, F.D., and Mouthon, M.A. (2013). Quiescent neural stem cells exit dormancy upon alteration of GABAAR signaling following radiation damage. Stem Cell Res. *11*, 516–528.

DeCordova, S., Shastri, A., Tsolaki, A.G., Yasmin, H., Klein, L., Singh, S.K., and Kishore, U. (2020). Molecular Heterogeneity and Immunosuppressive Microenvironment in Glioblastoma. Front. Immunol. *11*.

Delamarre, L., Pack, M., Chang, H., Mellman, I., and Trombetta, E.S. (2005). Differential lysosomal proteolysis in antigen-presenting cells determines antigen fate. Science *307*, 1630–1634.

Derecki, N.C., Cardani, A.N., Yang, C.H., Quinnies, K.M., Crihfield, A., Lynch, K.R., and Kipnis, J. (2010). Regulation of learning and memory by meningeal immunity: a key role for IL-4. J. Exp. Med. *207*, 1067–1080.

Deretic, V., Saitoh, T., and Akira, S. (2013). Autophagy in infection, inflammation and immunity. Nat. Rev. Immunol. *13*, 722–737.

Dhanwani, R., Lima-Junior, J.R., Sethi, A., Pham, J., Williams, G., Frazier, A., Xu, Y., Amara, A.W., Standaert, D.G., Goldman, J.G., et al. (2022). Transcriptional analysis of peripheral memory T cells reveals Parkinson's disease-specific gene signatures. NPJ Park. Dis. *8*.

Doetsch, F. (2003). The glial identity of neural stem cells. Nat. Neurosci. *6*, 1127–1134.

Doetsch, F., and Alvarez-Buylla, A. (1996). Network of tangential pathways for neuronal migration in adult mammalian brain. Proc. Natl. Acad. Sci. U. S. A. *93*, 14895–14900.

Doetsch, F., García-Verdugo, J.M., and Alvarez-Buylla, A. (1997). Cellular composition and three-dimensional organization of the subventricular germinal zone in the adult mammalian brain. J. Neurosci. *17*, 5046–5061.

Doetsch, F., García-Verdugo, J.M., and Alvarez-Buylla, A. (1999a). Regeneration of a germinal layer in the adult mammalian brain. Proc. Natl. Acad. Sci. U. S. A. *96*, 11619–11624.

Doetsch, F., Caille, I., Lim, D.A., Garcia-Verdugo, J.M., and Alvarez-Buylla, A. (1999b). Subventricular zone astrocytes are neural stem cells in the adult mammalian brain. Cell *97*, 703–716.

Donaldson, J.G., and Williams, D.B. (2009). Intracellular assembly and trafficking of MHC class I molecules. Traffic *10*, 1745–1752.

Drukker, M., Katz, G., Urbach, A., Schuldiner, M., Markel, G., Itskovitz-Eldor, J., Reubinoff, B., Mandelboim, O., and Benvenisty, N. (2002). Characterization of the expression of MHC proteins in human embryonic stem cells. Proc. Natl. Acad. Sci. U. S. A. *99*, 9864–9869.

Dulken, B.W., Leeman, D.S., Boutet, S.C., Hebestreit, K., and Brunet, A. (2017). Single-Cell Transcriptomic Analysis Defines Heterogeneity and Transcriptional Dynamics in the Adult Neural Stem Cell Lineage. Cell Rep. *18*, 777–790.

Dulken, B.W., Buckley, M.T., Navarro Negredo, P., Saligrama, N., Cayrol, R., Leeman, D.S., George, B.M., Boutet, S.C., Hebestreit, K., Pluvinage, J. V., et al. (2019). Single-cell analysis reveals T cell infiltration in old neurogenic niches. Nature *571*, 205–210.

Eisenbarth, S.C. (2019). Dendritic cell subsets in T cell programming: location dictates function. Nat. Rev. Immunol. *19*, 89–103.

Elmer, B.M., and McAllister, A.K. (2012). Major histocompatibility complex class I proteins in brain development and plasticity. Trends Neurosci. *35*, 660–670.

Engelhardt, B., and Ransohoff, R.M. (2012). Capture, crawl, cross: the T cell code to breach the blood–brain barriers. Trends Immunol. *33*, 579–589.

Engelhardt, B., Vajkoczy, P., and Weller, R.O. (2017). The movers and shapers in immune privilege of the CNS. Nat. Immunol. *18*, 123–131.

Ermolaeva, M., Neri, F., Ori, A., and Rudolph, K.L. (2018). Cellular and epigenetic drivers of stem cell ageing. Nat. Rev. Mol. Cell Biol. *19*, 594–610.

Faiz, M., Sachewsky, N., Gascón, S., Bang, K.W.A., Morshead, C.M., and Nagy, A. (2015). Adult Neural Stem Cells from the Subventricular Zone Give Rise to Reactive Astrocytes in the Cortex after Stroke. Cell Stem Cell *17*, 624–634.

Fehling, H.J., Swat, W., Laplace, C., Kühn, R., Rajewsky, K., Müller, U., and Von Boehmer, H. (1994). MHC class I expression in mice lacking the proteasome subunit LMP-7. Science *265*, 1234–1237.

Ferrón, S., Mira, H., Franco, S., Cano-Jimenez, M., Bellmunt, E., Ramírez, C., Fariñas, I., and Blasco, M.A. (2004). Telomere shortening and chromosomal instability abrogates proliferation of adult but not embryonic neural stem cells. Development *131*, 4059–4070.

Finn, J.D., Hui, D., Downey, H.D., Dunn, D., Pien, G.C., Mingozzi, F., Zhou, S., and High, K.A. (2010). Proteasome inhibitors decrease AAV2 capsid derived peptide epitope presentation on MHC class I following transduction. Mol. Ther. *18*, 135–142.

Forbes, S.J., and Rosenthal, N. (2014). Preparing the ground for tissue regeneration: from mechanism to therapy. Nat. Med. *20*, 857–869.

Fuentealba, L.C., Obernier, K., and Alvarez-Buylla, A. (2012). Adult neural stem cells bridge their niche. Cell Stem Cell *10*, 698–708.

Fuentealba, L.C., Rompani, S.B., Parraguez, J.I., Obernier, K., Romero, R., Cepko, C.L., and Alvarez-Buylla, A. (2015). Embryonic Origin of Postnatal Neural Stem Cells. Cell *161*, 1644–1655.

Fujisaki, J., Wu, J., Carlson, A.L., Silberstein, L., Putheti, P., Larocca, R., Gao, W., Saito, T.I., Celso, C. Lo, Tsuyuzaki, H., et al. (2011). In vivo imaging of Treg cells providing immune privilege to the haematopoietic stem-cell niche. Nature *474*, 216–220.

Furutachi, S., Miya, H., Watanabe, T., Kawai, H., Yamasaki, N., Harada, Y., Imayoshi, I., Nelson, M., Nakayama, K.I., Hirabayashi, Y., et al. (2015). Slowly dividing neural progenitors are an embryonic origin of adult neural stem cells. Nat. Neurosci. *18*, 657–665.

Galea, I., Bechmann, I., and Perry, V.H. (2007). What is immune privilege (not)? Trends Immunol. *28*, 12–18.

Galvao, R.P., Kasina, A., McNeill, R.S., Harbin, J.E., Foreman, O., Verhaak, R.G.W., Nishiyama, A., Ryan Miller, C., and Zong, H. (2014). Transformation of quiescent adult oligodendrocyte precursor cells into malignant glioma through a multistep reactivation process. Proc. Natl. Acad. Sci. U. S. A. *111*, E4214–E4223.

Gate, D., Saligrama, N., Leventhal, O., Yang, A.C., Unger, M.S., Middeldorp, J., Chen, K., Lehallier, B., Channappa, D., De Los Santos, M.B., et al. (2020). Clonally expanded CD8 T cells patrol the cerebrospinal fluid in Alzheimer's disease. Nature *577*, 399–404.

Ghannam, S., Bouffi, C., Djouad, F., Jorgensen, C., and Noël, D. (2010). Immunosuppression by mesenchymal stem cells: mechanisms and clinical applications. Stem Cell Res. Ther. *1*.

Ginhoux, F., Greter, M., Leboeuf, M., Nandi, S., See, P., Gokhan, S., Mehler, M.F., Conway, S.J., Ng, L.G., Stanley, E.R., et al. (2010). Fate mapping analysis reveals that adult microglia derive from primitive macrophages. Science *330*, 841–845.

Gobin, S.J.P., van Zutphen, M., Westerheide, S.D., Boss, J.M., and van den Elsen, P.J. (2001). The MHC-specific enhanceosome and its role in MHC class I and beta(2)-microglobulin gene transactivation. J. Immunol. *167*, 5175–5184.

Gomez Perdiguero, E., Schulz, C., and Geissmann, F. (2013). Development and homeostasis of "resident" myeloid cells: the case of the microglia. Glia *61*, 112–120.

Goodfellow, P.J., Darling, S.M., Thomas, N.S., and Goodfellow, P.N. (1986). A Pseudoautosomal Gene in Man. Science (80-.). *234*, 740–743.

Greenwald, R.J., Freeman, G.J., and Sharpe, A.H. (2005). The B7 family revisited. Annu. Rev. Immunol. *23*, 515–548.

Griffith, J.W., Sokol, C.L., and Luster, A.D. (2014). Chemokines and Chemokine Receptors: Positioning Cells for Host Defense and Immunity. Annu Rev Immunol *32*, 659–702.

Gruhler, A., and Früh, K. (2000). Control of MHC class I traffic from the endoplasmic reticulum by cellular chaperones and viral anti-chaperones. Traffic *1*, 306–311.

Gu, Z., Eils, R., and Schlesner, M. (2016). Complex heatmaps reveal patterns and correlations in multidimensional genomic data. Bioinformatics *32*, 2847–2849.

Guerder, S., and Flavell, R.A. (1995). T-cell activation. Two for T. Curr. Biol. *5*, 866–868.

Guermonprez, P., Valladeau, J., Zitvogel, L., Théry, C., and Amigorena, S. (2002). Antigen presentation and T cell stimulation by dendritic cells. Annu. Rev. Immunol. *20*, 621–667.

Hanahan, D. (2022). Hallmarks of Cancer: New Dimensions. Cancer Discov. *12*, 31–46.

Hanash, A.M., Dudakov, J.A., Hua, G., O'Connor, M.H., Young, L.F., Singer, N. V., West, M.L., Jenq, R.R., Holland, A.M., Kappel, L.W., et al. (2012). Interleukin-22 protects intestinal stem cells from immune-mediated tissue damage and regulates sensitivity to graft versus host disease. Immunity *37*, 339–350.

Hashimoto, D., Chow, A., Noizat, C., Teo, P., Beasley, M.B., Leboeuf, M., Becker, C.D., See, P., Price, J., Lucas, D., et al. (2013). Tissue-resident macrophages self-maintain locally throughout adult life with minimal contribution from circulating monocytes. Immunity *38*, 792–804.

He, X., and Xu, C. (2020). Immune checkpoint signaling and cancer immunotherapy. Cell Res. 2020 308 *30*, 660–669.

Holland, E.C., Celestino, J., Dai, C., Schaefer, L., Sawaya, R.E., and Fuller, G.N. (2000). Combined activation of Ras and Akt in neural progenitors induces glioblastoma formation in mice. Nat. Genet. *25*, 55–57.

Hozumi, K., Negishi, N., Tsuchiya, I., Abe, N., Hirano, K.I., Suzuki, D., Yamamoto, M., Engel, J.D., and Habu, S. (2008). Notch signaling is necessary for GATA3 function in the initiation of T cell development. Eur. J. Immunol. *38*, 977–985.

Hu, X., Deng, Q., Ma, L., Li, Q., Chen, Y., Liao, Y., Zhou, F., Zhang, C., Shao, L., Feng, J., et al. (2020). Meningeal lymphatic vessels regulate brain tumor drainage and immunity. Cell Res. 2020 303 *30*, 229–243.

Huang, G.-J., Smith, A.L., Gray, D.H.D., Cosgrove, C., Singer, B.H., Edwards, A., Sim, S., Parent, J.M., Johnsen, A., Mott, R., et al. (2010). A Genetic and Functional Relationship between T Cells and Cellular Proliferation in the Adult Hippocampus. PLoS Biol. *8*, e1000561.

Huse, J.T., and Holland, E.C. (2009). Genetically Engineered Mouse Models of Brain Cancer and the Promise of Preclinical Testing. Brain Pathol. *19*, 132–143.

Iliff, J.J., Wang, M., Liao, Y., Plogg, B.A., Peng, W., Gundersen, G.A., Benveniste, H., Vates, G.E., Deane, R., Goldman, S.A., et al. (2012). A paravascular pathway facilitates CSF flow through the brain parenchyma and the clearance of interstitial solutes, including amyloid β. Sci. Transl. Med. *4*, 147ra111.

Insinga, A., Cicalese, A., Faretta, M., Gallo, B., Albano, L., Ronzoni, S., Furia, L., Viale, A., and Pelicci, P.G. (2013). DNA damage in stem cells activates p21, inhibits p53, and induces symmetric self-renewing divisions. Proc. Natl. Acad. Sci. U. S. A. *110*, 3931–3936.

Iwasaki, A., and Medzhitov, R. (2015). Control of adaptive immunity by the innate immune system. Nat. Immunol. 2015 164 *16*, 343–353.

Jackson, C.M., Choi, J., and Lim, M. (2019). Mechanisms of immunotherapy resistance: lessons from glioblastoma. Nat. Immunol. *20*, 1100–1109.

Jain, N., Kalam, H., Singh, L., Sharma, V., Kedia, S., Das, P., Ahuja, V., and Kumar, D. (2020). Mesenchymal stem cells offer a drug-tolerant and immune-privileged niche to Mycobacterium tuberculosis. Nat. Commun. *11*.

Janeway, C.J., P, T., and -, M.W. (2001). The major histocompatibility complex and its functions. In Immunobiology: The Immune System in Health and Disease., (New York: Garland Science), p.

Jessen, N.A., Munk, A.S.F., Lundgaard, I., and Nedergaard, M. (2015). The Glymphatic System: A Beginner's Guide. Neurochem. Res. 2015 4012 *40*, 2583–2599.

Jiang, P., Gu, S., Pan, D., Fu, J., Sahu, A., Hu, X., Li, Z., Traugh, N., Bu, X., Li, B., et al. (2018). Signatures of T cell dysfunction and exclusion predict cancer immunotherapy response. Nat. Med. 2018 2410 *24*, 1550–1558.

Jiménez, A.J., Domínguez-Pinos, M.D., Guerra, M.M., Fernández-Llebrez, P., and Pérez-Fígares, J.M. (2014). Structure and function of the ependymal barrier and diseases associated with ependyma disruption. Tissue Barriers *2*.

Jung, S., Aliberti, J., Graemmel, P., Sunshine, M.J., Kreutzberg, G.W., Sher, A., and Littman, D.R. (2000). Analysis of fractalkine receptor CX(3)CR1 function by targeted deletion and green fluorescent protein reporter gene insertion. Mol. Cell. Biol. *20*, 4106–4114.

Kaech, S.M., Wherry, E.J., and Ahmed, R. (2002). Effector and memory T-cell differentiation: implications for vaccine development. Nat. Rev. Immunol. *2*, 251–262.

Kaiserman, D., and Bird, P.I. (2010). Control of granzymes by serpins. Cell Death Differ. *17*, 586–595.

Karin, N. (2018). Chemokines and cancer: new immune checkpoints for cancer therapy. Curr. Opin. Immunol. *51*, 140–145.

Kaskow, B.J., and Baecher-Allan, C. (2018). Effector T Cells in Multiple Sclerosis. Cold Spring Harb. Perspect. Med. *8*.

Kierdorf, K., Erny, D., Goldmann, T., Sander, V., Schulz, C., Perdiguero, E.G., Wieghofer, P., Heinrich, A., Riemke, P., Hölscher, C., et al. (2013). Microglia emerge from erythromyeloid precursors via Pu.1- and Irf8-dependent pathways. Nat. Neurosci. *16*, 273–280.

Kim, S.H., Choi, E.Y., Shin, Y.K., Kim, T.J., Chung, D.H., Chang, S.I., Kim, N.K., and Park, S.H. (1998). Generation of Cells With Hodgkin's and Reed-Sternberg Phenotype Through Downregulation of CD99 (Mic2). Blood *92*, 4287–4295.

Kipnis, J. (2016). Multifaceted interactions between adaptive immunity and the central nervous system. Science (80-.). *353*, 766–771.

Kipnis, J., Gadani, S., and Derecki, N.C. (2012). Pro-cognitive properties of T cells. Nat. Rev. Immunol. *12*, 663–669.

Kobayashi, K.S., and Van Den Elsen, P.J. (2012). NLRC5: A key regulator of MHC class I-dependent immune responses. Nat. Rev. Immunol. *12*, 813–820.

Kriegstein, A., and Alvarez-Buylla, A. (2009). The glial nature of embryonic and adult neural stem cells. Annu. Rev. Neurosci. *32*, 149–184.

Krot, M., and Rolls, A. (2021). Autoimmunity in neurodegeneration. Science (80-.). *374*, 823–824.

Kurd, N., and Robey, E.A. (2016). T-cell selection in the thymus: A spatial and temporal perspective. Immunol. Rev. *271*, 114–126.

Kwon, D. (2022). Guardians of the brain: how a special immune system protects our grey matter. Nature *606*, 22–24.

Ladasky, J.J., Boyle, S., Seth, M., Li, H., Pentcheva, T., Abe, F., Steinberg, S.J., and Edidin, M. (2006). Bap31 enhances the endoplasmic reticulum export and quality control of human class I MHC molecules. J. Immunol. *177*, 6172–6181.

Lampson, L.A. (1995). Interpreting MHC class I expression and class I/class II reciprocity in the CNS: reconciling divergent findings. Microsc. Res. Tech. *32*, 267–285.

Lan, X., Jörg, D.J., Cavalli, F.M.G., Richards, L.M., Nguyen, L. V., Vanner, R.J., Guilhamon, P., Lee, L., Kushida, M.M., Pellacani, D., et al. (2017). Fate mapping of human glioblastoma reveals an invariant stem cell hierarchy. Nature *549*, 227–232.

Laurenti, E., Frelin, C., Xie, S., Ferrari, R., Dunant, C.F., Zandi, S., Neumann, A., Plumb, I., Doulatov, S., Chen, J., et al. (2015). CDK6 levels regulate quiescence exit in human hematopoietic stem cells. Cell Stem Cell *16*, 302–313.

Lawson, L.J., Perry, V.H., Dri, P., and Gordon, S. (1990). Heterogeneity in the distribution and morphology of microglia in the normal adult mouse brain. Neuroscience *39*, 151–170.

Lee, J., Lee, J., Kahng, J., Kim, S., Park, J., Yoon, S., Um, J., Kim, W., Lee, J., Park, J., et al. (2018). Human glioblastoma arises from subventricular zone cells with low-level driver mutations. Nature *560*, 243–247.

Leeman, D.S., Hebestreit, K., Ruetz, T., Webb, A.E., Mckay, A., Pollina, E.A., Dulken, B.W., Zhao, X., Yeo, R.W., Ho, T.T., et al. (2018). Lysosome activation clears aggregates and enhances quiescent neural stem cell activation during aging HHS Public Access. Science (80-.). *359*, 1277–1283.

Ley, K., Laudanna, C., Cybulsky, M.I., and Nourshargh, S. (2007). Getting to the site of inflammation: the leukocyte adhesion cascade updated. Nat. Rev. Immunol. 2007 79 *7*, 678–689.

Li, H., Gang, Z., Yuling, H., Luokun, X., Jie, X., Hao, L., Li, W., Chunsong, H., Junyan, L., Mingshen, J., et al. (2006). Different neurotropic pathogens elicit neurotoxic CCR9- or neurosupportive CXCR3-expressing microglia. J. Immunol. *177*, 3644–3656.

Li, Q., Cheng, Z., Zhou, L., Darmanis, S., Neff, N.F., Okamoto, J., Gulati, G., Bennett, M.L., Sun, L.O., Clarke, L.E., et al. (2019). Developmental Heterogeneity of Microglia and Brain Myeloid Cells Revealed by Deep Single-Cell RNA Sequencing. Neuron *101*, 207-223.e10.

Lim, D.A., and Alvarez-Buylla, A. (2016). The adult ventricular–subventricular zone (V-SVZ) and olfactory bulb (OB) neurogenesis. Cold Spring Harb. Perspect. Biol. *8*, a018820.

Lim, M., Xia, Y., Bettegowda, C., and Weller, M. (2018). Current state of immunotherapy for glioblastoma. Nat. Rev. Clin. Oncol. *15*, 422–442.

Lin, K., Bieri, G., Gontier, G., Müller, S., Smith, L.K., Snethlage, C.E., White, C.W., Maybury-Lewis, S.Y., and Villeda, S.A. (2021). MHC class I H2-Kb negatively regulates neural progenitor cell proliferation by inhibiting FGFR signaling. PLoS Biol. *19*.

Liu, J., Shen, Y., Li, M., Lv, D., Zhang, A., Peng, Y., Miao, F., and Zhang, J. (2015). Spatial-Temporal Expression of Non-classical MHC Class I Molecules in the C57 Mouse Brain. Neurochem. Res. *40*, 1487–1496.

Liu, J.J., Shen, Y., Li, M., Shi, Q., Zhang, A., Miao, F., Liu, J.J., Wu, X., He, Y., and Zhang, J. (2013). The expression pattern of classical MHC class I molecules in the development of mouse central nervous system. Neurochem. Res. *38*, 290–299.

Liu, Z., Mi, F., Han, M., Tian, M., Deng, L., Meng, N., Luo, J., and Fu, R. (2021). Bone marrow-derived mesenchymal stem cells inhibit CD8+ T cell immune responses via PD-1/PD-L1 pathway in multiple myeloma. Clin. Exp. Immunol. *205*, 53–62.

Lledo, P.M., and Saghatelyan, A. (2005). Integrating new neurons into the adult olfactory bulb: joining the network, life-death decisions, and the effects of sensory experience. Trends Neurosci. *28*, 248–254.

Llorens-Bobadilla, E., Zhao, S., Baser, A., Saiz-Castro, G., Zwadlo, K., and Martin-Villalba, A. (2015). Single-Cell Transcriptomics Reveals a Population of Dormant Neural Stem Cells that Become Activated upon Brain Injury. Cell Stem Cell *17*, 329–340.

Lois, C., García-Verdugo, J.M., and Alvarez-Buylla, A. (1996). Chain migration of neuronal precursors. Science *271*, 978–981.

Louveau, A., Smirnov, I., Keyes, T.J., Eccles, J.D., Rouhani, S.J., Peske, J.D., Derecki, N.C., Castle, D., Mandell, J.W., Lee, K.S., et al. (2015a). Structural and functional features of central nervous system lymphatic vessels. Nature *523*, 337–341.

Louveau, A., Harris, T.H., and Kipnis, J. (2015b). Revisiting the Mechanisms of CNS Immune Privilege. Trends Immunol. *36*, 569–577.

Louveau, A., Herz, J., Alme, M.N., Salvador, A.F., Dong, M.Q., Viar, K.E., Herod, S.G., Knopp, J., Setliff, J.C., Lupi, A.L., et al. (2018). CNS lymphatic drainage and neuroinflammation are regulated by meningeal lymphatic vasculature. Nat. Neurosci. *21*, 1380–1391.

Ludigs, K., Seguín-Estévez, Q., Lemeille, S., Ferrero, I., Rota, G., Chelbi, S., Mattmann, C., MacDonald, H.R., Reith, W., and Guarda, G. (2015). NLRC5 exclusively transactivates MHC class I and related genes through a distinctive SXY module. PLoS Genet. *11*.

Luz-Crawford, P., Kurte, M., Bravo-Alegría, J., Contreras, R., Nova-Lamperti, E., Tejedor, G., Noël, D., Jorgensen, C., Figueroa, F., Djouad, F., et al. (2013). Mesenchymal stem cells generate a CD4+CD25+Foxp3+ regulatory T cell population during the differentiation process of Th1 and Th17 cells. Stem Cell Res. Ther. *4*.

Mahnke, Y.D., Brodie, T.M., Sallusto, F., Roederer, M., and Lugli, E. (2013). The who's who of T-cell differentiation: Human memory T-cell subsets. Eur. J. Immunol. *43*, 2797–2809.

Malladi, S., MacAlinao, D.G., Jin, X., He, L., Basnet, H., Zou, Y., De Stanchina, E., and Massagué, J. (2016). Metastatic Latency and Immune Evasion through Autocrine Inhibition of WNT. Cell *165*, 45–60.

Mandal, P.K., Blanpain, C., and Rossi, D.J. (2011). DNA damage response in adult stem cells: Pathways and consequences. Nat. Rev. Mol. Cell Biol. *12*, 198–202.

Martínez-Lostao, L., Anel, A., and Pardo, J. (2015). How Do Cytotoxic Lymphocytes Kill Cancer Cells? Clin. Cancer Res. *21*, 5047–5056.

Mastorakos, P., and McGavern, D. (2019). The anatomy and immunology of vasculature in the central nervous system. Sci. Immunol. *4*.

Matarredona, E.R., and Pastor, A.M. (2019). Neural stem cells of the subventricular zone as the origin of human glioblastoma stem cells. Therapeutic implications. Front. Oncol. *9*, 779.

Mateos-White, I., Fabra-Beser, J., de Agustín-Durán, D., and Gil-Sanz, C. (2020). Double In Utero Electroporation to Target Temporally and Spatially Separated Cell Populations. JoVE (Journal Vis. Exp. *2020*, e61046.

McLendon, R., Friedman, A., Bigner, D., Van Meir, E.G., Brat, D.J., Mastrogianakis, G.M., Olson, J.J., Mikkelsen, T., Lehman, N., Aldape, K., et al. (2008). Comprehensive genomic characterization defines human glioblastoma genes and core pathways. Nature *455*, 1061–1068.

Meissner, T.B., Li, A., Biswas, A., Lee, K.H., Liu, Y.J., Bayir, E., Iliopoulos, D., Van Den Elsen, P.J., and Kobayashi, K.S. (2010). NLR family member NLRC5 is a transcriptional regulator of MHC class I genes. Proc. Natl. Acad. Sci. U. S. A. *107*, 13794–13799.

Meissner, T.B., Liu, Y.-J., Lee, K.-H., Li, A., Biswas, A., van Eggermond, M.C.J.A., van den Elsen, P.J., and Kobayashi, K.S. (2012). NLRC5 cooperates with the RFX transcription factor complex to induce MHC class I gene expression. J. Immunol. *188*, 4951–4958.

Menn, B., Garcia-Verdugo, J.M., Yaschine, C., Gonzalez-Perez, O., Rowitch, D., and Alvarez-Buylla, A. (2006). Origin of oligodendrocytes in the subventricular zone of the adult brain. J. Neurosci. *26*, 7907–7918.

Merkle, F.T., Mirzadeh, Z., and Alvarez-Buylla, A. (2007). Mosaic organization of neural stem cells in the adult brain. Science *317*, 381–384.

Merkle, F.T., Fuentealba, L.C., Sanders, T.A., Magno, L., Kessaris, N., and Alvarez-Buylla, A. (2014). Adult neural stem cells in distinct microdomains generate previously unknown interneuron types. Nat. Neurosci. *17*, 207–214.

Da Mesquita, S., Fu, Z., and Kipnis, J. (2018). The Meningeal Lymphatic System: A New Player in Neurophysiology. Neuron *100*, 375–388.

Meyer-Franke, A., Wilkinson, G.A., Kruttgen, A., Hu, M., Munro, E., Hanson, M.G., Reichardt, L.F., and Barres, B.A. (1998). Depolarization and cAMP Elevation Rapidly Recruit TrkB to the Plasma Membrane of CNS Neurons. Neuron *21*, 681–693.

Miao, Y., Yang, H., Levorse, J., Yuan, S., Polak, L., Sribour, M., Singh, B., Rosenblum, M.D., and Fuchs, E. (2019). Adaptive Immune Resistance Emerges from Tumor-Initiating Stem Cells. Cell *177*, 1172-1186.e14.

Mich, J.K., Signer, R.A.J., Nakada, D., Pineda, A., Burgess, R.J., Vue, T.Y., Johnson, J.E., and Morrison, S.J. (2014). Prospective identification of functionally distinct stem cells and neurosphere-initiating cells in adult mouse forebrain. Elife *3*.

Mildner, A., Schmidt, H., Nitsche, M., Merkler, D., Hanisch, U.K., Mack, M., Heikenwalder, M., Brück, W., Priller, J., and Prinz, M. (2007). Microglia in the adult brain arise from Ly-6ChiCCR2+ monocytes only under defined host conditions. Nat. Neurosci. *10*, 1544–1553.

Mirzadeh, Z., Merkle, F.T., Soriano-Navarro, M., Garcia-Verdugo, J.M., and Alvarez-Buylla, A. (2008). Neural stem cells confer unique pinwheel architecture to the ventricular surface in neurogenic regions of the adult brain. Cell Stem Cell *3*, 265–278.

Mizrak, D., Levitin, H.M., Delgado, A.C., Crotet, V., Yuan, J., Chaker, Z., Silva-Vargas, V., Sims, P.A., and Doetsch, F. (2019). Single-Cell Analysis of Regional Differences in Adult V-SVZ Neural Stem Cell Lineages. Cell Rep. *26*, 394-406.e5.

Mombaerts, P., Iacomini, J., Johnson, R.S., Herrup, K., Tonegawa, S., and Papaioannou, V.E. (1992). RAG-1-deficient mice have no mature B and T lymphocytes. Cell *68*, 869–877.

Montealegre, S., and Van Endert, P.M. (2019). Endocytic recycling of MHC class I molecules in non-professional antigen presenting and dendritic cells. Front. Immunol. *10*, 3098.

Morante-Redolat, J.M., and Porlan, E. (2019). Neural Stem Cell Regulation by Adhesion Molecules Within the Subependymal Niche. Front. Cell Dev. Biol. *7*.

Mueller, S.N., Gebhardt, T., Carbone, F.R., and Heath, W.R. (2013). Memory T Cell Subsets, Migration Patterns, and Tissue Residence. Annu Rev Immunol *31*, 137–161.

Mundt, S., Greter, M., Flügel, A., and Becher, B. (2019a). The CNS Immune Landscape from the Viewpoint of a T Cell. Trends Neurosci. *42*, 667–679.

Mundt, S., Mrdjen, D., Utz, S.G., Greter, M., Schreiner, B., and Becher, B. (2019b). Conventional DCs sample and present myelin antigens in the healthy CNS and allow parenchymal T cell entry to initiate neuroinflammation. Sci. Immunol. *4*.

Muzumdar, M.D., Tasic, B., Miyamichi, K., Li, N., and Luo, L. (2007). A global double-fluorescent Cre reporter mouse. Genesis *45*, 593–605.

Naik, S., Larsen, S.B., Cowley, C.J., and Fuchs, E. (2018). Two to Tango: Dialog between Immunity and Stem Cells in Health and Disease. Cell *175*, 908–920.

Najar, M., Raicevic, G., Boufker, H.I., Kazan, H.F., Bruyn, C. De, Meuleman, N., Bron, D., Toungouz, M., and Lagneaux, L. (2010). Mesenchymal stromal cells use PGE2 to modulate activation and proliferation of lymphocyte subsets: Combined comparison of adipose tissue, Wharton's Jelly and bone marrow sources. Cell. Immunol. *264*, 171–179.

Neal, E.G., Acosta, S.A., Kaneko, Y., Ji, X., and Borlongan, C. V. (2019). Regulatory T-cells within bone marrow-derived stem cells actively confer immunomodulatory and neuroprotective effects against stroke. J. Cereb. Blood Flow Metab. *39*, 1750–1758.

Neefjes, J., Jongsma, M.L.M., Paul, P., and Bakke, O. (2011). Towards a systems understanding of MHC class i and MHC class II antigen presentation. Nat. Rev. Immunol. *11*, 823–836.

Negishi, H., Taniguchi, T., and Yanai, H. (2018). The Interferon (IFN) Class of Cytokines and the IFN Regulatory Factor (IRF) Transcription Factor Family. Cold Spring Harb. Perspect. Biol. *10*, a028423.

Nemazee, D. (2006). Receptor editing in lymphocyte development and central tolerance. Nat. Rev. Immunol. 2006 610 *6*, 728–740.

Németh, K., Leelahavanichkul, A., Yuen, P.S.T., Mayer, B., Parmelee, A., Doi, K., Robey, P.G., Leelahavanichkul, K., Koller, B.H., Brown, J.M., et al. (2009). Bone marrow stromal cells attenuate sepsis via prostaglandin E(2)-dependent reprogramming of host macrophages to increase their interleukin-10 production. Nat. Med. *15*, 42–49.

Neumann, H., Cavalié, A., Jenne, D.E., and Wekerle, H. (1995). Induction of MHC class I genes in neurons. Science *269*, 549–552.

Nimmerjahn, A., Kirchhoff, F., and Helmchen, F. (2005). Resting microglial cells are highly dynamic surveillants of brain parenchyma in vivo. Science *308*, 1314–1318.

Noorani, I. (2019). Genetically engineered mouse models of gliomas: Technological developments for translational discoveries. Cancers (Basel). *11*, 1335.

Obernier, K., and Alvarez-Buylla, A. (2019). Neural stem cells: Origin, heterogeneity and regulation in the adult mammalian brain. Dev. *146*.

Otsuki, L., and Brand, A.H. (2020). Quiescent Neural Stem Cells for Brain Repair and Regeneration: Lessons from Model Systems. Trends Neurosci. *43*, 213–226.

Pang, L.X., Cai, W.W., Li, Q., Li, H.J., Fei, M., Yuan, Y.S., Sheng, B., Zhang, K., An, R.C., Ou, Y.W., et al. (2021). Bone marrow-derived mesenchymal stem cells attenuate myocardial ischemia-reperfusion injury via upregulation of splenic regulatory T cells. BMC Cardiovasc. Disord. *21*.

Papadopoulos, Z., Herz, J., and Kipnis, J. (2020). Meningeal Lymphatics: From Anatomy to Central Nervous System Immune Surveillance. J. Immunol. *204*, 286–293.

Pasciuto, E., Burton, O.T., Roca, C.P., Lagou, V., Rajan, W.D., Theys, T., Mancuso, R., Tito, R.Y., Kouser, L., Callaerts-Vegh, Z., et al. (2020). Microglia Require CD4 T Cells to Complete the Fetal-to-Adult Transition. Cell *182*, 625-640.e24.

Pasello, M., Manara, M.C., and Scotlandi, K. (2018). CD99 at the crossroads of physiology and pathology. J. Cell Commun. Signal. 2018 121 *12*, 55–68.

Pastrana, E., Cheng, L.C., and Doetsch, F. (2009). Simultaneous prospective purification of adult subventricular zone neural stem cells and their progeny. Proc. Natl. Acad. Sci. U. S. A. *106*, 6387–6392.

Pata, S., Otáhal, P., Brdikča, T., Laopajon, W., Mahasongkram, K., and Kasinrerk, W. (2011). Association of CD99 short and long forms with MHC class I, MHC class II and tetraspanin CD81 and recruitment into immunological synapses. BMC Res. Notes *4*.

Patel, S., and Player, M. (2009). Colony-stimulating factor-1 receptor inhibitors for the treatment of cancer and inflammatory disease. Curr. Top. Med. Chem. *9*, 599–610.

Pavel, M., and Rubinsztein, D.C. (2017). Mammalian autophagy and the plasma membrane. FEBS J. *284*, 672–679.

Peaper, D.R., and Cresswell, P. (2008). Regulation of MHC class I assembly and peptide binding. Annu. Rev. Cell Dev. Biol. *24*, 343–368.

Pelvig, D.P., Pakkenberg, H., Stark, A.K., and Pakkenberg, B. (2008). Neocortical glial cell numbers in human brains. Neurobiol. Aging *29*, 1754–1762.

Pereira, E.A., and DaSilva, L.L.P. (2016). HIV-1 Nef: Taking Control of Protein Trafficking. Traffic *17*, 976–996.

Peruzzotti-Jametti, L., Bernstock, J.D., Vicario, N., Costa, A.S.H., Kwok, C.K., Leonardi, T., Booty, L.M., Bicci, I., Balzarotti, B., Volpe, G., et al. (2018). Macrophage-Derived Extracellular Succinate Licenses Neural Stem Cells to Suppress Chronic Neuroinflammation. Cell Stem Cell *22*, 355-368.e13.

Ponti, G., Obernier, K., Guinto, C., Jose, L., Bonfanti, L., and Alvarez-Buylla, A. (2013). Cell cycle and lineage progression of neural progenitors in the ventricular-subventricular zones of adult mice. Proc. Natl. Acad. Sci. U. S. A. *110*.

Porlan, E., Perez-Villalba, A., Delgado, A.C., and Ferrón, S.R. (2013). Paracrine regulation of neural stem cells in the subependymal zone. Arch. Biochem. Biophys. *534*, 11–19.

Prinz, M., and Priller, J. (2014). Microglia and brain macrophages in the molecular age: from origin to neuropsychiatric disease. Nat. Rev. Neurosci. *15*, 300–312.

Qi, F., Yang, J., Xia, Y., Yuan, Q., Guo, K., Zou, J., and Yao, Z. (2016). A(H1N1) vaccination recruits T lymphocytes to the choroid plexus for the promotion of hippocampal neurogenesis and working memory in pregnant mice. Brain. Behav. Immun. *53*, 72–83.

Radtke, F., Wilson, A., Mancini, S.J.C., and MacDonald, H.R. (2004). Notch regulation of lymphocyte development and function. Nat. Immunol. *5*, 247–253.

Rando, T.A., and Jones, D.L. (2021). Regeneration, Rejuvenation, and Replacement: Turning Back the Clock on Tissue Aging. Cold Spring Harb. Perspect. Biol. *13*.

Ransohoff, R.M., and Cardona, A.E. (2010). The myeloid cells of the central nervous system parenchyma. Nature *468*, 253–262.

Ransohoff, R.M., and Engelhardt, B. (2012). The anatomical and cellular basis of immune surveillance in the central nervous system. Nat. Rev. Immunol. *12*, 623–635.

Ricklefs, F.L., Alayo, Q., Krenzlin, H., Mahmoud, A.B., Speranza, M.C., Nakashima, H., Hayes, J.L., Lee, K., Balaj, L., Passaro, C., et al. (2018). Immune evasion mediated by PD-L1 on glioblastoma-derived extracellular vesicles. Sci. Adv. *4*.

Rock, K.L., Gramm, C., Rothstein, L., Clark, K., Stein, R., Dick, L., Hwang, D., and Goldberg, A.L. (1994). Inhibitors of the proteasome block the degradation of most cell proteins and the generation of peptides presented on MHC class I molecules. Cell *78*, 761–771.

Rodgers, J.T., King, K.Y., Brett, J.O., Cromie, M.J., Charville, G.W., Maguire, K.K., Brunson, C., Mastey, N., Liu, L., Tsai, C.R., et al. (2014). mTORC1 controls the adaptive transition of quiescent stem cells from G0 to G(Alert). Nature *510*, 393–396.

Rolls, A., Schori, H., London, A., and Schwartz, M. (2008). Decrease in hippocampal neurogenesis during pregnancy: a link to immunity. Mol. Psychiatry *13*, 468–469.

Rossi, D., and Zlotnik, A. (2000). The Biology of Chemokines and their Receptors. Annu. Rev. Immunol. *18*, 217–243.

Rustenhoven, J., Drieu, A., Mamuladze, T., de Lima, K.A., Dykstra, T., Wall, M., Papadopoulos, Z., Kanamori, M., Salvador, A.F., Baker, W., et al. (2021). Functional characterization of the dural sinuses as a neuroimmune interface. Cell *184*, 1000-1016.e27.

Sallusto, F., Geginat, J., and Lanzavecchia, A. (2004). Central memory and effector memory T cell subsets: function, generation, and maintenance. Annu. Rev. Immunol. *22*, 745–763.

Salter, M.W., and Stevens, B. (2017). Microglia emerge as central players in brain disease. Nat. Med. *23*, 1018–1027.

Salvioni, A., Belloy, M., Lebourg, A., Bassot, E., Cantaloube-Ferrieu, V., Vasseur, V., Blanié, S., Liblau, R.S., Suberbielle, E., Robey, E.A., et al. (2019). Robust Control of a Brain-Persisting Parasite through MHC I Presentation by Infected Neurons. Cell Rep. *27*, 3254-3268.e8.

Savino, W., Smaniotto, S., and Dardenne, M. (2005). Hematopoiesis. Adv. Exp. Med. Biol. *567*, 167–185.

Schläger, C., Körner, H., Krueger, M., Vidoli, S., Haberl, M., Mielke, D., Brylla, E., Issekutz, T., Cabanãs, C., Nelson, P.J., et al. (2016). Effector T-cell trafficking between the leptomeninges and the cerebrospinal fluid. Nat. 2016 5307590 *530*, 349–353.

Schoenberger, S.P., Toes, R.E.M., Van Dervoort, E.I.H., Offringa, R., and Melief, C.J.M. (1998). T-cell help for cytotoxic T lymphocytes is mediated by CD40–CD40L interactions. Nat. 1998 3936684 *393*, 480–483.

Schoenborn, J.R., and Wilson, C.B. (2007). Regulation of Interferon-γ During Innate and Adaptive Immune Responses. Adv. Immunol. *96*, 41–101.

Schoggins, J.W. (2019). Interferon-Stimulated Genes: What Do They All Do? Annu Rev Virol *6*, 567–584.

Schulz, C., Perdiguero, E.G., Chorro, L., Szabo-Rogers, H., Cagnard, N., Kierdorf, K., Prinz, M., Wu, B., Jacobsen, S.E.W., Pollard, J.W., et al. (2012). A lineage of myeloid cells independent of Myb and hematopoietic stem cells. Science *336*, 86–90.

Schwarz, K., de Giuli, R., Schmidtke, G., Kostka, S., van den Broek, M., Kim, K.B., Crews, C.M., Kraft, R., and Groettrup, M. (2000). The selective proteasome inhibitors lactacystin and epoxomicin can be used to either up- or down-regulate antigen presentation at nontoxic doses. J. Immunol. *164*, 6147–6157.

Sethna, M.P., and Lampson, L.A. (1991). Immune modulation within the brain: recruitment of inflammatory cells and increased major histocompatibility antigen expression following intracerebral injection of interferon-γ. J. Neuroimmunol. *34*, 121–132.

Shatz, C.J. (2009). MHC Class I: An Unexpected Role in Neuronal Plasticity. Neuron *64*, 40–45.

Shemer, A., Erny, D., Jung, S., and Prinz, M. (2015). Microglia Plasticity During Health and Disease: An Immunological Perspective. *36*, 614–624.

Shigemoto-Mogami, Y., Hoshikawa, K., Goldman, J.E., Sekino, Y., and Sato, K. (2014). Microglia enhance neurogenesis and oligodendrogenesis in the early postnatal subventricular zone. J. Neurosci. *34*, 2231–2243.

Silva-Vargas, V., Maldonado-Soto, A.R., Mizrak, D., Codega, P., and Doetsch, F. (2016). Age-Dependent Niche Signals from the Choroid Plexus Regulate Adult Neural Stem Cells. Cell Stem Cell *19*, 643–652.

Simeonova, I., and Huillard, E. (2014). In vivo models of brain tumors: roles of genetically engineered mouse models in understanding tumor biology and use in preclinical studies. Cell. Mol. Life Sci. *71*, 4007–4026.

Sirerol-Piquer, M.S., Belenguer, G., Morante-Redolat, J.M., Duart-Abadia, P., Perez-Villalba, A., and Fariñas, I. (2019). Physiological Interactions between Microglia and Neural Stem Cells in the Adult Subependymal Niche. Neuroscience *405*, 77–91.

Sleckman, B.P. (2005). Lymphocyte antigen receptor gene assembly: multiple layers of regulation. Immunol. Res. *32*, 253–258.

Smolders, J., Heutinck, K.M., Fransen, N.L., Remmerswaal, E.B.M.M., Hombrink, P., ten Berge, I.J.M.M., van Lier, R.A.W.W., Huitinga, I., and Hamann, J. (2018). Tissue-resident memory T cells populate the human brain. *9*.

Sohn, H.W., Shin, Y.K., Lee, I.-S., Bae, Y.M., Suh, Y.H., Kim, M.K., Kim, T.J., Jung, K.C., Park, W.S., Park, C.-S., et al. (2001). CD99 Regulates the Transport of MHC Class I Molecules from the Golgi Complex to the Cell Surface. J. Immunol. *166*, 787–794.

Sohn, J., Orosco, L., Guo, F., Chung, S.H., Bannerman, P., Ko, E.M., Zarbalis, K., Deng, W., and Pleasure, D. (2015). The subventricular zone continues to generate corpus callosum and rostral migratory stream astroglia in normal adult mice. J. Neurosci. *35*, 3756–3763.

Song, C., Nicholson, J.D., Clark, S.M., Li, X., Keegan, A.D., and Tonelli, L.H. (2016). Expansion of brain T cells in homeostatic conditions in lymphopenic Rag2(-/-) mice. Brain. Behav. Immun. *57*, 161–172.

Song, D., Qi, F., Liu, S.S., Tang, Z., Duan, J., and Yao, Z. (2020a). The adoptive transfer of BCG-induced T lymphocytes contributes to hippocampal cell proliferation and tempers anxiety-like behavior in immune deficient mice. *15*, e0225874.

Song, E., Mao, T., Dong, H., Boisserand, L.S.B., Antila, S., Bosenberg, M., Alitalo, K., Thomas, J.-L., and Iwasaki, A. (2020b). VEGF-C-driven lymphatic drainage enables immunosurveillance of brain tumours. Nature *577*, 689–694.

Sospedra, M., and Martin, R. (2005). Immunology of multiple sclerosis. Annu. Rev. Immunol. *23*, 683–747.

Sotoodehnejadnematalahi, F., Moghadasali, R., Hajinasrollah, M., Ehsani, E., Hajizadeh-Saffar, E., Sodeifi, N., Saidi, R.F., Zarrabi, M., Farzanehkhah, M., Sadeghi, B., et al. (2021). Immunomodulatory Activity of Human Bone Marrow and Adipose-Derived Mesenchymal Stem Cells Prolongs Allogenic Skin Graft Survival in Nonhuman Primates. Cell J. *23*, 1–13.

Steinman, L. (2004). Elaborate interactions between the immune and nervous systems. Nat. Immunol. *5*, 575–581.

Stritesky, G.L., Jameson, S.C., and Hogquist, K.A. (2012). Selection of Self-Reactive T Cells in the Thymus. Annu Rev Immunol *30*, 95–114.

Sulzer, D., Alcalay, R.N., Garretti, F., Cote, L., Kanter, E., Agin-Liebes, J., Liong, C., McMurtrey, C., Hildebrand, W.H., Mao, X., et al. (2017). T cells from patients with Parkinson's disease recognize α-synuclein peptides. Nature *546*, 656–661.

Sun, C., Mezzadra, R., and Schumacher, T.N. (2018). Regulation and Function of the PD-L1 Checkpoint. Immunity *48*, 434–452.

Swijnenburg, R.J., Schrepfer, S., Govaert, J.A., Cao, F., Ransohoff, K., Sheikh, A.Y., Haddad, M., Connolly, A.J., Davis, M.M., Robbins, R.C., et al. (2008). Immunosuppressive therapy mitigates immunological rejection of human embryonic stem cell xenografts. Proc. Natl. Acad. Sci. U. S. A. *105*, 12991–12996.

Takaba, H., and Takayanagi, H. (2017). The Mechanisms of T Cell Selection in the Thymus. Trends Immunol. *38*, 805–816.

Tan, E.K., Chao, Y.X., West, A., Chan, L.L., Poewe, W., and Jankovic, J. (2020). Parkinson disease and the immune system - associations, mechanisms and therapeutics. Nat. Rev. Neurol. *16*, 303–318.

Tanigaki, K., and Honjo, T. (2007). Regulation of lymphocyte development by Notch signaling. Nat. Immunol. 2007 85 *8*, 451–456.

Tavazoie, M., Van der Veken, L., Silva-Vargas, V., Louissaint, M., Colonna, L., Zaidi, B., Garcia-Verdugo, J.M., and Doetsch, F. (2008). A specialized vascular niche for adult neural stem cells. Cell Stem Cell *3*, 279–288.

Tomasetti, C., Li, L., and Vogelstein, B. (2017). Stem cell divisions, somatic mutations, cancer etiology, and cancer prevention. Science (80-.). *355*, 1330–1334.

Trapani, J.A., and Smyth, M.J. (2002). Functional significance of the perforin/granzyme cell death pathway. Nat. Rev. Immunol. 2002 210 *2*, 735–747.

Tscharke, D.C., Croft, N.P., Doherty, P.C., and La Gruta, N.L. (2015). Sizing up the key determinants of the CD8+ T cell response. Nat. Rev. Immunol. 2015 1511 *15*, 705–716.

Urbán, N., Blomfield, I.M., and Guillemot, F. (2019). Quiescence of Adult Mammalian Neural Stem Cells: A Highly Regulated Rest. Neuron *104*, 834–848.

Viola, A., Contento, R.L., and Molon, B. (2006). T cells and their partners: The chemokine dating agency. Trends Immunol. *27*, 421–427.

Voskoboinik, I., Smyth, M.J., and Trapani, J.A. (2006). Perforin-mediated target-cell death and immune homeostasis. Nat. Rev. Immunol. 2006 612 *6*, 940–952.

Voskoboinik, I., Whisstock, J.C., and Trapani, J.A. (2015). Perforin and granzymes: function, dysfunction and human pathology. Nat. Rev. Immunol. 2015 156 *15*, 388–400.

Wagner, C.A., Roqué, P.J., Mileur, T.R., Liggitt, D., and Goverman, J.M. (2020). Myelin-specific CD8+ T cells exacerbate brain inflammation in CNS autoimmunity. J. Clin. Invest. *130*, 203–213.

Walter, D., Lier, A., Geiselhart, A., Thalheimer, F., Huntscha, S., Sobotta, M., Moehrle, B., Brocks, D., and Bayindir, I. (2015). Exit From Dormancy Provokes DNA-damage-induced Attrition in Haematopoietic Stem Cells. Nature *520*.

Wang, H.X., Pan, W., Zheng, L., Zhong, X.P., Tan, L., Liang, Z., He, J., Feng, P., Zhao, Y., and Qiu, Y.R. (2020). Thymic Epithelial Cells Contribute to Thymopoiesis and T Cell Development. Front. Immunol. *10*.

Wenger, T., Terawaki, S., Camosseto, V., Abdelrassoul, R., Mies, A., Catalan, N., Claudio, N., Clavarino, G., De Gassart, A., Rigotti, F.D.A., et al. (2012). Autophagy inhibition promotes defective neosynthesized proteins storage in ALIS, and induces redirection toward proteasome processing and MHCI-restricted presentation. Autophagy *8*, 350–363.

Wickham, H. (2016). ggplot2: Elegant Graphics for Data Analysis (Cham: Springer-Verlag New York).

Wilson, E.H., Weninger, W., and Hunter, C.A. (2010). Trafficking of immune cells in the central nervous system. J. Clin. Invest. *120*, 1368–1379.

Wolf, S.A., Steiner, B., Akpinarli, A., Kammertoens, T., Nassenstein, C., Braun, A., Blankenstein, T., and Kempermann, G. (2009a). CD4-positive T lymphocytes provide a neuroimmunological link in the control of adult hippocampal neurogenesis. J. Immunol. *182*, 3979–3984.

Wolf, S.A., Steiner, B., Wengner, A., Lipp, M., Kammertoens, T., and Kempermann, G. (2009b). Adaptive peripheral immune response increases proliferation of neural precursor cells in the adult hippocampus. FASEB J. *23*, 3121–3128.

Wong, G.H.W., Bartlett, P.F., Clark-Lewis, I., Battye, F., and Schrader, J.W. (1984). Inducible expression of H–2 and Ia antigens on brain cells. Nat. 1984 3105979 *310*, 688–691.

Xie, L., Choudhury, G.R., Winters, A., Yang, S.H., and Jin, K. (2015). Cerebral regulatory T cells restrain microglia/macrophage-mediated inflammatory responses via IL-10. Eur. J. Immunol. *45*, 180–191.

Xu, Y., He, F., Qi, F., Yang, G., Zheng, F., Yang, J., Wang, X., Liu, J., and Zou, J. (2017). Remodeling the Th1 polarized systemic environment contributes to neurogenesis and cognitive function via the Wnt7a pathway in neonatal mice. Neurobiol. Learn. Mem. *141*, 60–71.

Yamamoto, K., Venida, A., Yano, J., Biancur, D.E., Kakiuchi, M., Gupta, S., W Sohn, A.S., Mukhopadhyay, S., Lin, E.Y., Parker, S.J., et al. (2020). Autophagy promotes immune evasion of pancreatic cancer by degrading MHC-I. Nature *581*.

Yang, W., Li, Y., Gao, R., Xiu, Z., and Sun, T. (2020). MHC class I dysfunction of glioma stem cells escapes from CTL-mediated immune response via activation of Wnt/β-catenin signaling pathway. Oncogene *39*, 1098–1111.

Yang, X., Yang, J., Li, X., Ma, W., and Zou, H. (2018). Bone marrow-derived mesenchymal stem cells inhibit T follicular helper cell in lupus-prone mice. Lupus *27*, 49–59.

Yeung, J.T., Hamilton, R.L., Ohnishi, K., Ikeura, M., Potter, D.M., Nikiforova, M.N., Ferrone, S., Jakacki, R.I., Pollack, I.F., and Okada, H. (2013). LOH in the HLA class I region at 6p21 is associated with shorter survival in newly diagnosed adult glioblastoma. Clin. Cancer Res. *19*, 1816–1826.

Zalocusky, K.A., Najm, R., Taubes, A.L., Hao, Y., Yoon, S.Y., Koutsodendris, N., Nelson, M.R., Rao, A., Bennett, D.A., Bant, J., et al. (2021). Neuronal ApoE upregulates MHC-I expression to drive selective neurodegeneration in Alzheimer's disease. Nat. Neurosci. 2021 246 *24*, 786–798.

Zarif, H., Nicolas, S., Guyot, M., Hosseiny, S., Lazzari, A., Canali, M.M., Cazareth, J., Brau, F., Golzné, V., Dourneau, E., et al. (2018). CD8 + T cells are essential for the effects of enriched environment on hippocampus-dependent behavior, hippocampal neurogenesis and synaptic plasticity. Brain. Behav. Immun. *69*, 235–254.

Zhang, N., and Bevan, M.J. (2011). CD8+ T Cells: Foot Soldiers of the Immune System. Immunity *35*, 161–168.

Zhang, D., Ren, J., Luo, Y., He, Q., Zhao, R., Chang, J., Yang, Y., and Guo, Z.N. (2021). T Cell Response in Ischemic Stroke: From Mechanisms to Translational Insights. Front. Immunol. *12*.

Zhu, J., Feng, B., Xu, Y., Chen, W., Sheng, X., Feng, X., Shi, X., Liu, J., Pan, Q., Yu, J., et al. (2020). Mesenchymal stem cells alleviate LPS-induced acute lung injury by inhibiting the proinflammatory function of Ly6C + CD8 + T cells. Cell Death Dis. *11*.

Zhu, Y., Guignard, F., Zhao, D., Liu, L., Burns, D.K., Mason, R.P., Messing, A., and Parada, L.F. (2005). Early inactivation of p53 tumor suppressor gene cooperating with NF1 loss induces malignant astrocytoma. Cancer Cell *8*, 119–130.

Zhuo, L., Theis, M., Alvarez-Maya, I., Brenner, M., Willecke, K., and Messing, A. (2001). hGFAP-cre transgenic mice for manipulation of glial and neuronal function in vivo. Genesis *31*, 85–94.

Zindl, C.L., and Chaplin, D.D. (2010). Immunology. Tumor immune evasion. Science *328*, 697–698.

Ziv, Y., Ron, N., Butovsky, O., Landa, G., Sudai, E., Greenberg, N., Cohen, H., Kipnis, J., and Schwartz, M. (2006). Immune cells contribute to the maintenance of neurogenesis and spatial learning abilities in adulthood. Nat. Neurosci. *9*, 268–275.